FHWA-NJ-2018-008

HVS Evaluation of Flexible Overlays on Composite Pavement

FINAL REPORT
August 2018

Submitted by

Yusuf Mehta, Ph.D., P.E.
Professor
Department of Civil and Environmental Engineering
Rowan University

Ayman Ali, Ph.D.
Research Assistant Professor and Manager
Center for Research and Education in Advanced Transportation Systems
Rowan University

Andraé Francois
Research Assistant
Department of Civil and Environmental Engineering
Rowan University

NJDOT Research Project Manager
Giri Venkiteela, Ph.D.

In cooperation with

New Jersey
Department of Transportation
Bureau of Research
And
U. S. Department of Transportation

DISCLAIMER STATEMENT

“The contents of this report reflect the views of the author(s) who is (are) responsible for the facts and the accuracy of the data presented herein. The contents do not necessarily reflect the official views or policies of the New Jersey Department of Transportation or the Federal Highway Administration. This report does not constitute a standard, specification, or regulation.”

1. Report No. FHWA-NJ-2018-008	2.Government Accession No.	3. Recipient's Catalog No.	
4. Title and Subtitle HVS EVALUATION OF FLEXIBLE OVERLAYS ON COMPOSITE PAVEMENT		5. Report Date August 2018 6. Performing Organization Code	
7 Author(s) Yusuf Mehta, Ph.D., P.E., Ayman Ali, Ph.D. and Andraé Francois		8. Performing Organization Report No.	
9. Performing Organization Name and Address Rowan University Center for Research and Education in Advanced Transportation Engineering Rowan (CREATEs) 107 Gilbreth Parkway Mullica Hill, NJ 08062		10. Work Unit No. 11. Contract or Grant No.	
12. Sponsoring Agency Name and Address New Jersey Department of Transportation PO 600 Trenton, NJ 08625 Federal Highway Administration U.S. Department of Transportation Washington, D.C.		13. Type of Report and Period Covered 14. Sponsoring Agency Code	
15. Supplementary Notes			
16. Abstract This study focused on evaluating the field performance and life expectancy of various asphalt overlay treatments commonly used in New Jersey through full-scale accelerated pavement testing. Six 30-ft. long and 12-ft. wide full-scale, composite field sections were evaluated in this study. All six field sections contained a similar substructure (i.e. 8-in. thick Portland cement concrete (PCC) base, 16-in thick New Jersey I-3 (A-1-a) granular subbase, and 12-in. thick compacted natural soil subgrade). The overlay on the test sections consisted of the following mixes a 3-in. thick 9.5ME Superpave mix for Section 1, a 3-in thick Stone Matrix Asphalt (SMA) mix for Section 2, and a 2-in. thick New Jersey High Performance Thin Overlay (NJHPTO) for Section 3. The overlays on sections 3 through 6, consisted of a combination of 1-in. thick layer of BRIC and a 2-in. layer of 9.5 ME Superpave, SMA, and NJHPTO, respectively. All sections were instrumented with two asphalt strain gauges, linear variable differential transformers, soil compression gauges, and one pressure cell. The test sections were subjected to accelerated pavement testing at the Rowan University Accelerated Pavement Testing Facility (RU-APTF) using a Heavy Vehicle Simulator (HVS). The accelerated pavement testing involved the application of 60-kN, dual-tire, single axle load configuration for 200,000 repetitions. The test sections were also evaluated through heavy weight deflectometer testing and transverse pavement profile assessment. A ranking system was developed to determine which asphalt overlay had the best overall field performance. Based on the ranking system, it was concluded that section containing the SMA overlay had the best overall performance followed the sections containing the 9.5ME, NJHPTO, 9.5ME and BRIC combination, SMA and BRIC combination, NJHPTO and BRIC combination. It was also found that the addition of a 1-in. layer of BRIC did not significantly improve the field performance of the overlays.			
17. Key Words Composite Pavements, Asphalt Overlays, Accelerated Pavement Testing, Fatigue Performance, Expected Fatigue Life,		18. Distribution Statement	
19. Security Classif (of this report) Unclassified	20. Security Classif. (of this page) Unclassified	21. No of Pages 92	22. Price

Form DOT F 1700.7 (8-69)

TABLE OF CONTENTS

LIST OF FIGURES

LIST OF TABLES

EXECUTIVE SUMMARY

In the state of New Jersey (NJ) approximately 50 percent of pavements are composite. These composite pavements are typically composed of a Portland Cement Concrete (PCC) layer overlaid with a thin layer of asphalt. The thin layer of asphalt (or asphalt overlay) in composite pavements functions as a means of preservation and rehabilitation for deteriorated rigid pavements. The use of asphalt overlays on rigid pavements as a preservation and rehabilitation technique has become quite common among many state transportation agencies (STAs). This is because the application of asphalt overlays is relatively quick and inexpensive in comparison to other surface treatments for rigid pavements. The addition of asphalt overlays on rigid pavements provide several advantages which include: extending the service life of the pavement, reducing surface permeability, maintaining grade, and slope geometry of the pavement improving the ride quality of the pavement surface, and minimizing noise at the tire-pavement interface.

This study was initiated with the goal of identifying and predicting the expected life of thin asphalt overlay treatments used for rehabilitating and preserving PCC pavements. In order to fulfill this goal, the study was divided into two main components. The first component involved evaluating the current state of practice with respect to thin asphalt overlays through a holistic review of existing literature. This component of the study also required the evaluation of PCC pavement conditions in the state of NJ using field distress surveys and collected data from New Jersey Pavement Management System (NJPMS) as well as the identification of commonly used asphalt overlay mixes in NJ. Based on the findings of the comprehensive literature review, PCC pavement condition evaluation, and asphalt overlay identification; four types of asphalt overlay mixes were selected for the second component of the study; a standard Superpave 9.5 ME mix, a stone matrix asphalt (SMA) mix, a New Jersey high performance thin overlay NJHPTO mix, and a binder rich intermediate course (BRIC).

The second component of the study consisted of laboratory and field evaluation of the four types of overlay asphalt mixes. Several tasks were performed including: laboratory mix design and performance evaluation of selected mixes, construction of six full-scale composite pavement sections (i.e. PCC layers overlaid with the four asphalt overlay mixes) at the Rowan University Accelerated Pavement Testing Facility (RU-APTF), as well as the subsequent application of full-scale accelerated pavement loading using a Heavy Vehicle Simulator (HVS). The study also involved monitoring pavement performance of the asphalt overlays on the full-scale sections during APT with respect to reflective cracking, rutting, International Roughness Index (IRI), and pavement deflections) as well as analyzing the results obtained for recommending life expectancy for each of the thin asphalt overlay treatments evaluated.

Based on the laboratory and field testing results and subsequent analyses, it was concluded that Section 2 (SMA) had the best overall performance followed by Section 1 (9.5 ME), Section 5 (SMA and BRIC), Section 3 (NJHPTO), Section 6 (NJHPTO and BRIC) and Section 4 (9.5 ME and BRIC). Additionally, it was found that the overall field performance of the test sections did not significantly improve with the addition of a 1-in. layer of BRIC. This was because the addition of the 1-in. BRIC layer slightly reduced the resistance of the test sections with respect to their reflective cracking susceptibility and surface permanent deformation.

INTRODUCTION

Background

In the state of New Jersey (NJ) approximately 50 percent of pavements are composite pavements. These composite pavements are typically composed of a Portland Cement Concrete (PCC) layer overlaid with a thin layer of asphalt. The thin layer of asphalt (or asphalt overlay) in composite pavements functions as a means of preservation and rehabilitation for deteriorated rigid pavements. The use of asphalt overlays on rigid pavements as a preservation and rehabilitation technique has become quite common among many state transportation agencies (STAs). This is because the application of asphalt overlays is relatively quick and inexpensive in comparison to other surface treatments for rigid pavements. The addition of asphalt overlays on rigid pavements provide several advantages which include: extending the service life of the pavement, reducing surface permeability, maintaining grade and slope geometry of the pavement improving the ride quality of the pavement surface, and minimizing noise at the tire-pavement interface. [1]

Several hot mix asphalt (HMA) mixes have been used to construct asphalt overlays which have performed successfully in the laboratory and field. These HMA mixes include: dense graded Superpave mixes with 4.75-mm, 9.5-mm and 12.5-mm nominal maximum aggregate sizes (NMAS), 9.5-mm and 12.5-mm stone matrix asphalt (SMA) mixes, ultra-thin bonded wearing courses (UTBWC), and open graded friction courses (OGFC). [1] Several studies conducted have demonstrated that thin asphalt overlays may be a viable options for rehabilitating and/or preserving pavements. However, the majority of these studies were limited to evaluating only the laboratory performance of asphalt overlay mixes. Very few studies have evaluated of the life expectancy of asphalt overlay mixtures and many of the studies conducted on these mixes have evaluated their performance under conditions that may not be representative of conditions that exist in New Jersey. Thus, there is currently no field performance available for asphalt overlay mixtures that are utilized as treatments for deteriorated PCC pavements in the state of New Jersey.

There is a need to evaluate the field performance and life expectancy of various asphalt overlay treatments through full-scale pavement testing before the New Jersey Department of Transportation (NJDOT) can consider fully implementing these treatments on its roadways. It should be noted that, obtaining results through long term field evaluation (i.e. full scale testing) is time-consuming and might not a viable option. However, an accelerated full scale testing facility equipped with a Heavy Vehicle Simulator (HVS) facilitates conducting long term evaluations of twenty years within a period of six months. This evaluation will be essential for determining the life cycle and cost effectiveness of thin asphalt overlays and provide critical information to the NJDOT regarding the feasibility of using asphalt overlays as a pavement preservation option.

Objectives

The primary goal of the proposed project is to identify and predict the expected life of thin asphalt overlay treatments used for rehabilitating and preserving PCC pavements.

The specific objectives to fulfill the primary goal are as follows:

- Conduct a comprehensive literature review to identify potential distresses in thin overlays, successes and challenges of different types of thin overlay treatments and performance prediction models.
- Evaluate the current conditions of PCC pavement sections in the state of NJ using field distress surveys or data obtained from New Jersey Pavement Management System (NJPMS) to identify the spectrum of conditions on which thin asphalt overlays might be applied.
- Identify the most common thin asphalt overlay mixes used for rehabilitating/preserving PCC pavement in NJ and the major factors that influence performance of these mixes.
- Conduct laboratory mix design and laboratory performance evaluation of up to four asphalt overlay mixes commonly used in NJ.
- Construct six full-scale PCC pavement sections with up to four thin asphalt overlay treatments in the Rowan University Accelerated Pavement Testing Facility (RU-APTF).
- Conduct full-scale accelerated pavement loading using the Rowan University Heavy Vehicle Simulator (RU-HVS).
- Monitor pavement performance (reflective cracking, rutting, International Roughness Index (IRI), and modulus values using Falling Weight Deflectometer (FWD) of the thin asphalt overlays).
- Analyze results and recommend life expectancy for each of the thin asphalt overlay treatments evaluated.

Report Organization

This report is organized into nine chapters. In Chapter one, the problem statement, objectives, and outline of the report are presented. Chapter two presents a comprehensive literature review summarizing the studies that have evaluated the performance of commonly used asphalt overlay mixes. Chapter three provides a detailed discussion related to the types of asphalt overlay mixtures evaluated in this this study. Chapter four describes the entire construction process of the full-scale field sections at Rowan University Accelerated Pavement Testing Facility (RU-APTF). In Chapter five, a detailed discussion is presented with respect to the instrumentation of the full-scale test sections. Chapter six discusses the overall field evaluation plan adopted in this study. Chapter seven provides an in depth discussion on the overall analysis approach and procedures employed in this study to evaluate the relative performance of the full-scale test sections. A field performance comparison of the test sections is also presented in this chapter. Chapter 8 summarizes the findings of the field performance comparisons of the full-scale sections and provides the final conclusions about the overall performance ranking of the field sections.

LITERATURE REVIEW

This section provides a comprehensive overview of previous studies that have investigated the laboratory and field performance of commonly used asphalt overlay mixtures. The findings of these studies are detailed in the following subsections.

Laboratory Performance of Asphalt Overlay Mixtures

Stone Matrix Asphalt Mixtures

Stone matrix asphalt mixes are gap-graded asphalt mixtures that have a high coarse aggregate content. This mixture originated in Europe in the 1960's and has been successfully used in the United States (US) since 1991. [2] The preparation of SMA mixes involves utilizing coarse aggregates, fine aggregates and mineral filler depending on the NMAS selected for design. A key feature of SMA mixes is a coarse aggregate skeleton which forms as a result of the stone-on-stone contact between the coarse aggregates in the mix. This stone-on-stone contact is maintained by a rich asphalt cement mortar, mineral filler, and fiber. The lack of intermediate aggregate sizes in SMA mixes allows for more asphalt cement mortar to be present in the mix. The increased aggregate interlock in the coarse aggregate skeleton of SMA mixes increases the shear strength of the aggregates and this provides SMA mixes with increased load transfer efficiency and a high resistance to permanent deformation (i.e. rutting). The high binder content and low air voids of SMA mixes also improves the ability of the mix to resist reflective cracking and increases its durability. [2]

The National Cooperative Highway Research Program (NCHRP) previously conducted a study which evaluated a suitable mix design for stone matrix asphalt mixes in the US. From the results of this study the NCHRP recommended that a particular gradation (i.e. 4.75mm NMAS) should be utilized for SMA mixes. [3] As a result, subsequent studies involving the performance of SMA mixes have focused on improving the design of a 4.75mm NMAS SMA mixes. [3] For instance Xie et al (2003) [3] conducted a study which investigated the gradation requirements for the percent passing the 0.075mm sieve and the feasibility of the draindown basket used in the mix design process of MSA. Eight SMA mixes were designed using; (1) Two kinds of aggregate; granite and limestone, (2) One gradation using two fractions passing the 0.075mm sieve; 9% and 12%, and (3) PG 64-22 binder. Draindown tests were conducted along with the Asphalt Pavement Analyzer (APA) to observe the viability of the previously reported SMA specifications. Two different wire baskets were used in the study; 6.3-mm and 2.36-mm. The larger draindown basket allowed aggregates to pass through and it was recommended that a basket size of 2.36mm be used with 4.75-mm NMAS mixes. Depending on aggregate type, average rut depths ranged from 10.2-mm, for the granite mix and 12.5-mm, for the limestone mix. When asphalt content decreased due to raising the dust content to 12%, the values for average rut depth went down from 12.1-mm to 10.6-mm. Considering the high rut depths from the APA tests, it was recommended that a non-modified asphalt binder should not be used on roads with high traffic. Changing the gradation requirements for the 0.075-mm was also recommended from 12%-15%, to 9%-15%.

Cooley et al. (2003) [4] evaluated the potential for using fine stone matrix asphalt mixes (i.e. NMAS of 9.5-mm or 4.75-mm) for thin overlays by assessing their laboratory performance. A total of eight mixes were evaluated in the study; four controlled mixes (12.5 mm and 19.5 mm NMAS) and four mixes with a 9.5-mm and 4.75-mm NMAS. The researchers investigated two break point (BP) sieves for each mix with the exception of the 9.5-mm NMAS mix. It is important to note that the BP identified the point at which the gap in the gradation began. The break points for the 4.75-mm NMAS mix were 2.36-mm and 1.18 mm, the break points for the 9.5-mmm NMAS mix was 4.75-mm and 2.36-mm, and the break points for the 12.5-mm mix was 9.5-mm and 4.75-mm. Cooley et al. (2003) [4] conducted asphalt pavement analyzer tests at 50ºC and 64ºC respectively on each mix in order to investigate their rutting potential. Each SMA mixture sample were subjected to 8,000 loading cycles of the APA and the maximum rut depth criteria utilized for the testing was 5.0 mm. Testing results, according to Cooley et al. (2003) [4] indicated that rut depths increased when testing temperature was increased from 50ºC to 64ºC as expected. However, the researchers found that the magnitude of the rut depths remained relatively low; below the specified rutting criteria in spite of the temperature increase. Cooley et al. (2003) [4] therefore concluded based on APA testing that fine SMA mixtures can be designed to be rut resistant.

Cantrell (2013) [5] conducted a study which evaluated the potential of using 4.75-mm NMAS thin overlays in Washington State. In the study, Cantrell (2013) [5] developed four mix designs using two binder types (i.e. PG 70-28 and PG 76-28) and two gradations (i.e. course and medium) and investigated the cracking, rutting and moisture susceptibility of the mixes. The cracking and rutting potential of the mixes were evaluated using the laboratory indirect tensile test and the Hamburg wheel tracking test respectively. In regard to the indirect tension tests six specimen were prepared for each mixture. These specimen had a diameter of 102 mm and were cut to a height of 38.1 mm. With respect to the Hamburg wheel track test four specimen with a diameter of 150 mm were compacted to a height of 62 mm for each mixture and subsequently tested. The results of the indirect tension tests according to Cantrell (2013) [5] indicated that the crack resistance of the 4.75-mm mixtures were comparable to conventional 12.5-mm mixtures resistance of mm mixtures. However the coarse 4.75-mm mixtures had better cracking resistance based on work of fracture. With respect to rutting and moisture susceptibility, the results of the Hamburg Wheel track test showed that the course and medium graded PG76 mixtures performed similar to 12.5-mm mixtures.

Al-Qadi et al (2015) [6] conducted a study which evaluated for the ability of a 4.75-mm NMAS stone matrix asphalt mix to perform as a wearing course. All mixes analyzed in the study consisted of dolomite aggregates and quartzite aggregates. Al-Qadi et al (2015) [6] compared the 4.75-mm SMA mix with two control mixes; a 9.5-mm NMAS coarse dense-graded mixture and a 12.5-mm SMA mixture. The 4.75-mm NMAS mix contained 84 percent steel slag as a durable, friction aggregate, while the 9.5-mm NMAS mix contained 10 percent RAP and 35.7percent steel slag. The asphalt binder used in the 4.75-mm and 9.5-mm mixes was a PG 70-22 SBS modified binder, while the 12.5-mm mix contained a PG 76-22 SBS modified binder. Al-Qadi et al (2015) [6] conducted five laboratory performance tests which included: complex modulus, rutting potential, fracture potential,

moisture susceptibility, and durability tests. Based on the results of the testing, the researchers found that the control 12.5-mm SMA had the highest complex modulus, which indicated that this mix may have the best rutting resistance. The researchers also found that the 4.75-mm SMA mix had the lowest complex modulus at higher test frequencies. According to Al-Qadi et al (2015) [6] this indicated that this mixtures may perform better in terms of low temperature cracking. Additionally, the researchers also reported that the indirect tensile strength was highest in the 4.75-mm mix, in both wet and dry conditions. However, the tensile strength ratio fell between the control 12.5-mm SMA and the 9.5-mm control mix.

Dense Graded Hot Mix Asphalt Mixtures

In the state of New Jersey, dense graded hot mix asphalt mixtures are typically used for constructing a specialty asphalt overlay mixture referred to as High Performance Thin Overlay (HPTO). High Performance Thin Overlay mixtures are typically defined as having a thickness of 1 in. These mixtures are generally placed on existing pavements in order to improve their rutting and fatigue resistance (i.e. HPTO is commonly used as a pavement preservation strategy). Additionally, HPTO is also placed on pavements when the remaining structural capacity of a pavement is expected to exceed that of an already existing pavement preservation strategy [7]. HPTO mixtures provide several advantages when utilized on rigid and flexible pavements. These advantages include: reducing the rate of pavement deterioration, reducing pavement surface permeability, improving ride quality, and correcting surface deficiencies [7]. It should be noted that HPTO mixtures are relatively easy to apply (i.e. HPTO can be placed with a conventional paver or spray paver) and have a relatively short curing time. [1]

Several studies have been previously undertaken to evaluate the performance of dense graded HMA mixes commonly used in asphalt overlays. Kandhal and Cooley (2002) [8] conducted a study that compared coarse-graded and fine-graded Superpave mixtures based on their ability to resist rutting. In the study, fourteen (14) mixes in total were evaluated. These mixes consisted of the following gradations: 9.5mm NMAS and 19.5mm NMAS. Various combinations of aggregate types were utilized in the mixes. The aggregate types included: granite and crushed gravel (as coarse aggregates) and limestone, sandstone, and diabase (i.e. traprock) (as fine aggregates). Asphalt Pavement Analyzer (APA) tests were conducted on all mixture samples and the results indicated that both gradation types exhibited a similar rutting potential. As a result, Kandhal and Cooley (2002) [8] concluded that both the coarse and fine-graded mixtures can be designed to be rut resistant. The researchers also indicated that finer mixes may be more desirable since they are more workable, less permeable, less likely to segregate, and more cost effect in thinner layers.

Rahman (2011) [9] evaluated the laboratory performance of 4.75-mm NMAS Superpave mixes. In the study, Rahman (2011) [9] conducted beam fatigue tests to estimate the fatigue life and failure energy of 4.75-mm mixes when they are subjected to repeated loading conditions. The researcher evaluated four different mix designs in the study, which consisted of either PG 64-22 or PG 70-22 binder mixed with two aggregate blends with contained different proportions of fines (i.e. river sand). Rahman (2011) [9] prepared

twenty four 15 in. x 2 in. x 2.5 in. samples which were compacted at 7.0 ± 0.5 percent air voids. The flexural strength of these samples were analyzed in a two point loading arrangement in a conditioned chamber at 300 micro-strains (3). It should be noted that the researcher utilized the change between the initial flexural stiffness (i.e. at 50 loading cycles) and the final flexural stiffness (i.e. at 2 x 10^6 loading cycles) as the fatigue performance measure. Based on the results of the laboratory testing, Rahman (2011) [9] concluded that the laboratory fatigue performance of the 4.75-mm mixes were significantly influenced by the percentage of fines in the mix and PG grade of the binder. The researcher found that the flexural strength of 4.75-mm mixes increased as the percentage of natural sand content in the mix decreased.

Suleiman (2011) [10] evaluated the laboratory performance 4.75-mm Superpave mixes in order to assess if they can be used in thin overlays on non-Interstate highway pavements and maintenance applications. In the study, Suleiman (2011) [10] utilized the asphalt pavement analyzer test to investigate the rut resistance of hot mix asphalt (HMA) mixes with a NMAS of 4.75-mm. The researcher evaluated four mix design cases in which either PG 64-28 or PG 58-28 binder was mixed with two aggregate blends consisting of different proportions of natural and crushed fines. Suleiman (2011) [10] prepared laboratory specimen at 7.0 percent air voids, heated them at 64°C or 58°C for 6 hours; depending on the type of binder used in the mix, and subjected the specimen to 8,000 loading cycles of the APA. It is important to note that the specified rut depth criterion for the 4.75-mm mixes was 9.5-mm. Based on the testing results, Suleiman (2011) [10] concluded that the that the all the mix design cases were rut resistant however there was an increase in rut depth as binder content increased. Additionally, Suleiman (2011) [10] found that mixes which contained high percentages of crushed fines performed superior to mixes which contained lesser amounts of crushed fines. The researcher also found that mixes which contained high percentages of natural fines generally failed the APA test.

Ultrathin Bonded Wearing Course

Ultrathin bonded wearing course (UTBWC) mixtures are gap-graded asphalt mixtures which were first developed in France in 1986. These asphalt mixtures were designed specifically to be a functional layer in pavements as opposed to a structural layer. [11] The role of UTBWC in asphalt overlays according to Gilbert et al. (2004) [11] is to provide the following functions: improve skid resistance, minimize noise on road surface, and reduce water spray in wet traffic conditions. Additionally, it should be noted that UTBWC mixtures are typically prepared using gap-graded aggregates.

Ahmed et al. (2010) [12] evaluated the fracture characterization of gap-graded asphalt mixtures and thin bonded wearing courses. The researchers tested cored field samples in order to evaluate the low temperature fracture energy of the asphalt concrete. The researchers also prepared laboratory specimen of plant-produced hot mix asphalt mixture which was obtained during the construction of the field sections in order to assess the impact of tack coat application rate, air voids, and overlay thickness on the fracture energy of thin bonded wearing courses. Ahmed et al. (2010) [12] compared the fracture energy results of the field cores with that of the laboratory compacted specimen in the study. The researchers also compared the fracture toughness of typical dense-graded asphalt

mixtures, a laboratory compacted gap-graded mixture, and the thin bonded wearing courses. The results of the study according to Ahmed et al. (2010) [12] indicated that the gap-graded thin bonded wearing course had a higher fracture resistance when compared to typical wearing course mixtures.

Open Graded Friction Course

Open Graded Friction Course (OGFC) mixtures have been used in the United States since 1950. [13] These asphalt mixes are typically prepared using single size coarse aggregates and a small portion of fine aggregates. OGFCs provide many benefits when used as asphalt overlays. These benefits include: improved skid resistance on pavement surface, and reduced water spray during periods of inclement weather [13]. Additionally, Belshe et al. (2007) [14], performed a study which found that OGFC mixtures provided an insulation effect which extended the life of jointed Portland cement concrete (PCC) because it reduced the curling stresses on the PCC slabs.

Several other studies have been conducted to evaluate the performance of OGFC mixes. For instance, Qi and Harvey (2011) [15] performed a study which evaluated the laboratory performance of open graded asphalt mixes consisting of fine aggregates and various binders and additives. In the study Qi and Harvey (2011) [15] evaluated 4.75-mm NMAS asphalt mixtures containing six different combinations of binder types and additives to determine the optimal binder and additive combination which improved the performance of the asphalt mixes. The five binders utilized by the researchers in the study were PG 64-16, PG 58-34, PG 76-22, asphalt rubber, and PG 76-22 (modified with rubber) and the two additives used were hydrated lime and cellulose fiber. The permeability, moisture susceptibility, reflective cracking resistance, permanent deformation susceptibility, and raveling resistance of all six mixes were analyzed. For each of the six combinations, the researchers tested three unaged and aged 101-mm diameter specimen using the Cantabro test and three conditioned and unconditioned specimen using the moisture susceptibility test. Qi and Harvey (2011) [15] also tested four (159 mm x 560 mm x 38 mm specimen) using the Hamburg wheel test, nine (50-mm diameter cored) specimen using the shear and overlay test and five specimen using the nine (100-mm diameter cored) specimen using the impedance tube test. Based on the results of the study, Qi and Harvey (2011) [15] reported that OGFC mixes containing polymer modified binders or additives (i.e. asphalt rubber and hydrated lime) had less interconnected air voids than OGFC mixes containing conventional untreated binder. The researchers also reported that the use of hydrated lime did not improve resistance of mix to moisture failure, but improved resistance to raveling. Additionally, Qi and Harvey (2011) [15] concluded that the addition of asphalt rubber increased the rutting resistance but reduced the reflective cracking resistance of OGFC mixes.

Performance Comparison of Various Types of Asphalt Overlay Mixtures

Butler and Gibney (2005) [16] performed a study which investigated the resistance of a variety of bituminous mixes used in overlays in Ireland to reflective cracking. In the study the researchers evaluated three mixes bituminous mixtures; a 14-mm hot rolled asphalt mix, 20-mm dense base course mix, and a 10-mm stone matrix asphalt mix. In the study, two specimen (140 mm x 280 mm x 50 mm) and two specimen (140 mm x 260 mm x 50

mm), were compacted using a laboratory scaled roller compactor and aged for 24 hours at 60°C prior to reflective cracking test. The reflective cracking testing conducted in the study simulated bottom-up cracking and top-down cracking which occurs in asphalt overlays due to joint opening (or deterioration) in underlying concrete slab and differential movements of underlying concrete slabs respectively. To simulate bottom-up cracking, the researchers utilized a test setup similar to a simply supported beam where the ends of the aged specimen were supported on timber blocks, 10-mm metal plates were placed under the specimen (to mimic a concrete layer), and foam was placed under the metal plates along the specimen span to simulate a weak foundation. To simulate top-down cracking, the researchers utilized a test setup similar to a cantilever beam where the aged specimen were supported on a rigid timber block, 10-mm metal plates were placed under the specimen (to mimic a concrete layer), foam was placed under the cantilever end of the specimen for support, and a 10-mm joint was allowed between the timber and foam supports. Butler and Gibney (2005) [16] performed a standard wheel tracking test where a wheel load of 520 ± 5 N was applied to the specimen at a frequency of 21 cycles per minute at 25°C. Butler and Gibney (2005) [16] indicated that the 14-mm hot rolled asphalt mix showed more than 1.8 times more resistance to cracking when compared to the stone matrix asphalt mix. The researchers also suggested that increasing the depth of the overlay increased its resistance to cracking (i.e. increase of 5 mm increased cracking resistance by a factor of 1.3).

Bennert (2010) [17] assessed the potential for optimizing the use of thin asphalt overlays when rehabilitating PCC pavement in New Jersey. In this study, the researcher conducted a field evaluation with the objective of determining PCC pavement joint movements along with pavement specific traffic conditions. Using the data obtained, Bennert (2010) [17] conducted Overlay Tests (OT) to simulate the PCC pavement joint movements and traffic conditions, on asphalt overlay mixtures in New Jersey. Based on the results of the study, Bennert (2010) [17] reported that dense graded asphalt overlay mixes were not capable of resisting cracks with movements greater than 0.01-in. without cracking. The researcher recommended that a reflective crack relief interlayer (RCRI) should be placed under the asphalt overlay if the cracks have movements greater than 0.01-in. Furthermore, Bennert (2010) [17] also reported that testing results and collected information provided a procedure for designing asphalt overlay mixes. However, the researcher suggested that this procedure is only capable of predicting early reflective cracking occurring within the first two years of the asphalt overlays' lives.

Druta et al. (2014) [18] carried out a study which evaluated the rutting performance of thin asphalt overlays. In the study, the researchers performed asphalt pavement analyzer test (APA) tests on three types of dense graded asphalt overlay mixes and one gap-graded mixture. The dense graded mixtures had the following NMAS: 4.75-mm, 9.5-mm NMAS, and 12.5-mm NMAS, while the gap graded mixture had an NMAS of 9.5 mm. It is noted that the APA test were conducted at 64°C. Based on the results of the laboratory testing, Druta et al. (2014) [18] concluded that the (4.75-mm NMAS) dense graded mixture had the lowest rut depth at the end of 8000 cycles followed by the (9.5-mm NMAS) gap graded, (9.5-mm NMAS) dense graded and (12.5-mm NMAS) dense graded mixtures respectively.

Powell et al. (2012) [19] conducted a study which evaluated the long term performance of thin asphalt overlays using the National Center for Asphalt Technology (NCAT) test track. The mixtures analyzed in the study had a NMAS of 12.5 mm, 9.5 mm, and 4.75 mm respectively. The researchers measured the rutting, roughness, and cracking characteristics for all three mixes in the NCAT test track and compared field rutting results to laboratory asphalt pavement analyzer results. The pavement test track contained forty-six 60 m long pavement sections, in which 10 million ESALs were applied over the span of two years. This loading was equivalent to the traffic volume (i.e. design ESALs) of the pavement structure on the test track. In terms of rutting, Powell et al. (2012) [19] reported that the 4.75-mm, 9.5-mm, and 12.5-mm mixes experienced 6 mm, 4 mm, and 4 mm of rutting in the field, respectively, after the application of 30 million ESALs. The researchers also reported that the results of laboratory APA tests indicated that the 4.75-mm, 9.5-mm, and 12.5-mm mixes had a rut depth of 2.2 mm, 3.4 mm, and 3.4 mm, respectively after 8000 load cycles. Additionally, Powell et al. (2012) [19] reported that the field test section containing the 9.5-mm mix was the only section with visible cracking after 21 million ESALs were applied. All three pavements performed comparably in terms of roughness. Powell et al. (2012) [19] reported, based on field evaluation results, that the 4.75-mm NMAS thin asphalt overlay mixes had comparable performance to the 12.5-mm and 9.5-mm NMAS mixes.

Li et al. (2012) [20] compared the fatigue cracking performance of pavement sections containing a 4.75-mm NAMS dense graded Superpave asphalt overlay to that of sections containing no asphalt overlay. In the study, the researchers conducted full-scale accelerated pavement testing on field sections consisting of a 25-mm thick asphalt overlay and sections containing no asphalt overlay (i.e. control sections). The asphalt overlay utilized in the study consisted of 20% recycled asphalt pavement (RAP) and a polymer modified, PG 76-22 asphalt binder. The results of the study indicated that fatigue cracking initiated after 500,000 wheel passes for the unaged, untreated section (i.e. section containing no overlay) while cracking began after 425,000 wheel passes on the section which contained an unaged asphalt overlay. The results of the study also showed that cracking initiated after 50,000 wheel passes for the section containing an aged overlay. Based on these results Li et al. 2012 [20] concluded that fatigue cracking can be delayed with the use of a thin overlay treatment however, once the overlay became brittle due to aging, this benefit was lost.

Modeling Techniques Utilized to Predict Service Life of Asphalt Overlays

Nur et al. (2013) [21] carried out a study which developed a model to predict rutting on composite pavements in Louisiana. In the study the researchers analyzed pavement distress data from 199 pavement sections in Louisiana which totaled 579.7 miles of roadway. Nur et al. (2013) [21] performed a regression analysis which yielded a reasonable prediction for rutting. The researcher modeled rutting as a power function since the rutting was expected to increase with load repetitions (or time). The equivalent single axle load (ESALs) applied to the pavement, pavement thickness, functional classification of the roadway, and existing pavement condition (i.e., distress data) were all accounted for in the model. Based on the results of a sensitivity analysis performed on the developed

model, Nur et al. (2013) [21] concluded that rutting was largely affected by cumulative ESAL, thickness of the PCC layer, highway functional classification, and surface age.

Al-Qadi et al. (2009) [22] conducted a study to evaluate the effectiveness of HMA interlayers in retarding reflective cracking in asphalt overlays. In the study, the researchers developed a method to predict the years of service life added by introducing an HMA interlayer in a composite pavement. Al-Qadi et al. (2009) [22] predicted the years of service life added by an HMA interlayer using a performance benefit ratio. The computation of this performance benefit ratio is illustrated in Figure 1. From this figure it can be observed that the researchers plotted the reflective cracking index against the age of an overlay with and without an HMA interlayer. They then determined the service life of the overlays when the reflective cracking index (RCI) reached a certain threshold value. The extension in service life granted by the HMA interlayer was then determined by computing the difference between the RCI versus overlay age graph for the asphalt overlays with and without an HMA interlayer. Al-Qadi et al. (2009) [22] determined the performance benefit ratio by computing the ratio between the lifespan of the overlay containing the HMA interlayer and to that of the overlay that did not contain the HMA interlayer.

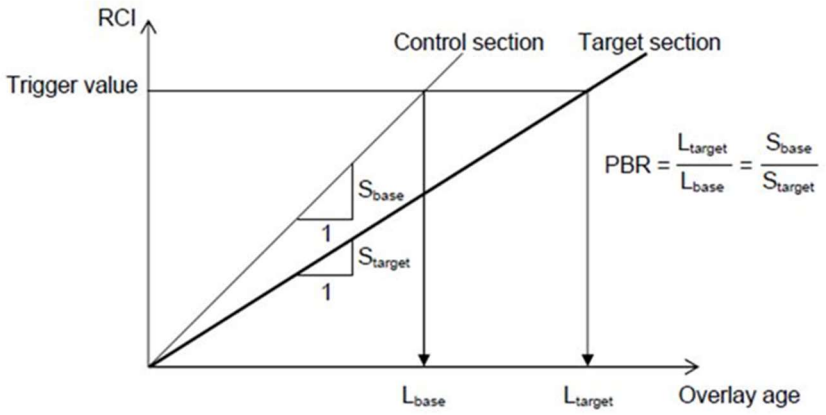

Figure 1 Performance benefit ratio and service life of HMA overlays (Al-Qadi et al. (2009) [20])

Summary of Literature Review

In summary, there seems to be consensus among researchers that thin asphalt overlays constructed using dense grade mixes, SMA mixes, UTBWC, and OGFC mixes are viable options for rehabilitating and/or preserving rigid pavements. However, the majority of the studies presented above have mainly focused on evaluating the laboratory performance of dense graded, SMA, UTBWC and OGFC mixes that are not typically utilized in the construction of asphalt overlays state of New Jersey. Additionally very few of the studies presented above have sought to evaluate the field performance of the previously mentioned mixes. Therefore the research presented in the following chapters will seek to evaluate the field performance of dense graded, SMA, UTBWC and OGFC mixes that are typically used in New Jersey under conditions that reflect those that exist in New Jersey.

MATERIALS DESCRIPTION

This section provides a detailed description of the HMA overlay mixes evaluated in the study. Four types of plant-produced HMA overlay mixes were considered in this study. These HMA mixes included: a 9.5 ME mix, a stone matrix asphalt (SMA) mix, a high performance thin overlay (HPTO) mix, and a binder rich intermediate course (BRIC) mix. Since these mixes were obtained from a local plant in Southern NJ, the research team also obtained the Job Mix Formulas (JMFs) for these mixes. The JMFs for all the mixes were verified by conducting volumetric testing (Bulk Specific Gravity, G_{mb}; and Rice Specific Graivity, G_{mm}), binder extraction and recovery to determine binder content, and the specified NJDOT performance tests (i.e., Asphalt Pavement Analyzer (APA) for rutting and Overlay Tester (OT) for fatigue/reflective cracking). In addition, the research team evaluated the moisture susceptibility of the selected HMA overlay mixes. The following sections provide a discussion of the four overlay mixes evaluated in this study along with the testing conducted to verify the designs of these mixes.

Description of HMA Overlay Mixes

9.5 ME Mix

A dense graded HMA mixture was utilized as the control mix in this study (Table 1 shows extraction recovery and volumetric testing results; Figure 2a shows aggregate gradation). This mixture was prepared according to the standard Superpave mix design procedure while meeting NJDOT specifications. The nominal maximum aggregate size (NMAS) of this mix was 9.5-mm (0.374-in.). From Figure 2a it can be seen that the aggregate gradation of the control mix fell within NJDOT's specified control point requirements. The type of binder utilized in the control mix was PG 76-22. The binder content and the air voids of the control mix were 5.68 % and 3.76 % respectively as shown in Table 1. It should be noted that the volumetric properties (i.e. binder content and percent air voids) of the mix fell within the NJDOT requirements.

Stone Matrix Asphalt (SMA) Mix

The stone matrix asphalt mix considered in this study had a NMAS of 12.5-mm (0.49-in). The gradation of the SMA mix is presented in Figure 2b. From this figure it can be observed that the aggregate gradation of this mix fell within the NJDOT specified control points. The type of binder utilized in the SMA mix was PG 76-22 and the binder content and air voids of the mix were 7.02 % and 4.44% respectively as illustrated in Table 1. It can be seen from Table 1 that the volumetric properties of the SMA mix fell within NJDOT specifications.

High Performance Thin Overlay (HPTO) Mix

The high performance thin overlay mix analyzed in this study contained a NMAS of 4.75-mm (0.187-in.). The aggregate gradation of this mix is illustrated in Figure 2c. It can be seen from this figure that the gradation of the HPTO mix generally lied within the control point requirements for that mix. However, the cumulative percent of aggregate passing (CPP) the No.4 sieve fell slightly outside the upper limit of the specified range. The

contractor was notified of this issue in the gradation and was instructed to make changes to ensure meeting NJDOT control points for this mix.

The type of binder utilized in the HPTO mixture was PG 76-22. The binder content of the mix was 7.60 % and the percent air voids was 3.18 %. The binder content and percent air voids both met the NJDOT volumetric requirements for HPTO mixes. This was achieved after making adjustments in gradation.

Binder Rich Intermediate Course (BRIC) Mix

The binder rich intermediate course mix evaluated in this study had an NMAS of 4.75-mm (0.187-in.). The aggregate gradation of the BRIC mix is shown in Figure 2d. It can be seen from this figure that the BRIC mixture had an open gradation. The type of binder utilized in the mixture was a polymer modified PG 70-28 binder. The binder content of BRIC mixture was 7.41% and the percent air voids was 2.54 % as shown in Table 1. From this table it can be observed that the volumetric properties of the BRIC mix met all NJDOT specifications.

Table 1– Extraction Recovery and Volumetric Testing Results

Mixture Type	Binder Content (%)		Air Voids (%)	
	Target	Actual	Target	Average
9.5 ME (control mix)	5.7	5.68	4.0 ± 1	3.76
Stone Matrix Asphalt (SMA)	6.7 – 7.5	7.02	4.0 ± 1	4.44
High Performance Thin Overlay (HPTO)	>7	7.60	3.5 ± 1	3.18
Binder Rich Intermediate Course (BRIC)	>7	7.41	2.5 ± 1	2.54

Verification of Job Mix Formulas

In addition to the testing conducted above, NJDOT specifies that certain asphalt mixtures be tested for certain performance characteristics before being approved. For this purpose, the research team conducted performance testing to verify that all the overlay mixes are meeting NJDOT specifications for rutting and fatigue/reflective cracking. Testing was performed on all the HMA overlay mixes at AASHTO re:source accredited Rowan University Construction and Materials laboratory (RUCOM) prior to the construction of full-scale sections (i.e. placement of the HMA overlays discussed in the following chapters). Three laboratory performance tests were conducted; APA (AASHTO T340) test for rutting, OT (Tex-248f and NJDOT B-10) test for fatigue/reflective cracking, and the modified Lottman (AASHTO T283) test for susceptibility to moisture induced damage.

Rutting Performance (APA Results)

The APA test was conducted in order to evaluate the rutting susceptibility of each of the four HMA overlay mixtures. These tests were performed according to AASHTO T340 specifications. Samples for this tests were prepared using plant-produced mixtures

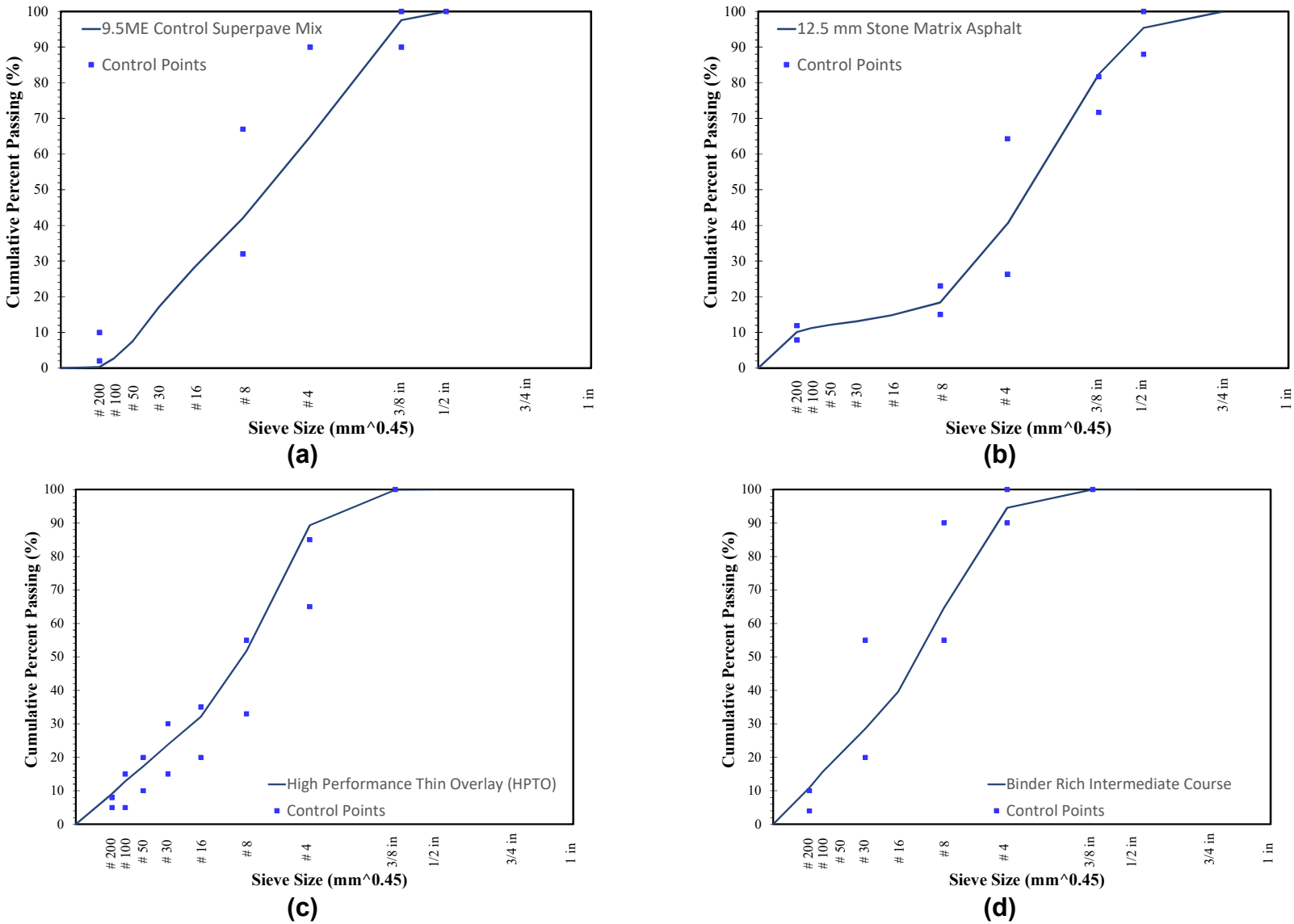

Figure 2. Gradation of HMA mixtures; (a) 9.5ME, (b) SMA, (c) HPTO, and (d) BRIC

compacted in RUCOM. The test was conducted by subjecting the compacted samples to a total of 8000 loading cycles. In each cycle a 100-lbf wheel load was applied over the sample with the load being transmitted to the sample using 100-psi pressurized rubber hoses in the APA chamber. Before the application of lo0ading cycles the samples were condition to reach a temperature of 64°C for a minimum of 6 hours.

The results of the APA tests conducted on all HMA overlay mixtures are presented in Figure 3. As can be seen from this figure, the average rut depth threshold specified by the New Jersey Department of Transportation (NJDOT) for the 9.5 ME Superpave, SMA, New Jersey HPTO, and BRIC mixes at the end of 8000 cycles are 5.5-mm, 5-mm, and 4-mm respectively. Based on the results illustrated in Figure 3, the average rut depth of all mixes (i.e. both laboratory-produced and plant-produced) fell well below their respective NJDOT specified thresholds for rutting. Therefore, all mixes met the NJDOT specialty mixes approval specifications for rutting.

By comparing the APA results (Figure 3) for all mixes, the relative rutting performance of these mixes can be evaluated. As illustrated in Figure 3, the APA rut depths for the 9.5 ME control mix and the New Jersey HPTO mixes had a similar average rut depth (~3.5-mm) at the end of 8000 cycles. The stone matrix asphalt mix had the next highest average rut depth after 8000 cycles of the APA (~1.75-mm) and the BRIC mix had the lowest average sample rut depth of all the overlay mixes (~0.75-mm). This trend indicates that the NJ HPTO mix had a similar susceptibility to rutting as the control mix and. The observed trends also indicate that the HPTO and the control mixes had a higher susceptibility to rutting than the SMA and BRIC overlay mixes.

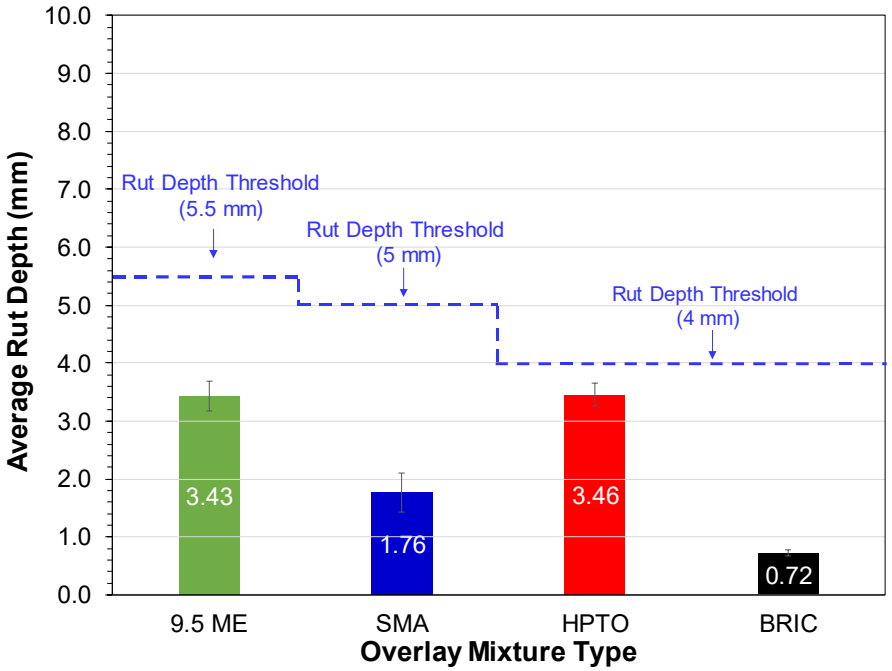

Figure 3. Average sample rut depth of laboratory produced and plant-produced overlay mixes after 8000 cycles of APA

Fatigue/Reflective Cracking Performance (OT Results)

The overlay test (OT) was performed on all HMA overlay mixes according to NJDOT B-10 and Tex-248f specifications. This test involved the preparation of three (6-in. x 3-in x 1.5-in.) OT specimens for each HMA overlay mixture (i.e. two per specialty mix), the application of 16-g of (NJDOT B-10) two part epoxy on the specimen, the placement of the epoxied specimen on OT base plates, the placement of test assembly (i.e. the base plates and specimen) into the OT chamber at 25 ± 0.5°C for 4 hours before the initiation of the test. The test was conducted using an asphalt pavement performance tester (AMPT) retrofitted with an OT jig. In the AMPT, the OT test involved the application of a constant displacement of 0.65-mm. by moving one of the plates on which a sample is glued. The load required to pull the sample the required displacement is also recorded for each pass and the percent reduction in this load per loading cycle is recorded. The test it typically terminated when a 93% reduction of the initial load (i.e. the specimen failed) or 1200 loading cycles were achieved. The 9.5 ME Superpave and the stone matrix asphalt mixtures were compacted at 7.0 ± 0.5 % air voids while the specimen of the NJ HPTO mix and the BRIC mix were compacted at 5.5 ± 0.5 % air voids and 3.5 ± 0.5 % air voids respectively.

Figure 4 below presents the results of the overlay tests performed on all overlay mixes evaluated in this study. From this figure, it can be observed that the average load reduction of all the laboratory produced overlay mixes met the required maximum load reduction of 93% at the 1200th load cycle of the OT tester as specified by the NJDOT-B10 standards. The results presented in this figure indicate that the SMA mix had the highest maximum load reduction at the end of the 1200th cycle (~87 %). This was followed by the control and BRIC mixes which had maximum load reductions of approximately 78 % respectively. The New Jersey HPTO mix had the lowest load reduction at the end of the 1200th load cycle (~70%).

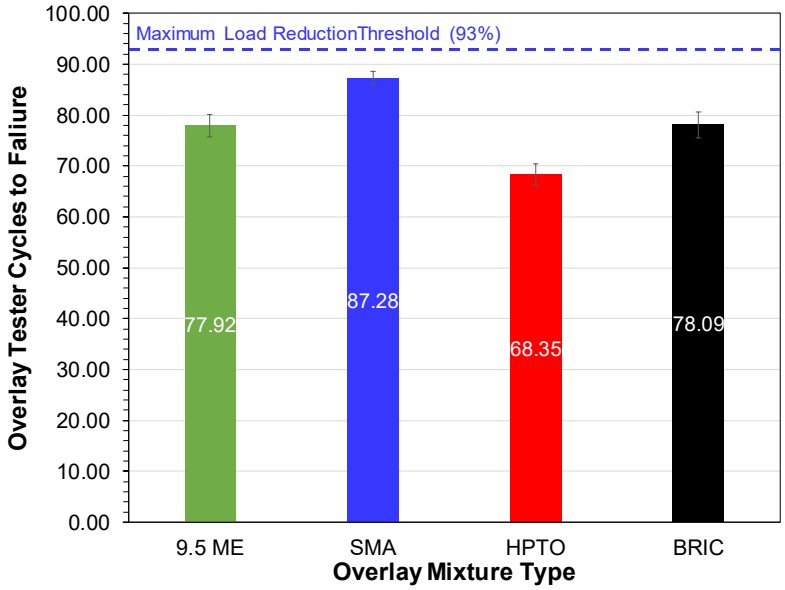

Figure 4. Average Percent Reduction in Initial OT Load after the Application of 1200 Loading Cycles

Moisture Induced Damage Susceptibility (AASHTO T283)

The Modified Lottman Test (AASHTO T283) was used to determine the resistance of compacted asphalt mixtures to moisture induced damage. For this test, six cylindrical specimens; each with a diameter of 6 in. and a height of 3.75-in. were prepared from each of the HMA overlay mixes. The 9.5 ME Superpave and the stone matrix asphalt mixtures were compacted at 7.0 ± 0.5 % air voids while the specimen of the NJ HPTO mix and the BRIC mix were compacted at 5.5 ± 0.5 % air voids and 3.5 ± 0.5 % air voids respectively. These air voids were similar to NJDOT's air voids specifications for the APA and OT tests. Three of the six specimens were kept without conditioning at 25^{o}C, while the other three specimen were conditioned. The conditioning involved partially water saturating the samples then subjecting them to a freeze and thaw cycle (i.e., in a freezer at -18 ± 3^{o}C for 16 hours and subsequently placed in a water bath at 60 ± 1^{o}C for 24 hours). All the samples (i.e. conditioned and unconditioned) were then broken diametrically using a specialized fixture at 77^{o}F and using a loading rate of 50 mm/min.

Figure 5a shows that the tensile strength ratio (TSR) for all mixes tested and Figure 5b presents the peak loads required to break both unconditioned and conditioned samples for all four HMA overlay mixes. As can be seen from Figure 5a, the SMA, HPTO mixes had TSR values well above the 80% threshold. The BRIC had a TSR value slightly lower than 80% while the control mix (9.5ME) had the lowest TSR value. In terms of moisture induced damage susceptibility, these observations indicate that the control mix was the most susceptible, followed by BRIC and with SMA and HPTO being the least susceptible. It is noted that NJDOT does not require this test for the approval of specialty mixes (i.e., SMA, HPTO, and BRIC). Nonetheless, all these specialty mixes had met the typical 80% TSR value specified by the Superpave mix design.

In addition, by comparing the condition and unconditioned peak loads for all mixtures (Figure 5b), one can evaluate the extent of moisture susceptibility of these mixtures. As can be seen from Figure 5b, the difference in peak loads between condition and unconditioned samples for the control mix was the highest followed by the same difference for the BRIC mix. Figure 5b also shows that the difference in peak loads (condition and unconditioned) for SMA and HPTO mixes were relatively similar. These observations indicate that the control mix is the most susceptible to moisture induced damaged followed by BRIC and to a lower degree the SMA and HPTO mixes.

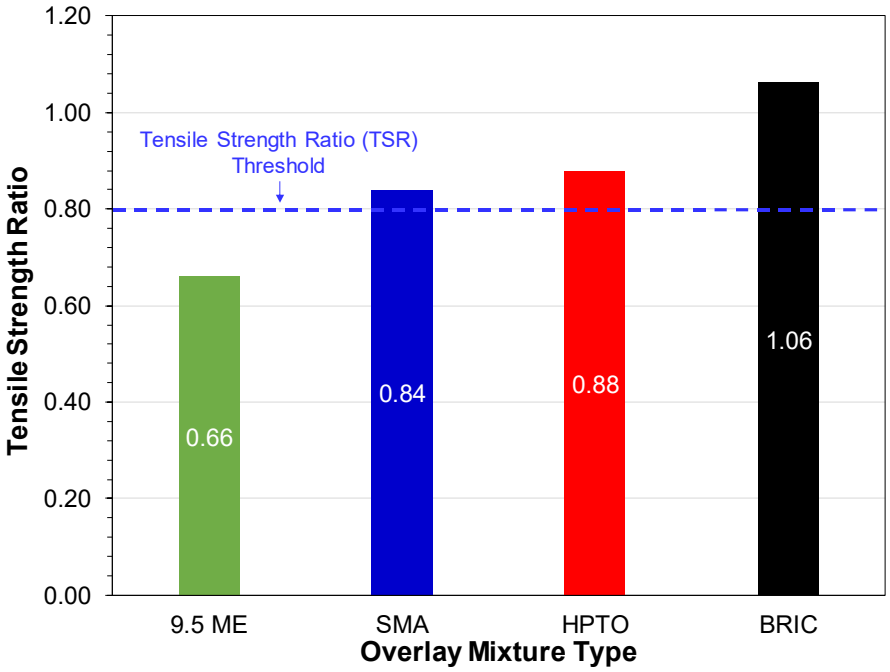

(a)

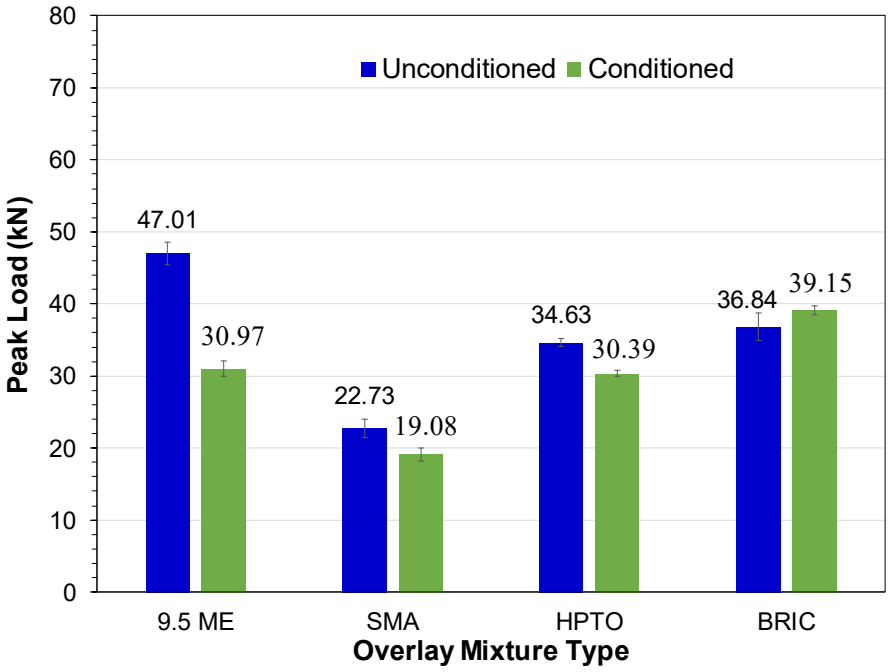

(b)

Figure 5. Modified Lottman Test Results; (a) Average Tensile Strength Ratio (TSR) and (b) Average Peak Loads

CONSTRUCTION OF FIELD SECTIONS

A total of six full scale, composite pavement field sections were evaluated in this study. These pavement sections were 30-ft. long and 12-ft. wide as shown in Figure 6. All six field sections contained a similar substructure (i.e. base, subbase, and subgrade). Each section had an 8-in. thick Portland cement concrete (PCC) base, 16-in thick New Jersey I-3 (A-1-a) granular subbase, and a 12-in. thick compacted natural soil subgrade. The differences between the sections came from the hot mix asphalt (HMA) overlay placed over the PCC layer. That is, for Section 1, a 3-in. thick 9.5-mm Superpave mix was used, for Section 2, a 3-in thick Stone Matrix Asphalt (SMA) mix was used, and for Section 3 a 2-in. thick New Jersey High Performance Thin Overlay (NJHPTO) was used. With respect to sections 3 through 6, a combination of HMA mixes were used in the overlays. For instance, the overlay in Section 4 consisted of a 2-in. thick 9.5-mm Superpave mix placed on top of a 1-in. thick BRIC mix, the overlay in Section 5 contained a 2-in. (50.8 mm) thick SMA mix placed on top of a 1-in. thick BRIC mix, and the overlay in Section 6 was comprised of a 2-in. NJHPTO mix placed on top of a 1-in. thick BRIC mix.

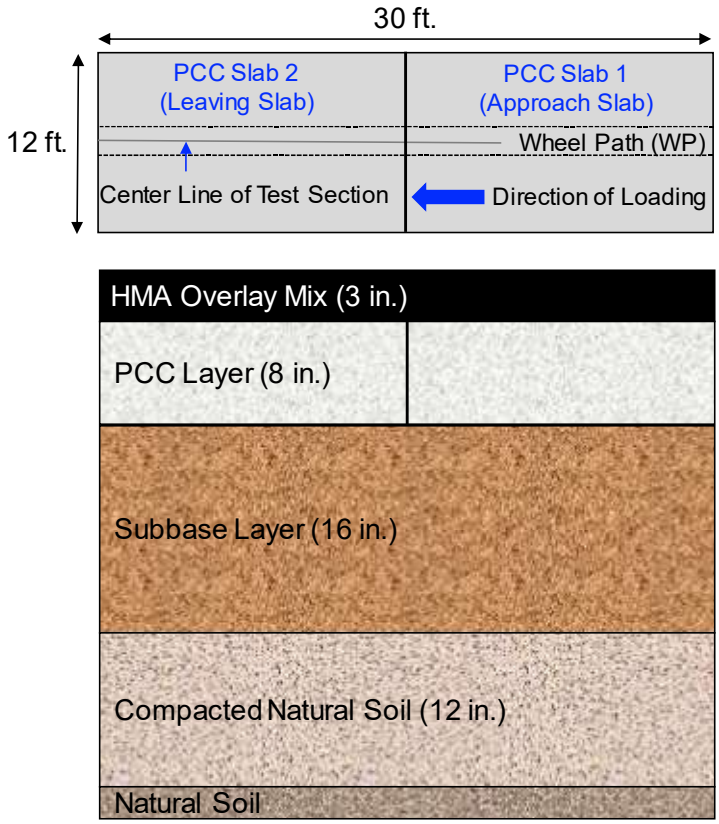

Figure 6. Overall layout of test sections evaluated in this study

The construction of the six full scale field sections was conducted in several phases. These phase included: (1) the subgrade and subbase layer preparation, (2) instrumentation of the field sections with embedded sensors, (3) placement and subsequent milling of the asphalt layer constructed for the commissioning of the Rowan University APTF, (4) installation the of the Portland cement concrete (PCC) slabs (i.e.

rigid layer), and (5) placement of the HMA overlays evaluated in this study. The construction of the field sections began with the compaction of 12-in. (304.8-mm) of natural soil as illustrated in Figure 7(a). This was then followed by the placement and compaction of 8-in. (203.2-mm) of New Jersey I-3 granular subbase material Figure 7(b). Following this step, temperature sensors (i.e. thermocouples), pressure cells, and soil compression gauges were embedded in the 8 in. (203.2-mm), I-3 layer in each field section. A second 8 in. (203.2-mm) layer of NJ I-3 soil was then placed and compacted over the existing 8 in. (203.2-mm), NJ I-3 layer. An 11 in. (279.4-mm) asphalt layer was then constructed on top the I-3 subbase material for the commissioning of the Rowan University APTF. After the commissioning of the test facility, the asphalt layer was milled at the predetermined locations of the test sections in preparation for test section construction. Two 15-ft. (4.5-m) long by 12-ft. (3.65-m) wide PCC slabs were then placed over the milled surfaces in each test section and the overlays were subsequently constructed on top of the PCC slabs after PCC slabs fully cured (i.e. 28 days after PCC slab placement). During the construction of the overlays in each test section, two asphalt strain gauges and three T-type thermocouples were embedded in the HMA overlay layer. The detailed construction procedure utilized for the PCC slabs and HMA overlays is detailed in the following subsections.

Construction of the Portland Cement Concrete Slabs in the Test Sections

As was previously mentioned, the construction of the PCC slabs (i.e. rigid layer) was preceded by the milling of an 11-in. (279.4-mm) asphalt layer that was placed over the New Jersey I-3, subbase layer for the commissioning of the Rowan University APTF. As such, the construction procedure for the PCC slabs began with initial preparation of the milled surfaces. This preparation involved adding granular material in areas where I-3 material was removed during the milling process (i.e. leveling the milled surface) and smoothening the milled surface using a vibratory compactor (Figure 7(f)). Two 15-ft. (4.5-m) long by 12-ft. (3.65-m) wide wooden forms were then staked into the I-3 subbase layer in each test section. The interface between the wooden forms were separated by a 1 in. (25.4-mm) fiber impregnated spacer. Cement mix was then poured into each form via concrete mixer as shown in Figure 7(g). A total of six concrete mixers were used during the construction of the PCC slabs. Before the cement mix in each form was consolidated and finished, cement samples were taken for quality assurance testing. It is noted that cement samples from each of the six concrete mixers were taken for quality control testing. After the samples were obtained, the cement mixes in each wooden form were consolidated and finished using bull and hand-held floats as illustrated in Figure 7(h). The concrete slabs were then covered and left to cure for 30 days in the wooden forms.

(a)

(b)

(c)

(d)

(e)

(f)

(g) (h) (i)

(j) (k) (l)

Figure 7.Overall construction of the test sections evaluated in this study

Quality assurance testing was performed on 27 cement samples obtained during PCC slab construction. This testing involved evaluating the compressive strength of the concrete samples after 7 days, 14 days, and 28 days respectively. A total of seven cylindrical specimen were evaluated after 7 days, seven specimen after 14 days, and thirteen after 28 days. The results of the quality assurance testing is shown in Figure 8. From this figure it can be observed that the average compressive strength of the concrete specimen progressively increased during each 7 day intervals as expected. It is noted that the average 28 day compressive strength of the concrete samples was 4403 psi; which exceeded the specified 3700 psi minimum 28 day compressive strength NJDOT requirement.

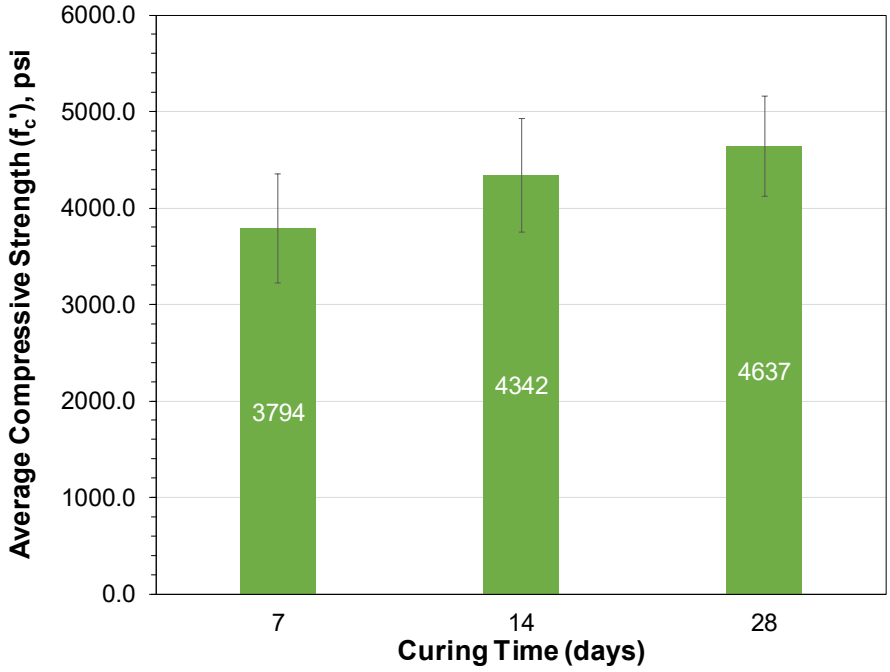

Figure 8. Results of quality assurance testing performed on cement samples

Construction of the HMA Overlays in the Test Sections

The construction of the HMA overlays in each test section was conducted in accordance to NJDOT standards by a contactor approved by NJDOT. The construction process for the overlays began with the installation of two asphalt strain gauges on top of a 0.5-in. (12.7-mm) thick HMA bed and three T-type thermocouples at 0.5-in intervals (starting from the top of the PCC slabs). A detailed installation procedure for the asphalt strain gauges and T-type thermocouples is provided in the following chapter). After the sensors were installed, a tack coat was then applied on top the PCC slabs. In preparation for the placement of the asphalt overlays. The plant-produced HMA overlays were then placed over the PCC slabs in each test section using a paver as shown in Figure 7(j). Following the placement of the HMA by the paver, the HMA was spread evenly across the width of the test section using shovels and lutes Figure 7(k). The HMA was then compacted using a steel tired, vibratory roller. Field densities were then measured at ten random locations

on each test section using a nuclear density gauge to ensure that the compaction quality of the overlays was sufficient. The results of the field density verification testing on each test section is presented in Table 2.

Table 2 – Average Field Density obtained for Overlays in each Test Section

Test Section	Average Rice Number (%)
1 (9.5 ME)	93.5
2 (SMA)	94.2
3 (HPTO)	95.2
4 (9.5 ME and BRIC)	92.7
5 (SMA and BRIC)	93.2
5 (HPTO and BRIC)	95.4

HMA Overlay Quality Acceptance Testing

Prior to construction of the overlays, HMA mixture samples were taken from the trucks that transported the mixes to Rowan University APTF at the asphalt plant of the contractor. These samples were obtained in order to perform quality acceptance testing on the HMA mixes. The quality acceptance testing in this study consisted of three performance tests which were conducted evaluate the rutting, fatigue cracking and moisture induced damage susceptibility of the overlay mixes. The quality acceptance testing involved the following laboratory tests: the APA test, the OT test, and the Modified Lottman Test. The results of the quality acceptance testing is presented in the following subsections.

Rutting Performance (APA Results)

The results of the APA tests conducted on all HMA overlay mixtures are presented in Figure 9. As can be observed from the figure, the 9.5 ME Superpave, SMA, New Jersey HPTO, and BRIC mixes at the end of 8000 cycles were 0.8-mm, 1.9-mm, 2.0-mm and 0.6-mm respectively. These rutting values all met the maximum rutting requirements specified by NJDOT for each HMA mixture. Therefore, all the plant produced mixes were approved with respect to rutting.

By comparing the APA results (Figure 3) for all mixes, the relative rutting performance of these mixes can be evaluated. As illustrated in Figure 3, the APA rut depths for the SMA and the New Jersey HPTO mixes had a similar average rut depth (~2-mm) at the end of 8000 cycles. The 9.5 ME (control mix) had the next highest average rut depth after 8000 cycles followed by the BRIC mix; which had the lowest average sample rut depth of all the overlay mixes. This trend indicated that the in place HPTO mix had a similar susceptibility to rutting as the SMA mix. The observed trends also indicate that the 9.5 ME (control mix) and BRIC mixture had a higher susceptibility to rutting than the HPTO and BRIC overlay mixes.

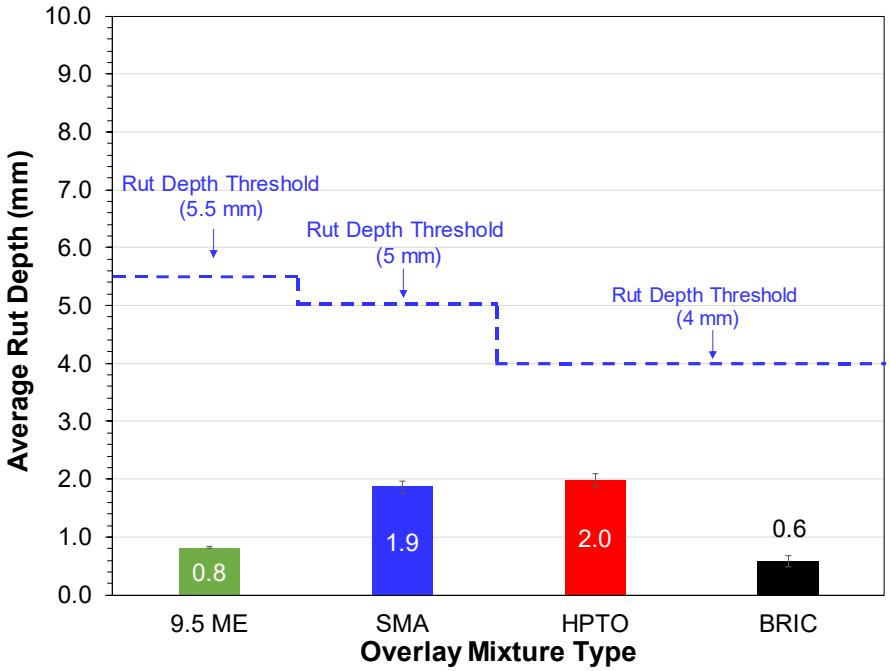

Figure 9. Average sample rut depth of laboratory produced and plant-produced overlay mixes after 8000 cycles of APA

Fatigue/Reflective Cracking Performance (OT Results)

Figure 10 below presents the results of the overlay tests performed on all overlay mixes during quality acceptance testing. From this figure, it can be observed that the average number of cycles to failure of the SMA, HPTO, and BRIC mixes were 150, 1034, and 2140 loading cycles respectively. These results suggested that the in place SMA overlay mix may be the most susceptible to reflective cracking during accelerated pavement testing. The results also implied that the HMA mix with the next highest reflective cracking susceptibility during accelerated pavement testing was the HPTO mix followed by the BRIC mix.

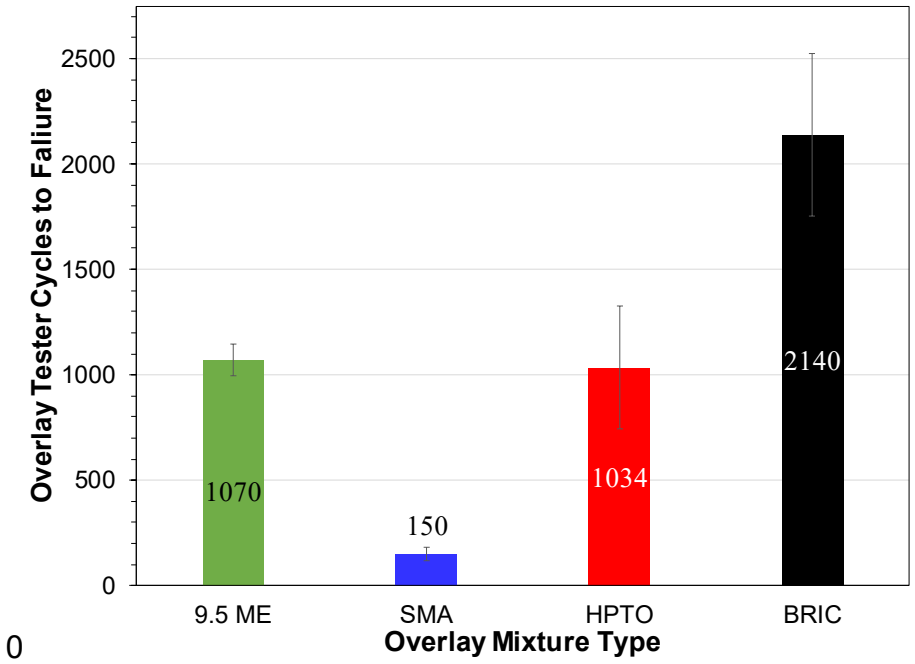

Figure 10. Average Number over Overlay Tester Cycles to Failure.

Moisture Induced Damage Susceptibility (AASHTO T283)

Figure 11a shows that the tensile strength ratio (TSR) for all mixes tested and Figure 11b presents the peak loads required to break both unconditioned and conditioned samples for all four HMA overlay mixes. As can be seen from Figure 5a, only the in place HPTO mix had a TSR value above the 80% threshold while the in place 9.5 ME (control mix), SMA and BRIC mixes all had TSR values lower than 80%. The SMA mix had the next highest TSR value after the HPTO mix, followed by the BRIC and 9.5 ME (control mix). It is noted that NJDOT does not require this test for the approval of specialty mixes (i.e., SMA, HPTO, and BRIC). Additionally, since this study was primarily concerned with the impact of loading on pavement performance as opposed to moisture induced damage all the mixtures were approved. The results in regard to the moisture induced damage susceptibility of the in place mixes indicated that the control mix was the most susceptible, followed by BRIC and with SMA and HPTO being the least susceptible.

The extent of moisture susceptibility of the in place mixes were also evaluated during quality acceptance testing by comparing the condition and unconditioned peak loads for all mixtures (Figure 11b). As can be observed from Figure 11b, the difference in peak loads between condition and unconditioned samples for the control mix was the highest followed by SMA and BRIC mixes; which had a similar difference, and the HPTO mix; which had the least difference between conditioned and unconditioned samples. These observations indicate that the control mix is the most susceptible to moisture induced damaged during accelerated pavement testing followed by the SMA and BRIC mixes. The results also confirmed that the in place HPTO mix had the lowest susceptibility to moisture induced damage.

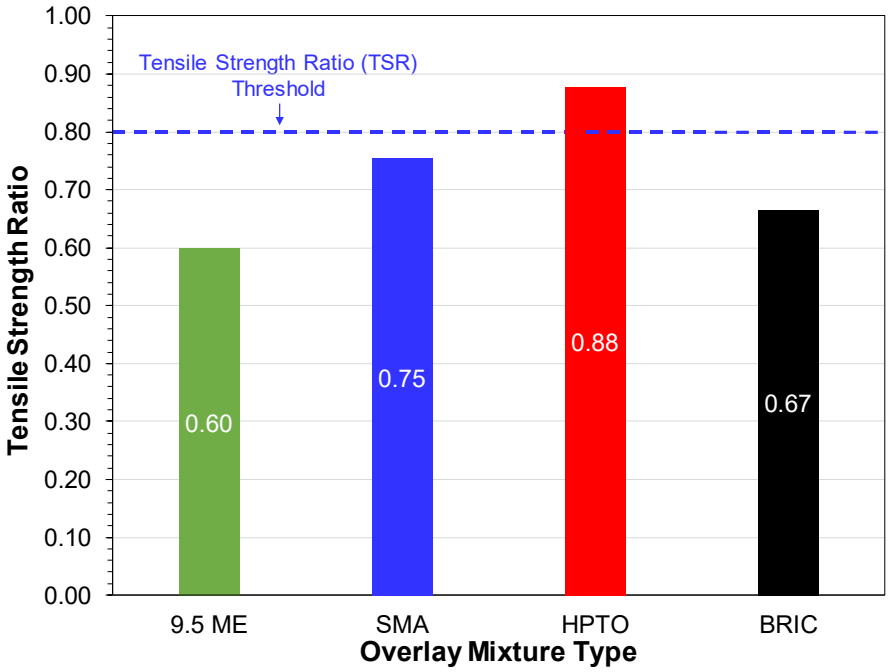

(a)

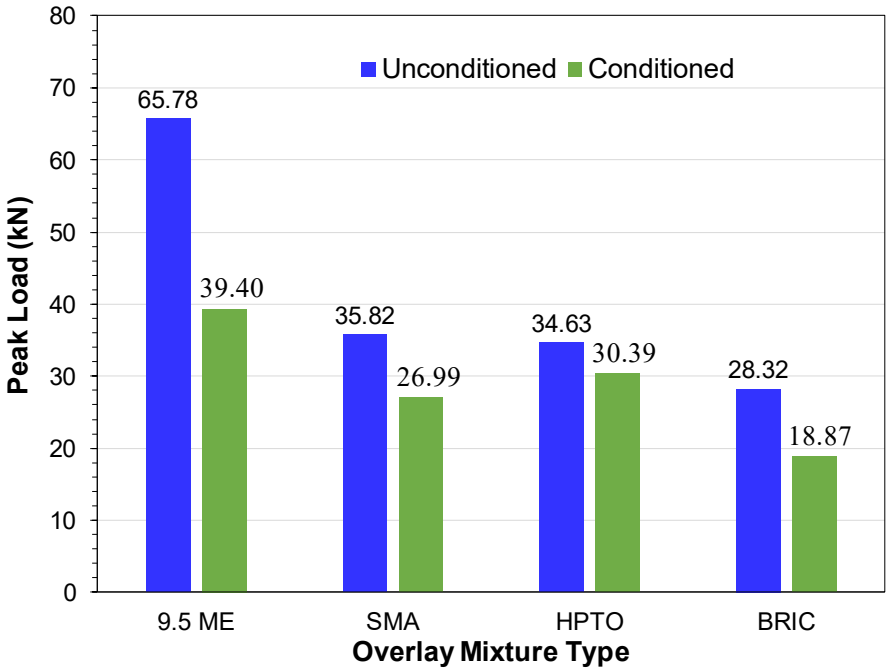

(b)

Figure 11. Modified Lottman Test Results; (a) Average Tensile Strength Ratio (TSR) and (b) Average Peak Loads

INSTRUMENTATION OF FIELD SECTIONS

This chapter presents the steps taken to instrument all six full-scale pavement sections discussed in the previous chapter. The goal of instrumenting the sections was to obtain insights on how the materials behaved under the application of full-scale loading (discussed in the following chapter). In particular, sensors were installed within each pavement section in order to achieve the following objectives:

- Measure the tensile strains at the bottom of the HMA overlay layers. Tensile strains at the bottom of HMA layers are directly related to their fatigue life; thus, such measurements facilitate the estimation of the fatigue life of thin asphalt overlays;
- Measure the increase or decrease in the gap between the two PCC slabs within a sections (i.e., horizontal joint opening or closing). Similar to tensile strains, having an opening (or crack) underneath the pavement may increase the deterioration of overlays (increased potential for reflective cracking); thus, having joint opening/closing measurements are essentials for quantifying effect, if any;
- Measure the vertical movements of the two PCC slabs in a section and determine the relative vertical displacement between these two slabs. Such information will in determining the effect of vertical joint movements on the life of thin asphalt overlays;
- Monitor the temperature within the pavement structure (especially in HMA overlays). This is essential to ensuring that all sections are tested at relatively similar temperatures; and,
- Measure the stresses, due to applied full-scale loading, at the same depth within all sections. Such measurements will be valuable to estimating the rate of deterioration in the structural integrity of the sections.

Figure 12 presents the instrumentation plan prepared to fulfill the objectives above. As can be seen from this figure, for each of the six sections, two asphalt strain gauges (ASGs) were placed at the bottom of the HMA overlay layer (i.e., total 12 for all six sections). For horizontal joint movements, two Linear Variable Differential Transducers (LVDTs) were utilized (Figure 12) while for the vertical joint movement two Soil Compression Gauges (SCGs). Figure 12 also shows that the stresses at the in the unbound base layer (I-3 aggregates) were measured using one pressure cell for each section (i.e., a total of six pressure cells installed). The installation procedure for the employed sensors is presented in the follow subsections.

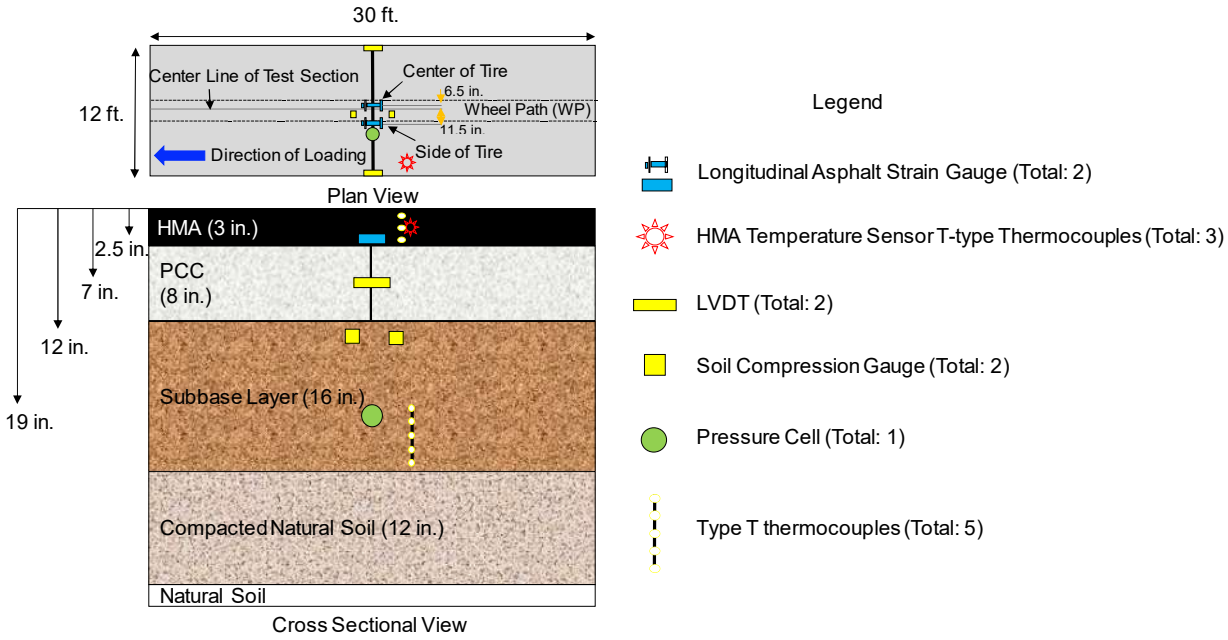

Figure 12. Plan for Instrumenting All Six Thin Asphalt Overlay Sections

Asphalt Strain Gauges (ASG) Installation Procedure

Asphalt Strain Gauges (or H-type gauges) are typically used to simultaneously measure longitudinal and transverse strains in asphalt pavement layers. A typical H-type gauge consists of an electrical resistance strain gauge embedded within a strip of glass-fiber reinforced epoxy with transverse stainless steel anchors at each end of the strip to form an H-type shape (Figure 13). These gauges are typically manufactured using a strip stiffness that is approximately the same as HMA stiffness Gokhale (2009) [23]. In addition, ASGs are designed especially to withstand the high temperature and loads associated with pavement construction. The step by step procedure employed for installing these sensors in all six sections at CREATEs is presented as follows:

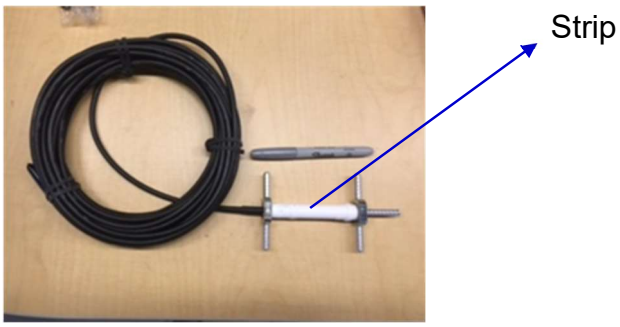

Figure 13. Picture of an Asphalt Strain Gauge (H-type)

- Step 1: Check if ASGs are working properly: ASGs were tested prior to installation in the test sections. The initial voltage readings were recorded to ensure that the sensors are working properly (i.e., responding to applied pulling action or tensile force);
- Step 2: Prepare placement location: the predetermined locations of the ASGs were carefully marked in reference to sides and center of the slabs in each section. Figure 14 shows that one of the ASGs in each test section is under the right tire of the wheel; whereas, the other one is on the side of the left tire of the wheel. The sections were prepared to receive the ASGs by first saw cut trenches in which the ASG cords will be placed (Figure 15a). These trenches were important to prevent damage to the cords due to paving operations;
- Step 3: Apply tack coat: the asphalt emulsion utilized as a tack coat for bonding the PCC slabs to the HMA overlays was sprayed at the locations where the ASGs were to be placed. A 12.5-mm (0.5-in.) bed of loose HMA was then manually compacted using a tamping rod (Figure 15b);
- Step 4: Place ASGs and cover with hand compacted HMA mix: the ASGs were placed at the desired locations and were covered by a layer of loose HMA mix (Figure 15c). The loose mix was then manually compacted to a height less than the thickness of the pavement layer;
- Step 5: Obtain GPS coordinates of ASGs' locations: the ASGs' were located using a Global Positioning System (GPS) device; and,
- Step 6: Place HMA overlay using paver and compact: a paver was utilized to place the HMA overlay mixes after placing the ASGs. A roller was then utilized to compact the HMA overlays to NJDOT acceptable field density levels. Paint marks were applied on top of the paved surface after placement to mark the locations of the ASGs (Figure 15d).

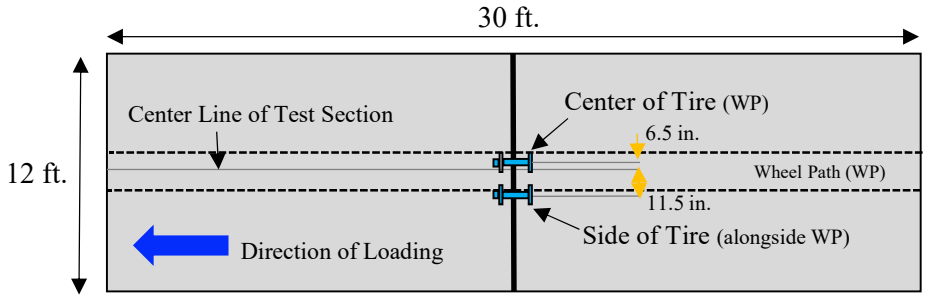

Figure 14. Location of H-type asphalt strain gauges in the test sections

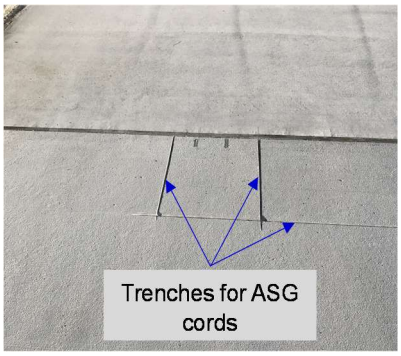

(a)Step 2

(b)Step 3

(c)Step 4

(d)Step 6

Figure 15. Asphalt strain gauge installation procedure

Temperature Sensor Installation Procedure in HMA Overlays

Thermocouples were utilized as temperature sensors in the HMA layer of the test sections because of their ability to measure a wide range of temperatures, ease of installation, and cost effectiveness. The type of thermocouples installed in the HMA overlays were T-type thermocouples. T-type thermocouples consist of two dissimilar metal wires (i.e. copper and constantan wires) welded together at one end to create a junction. Typically, when this junction experiences a change in temperature, an electrical voltage is generated. This electrical signal can then be converted to temperature measurements using reference tables or a digital thermometer. The step by step procedure employed for installing the thermocouple wires in HMA layer of all six sections at CREATEs is presented as follows:

- Step 1: Cut thermocouple wires to required length and pair corresponding thermocouple wires: The copper and constantan thermocouple wires were measured and cut at intervals of 8-ft. The respective copper and constantan wires were then labeled numerically in ascending order, and the paired according to their labels (i.e. 1-1, 2-2, etc). This step was critical because in correct pairing (i.e. pairing similar wires) would lead to erratic temperature measurements. ASGs were tested prior to installation in the test sections. The initial voltage readings were recorded to ensure that the sensors are working properly (i.e., responding to applied pulling action or tensile force);

- Step 2: Check if thermocouple wire pairs are working properly: The copper and constantan thermocouple wire pairs were inserted into a digital thermometer and it was verified whether the temperature readings fell within the 75°F to 80°F range (Figure 16). This is because the verification process was conducted at room temperature;
- Step 3: Connect the thermocouple wire pairs at one end: Quick tip connectors were used to connect the copper and constantan wire pairs. Shrink tubing was then placed over the Quick tips connectors and heat was applied to the shrink tubing in order to hold the quick tip connections in place and seal the end of the thermocouple where the wires were connected;
- Step 4: Place thermocouples and cover with hand compacted HMA mix: A total of three thermocouples were embedded in the HMA overlay on each test section. In each test section, the first thermocouple was placed directly on the PCC slab at the desired location and loose HMA was placed over the installed thermocouple. The loose HMA was then compacted by hand to a height of 1.5-in. The second thermocouple was then placed on top of the compacted HMA (Figure 16a). Additional loose HMA was placed over the second thermocouple and mound of HMA was compacted to a height of 2.5-in (Figure 16b and c). The third thermocouple was placed over the 2.5-in. mound of compacted HMA and was subsequently covered with loose HMA. This loose HMA was compacted until the thickness of the HMA mound was 3-in.

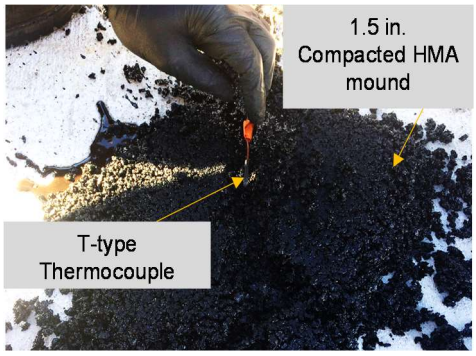

(a)

(b)

(c)

Figure 16. HMA overlay temperature sensor installation procedure: (a) placement of thermocouple on 1.5 in HMA bed; (b) compaction of loose HMA; (c) 2.5 in mound of compacted HMA

LVDT Mounting Procedure

Linear variable displacement transformers (LVDTs), as its name suggests, are electrical transformers used to measure the displacements or position. The type of LVDT utilized in the test sections during accelerated pavement testing were Macro Sensors GHS 750-100 sensors. These LVDTs consisted of a spring loaded probe shaft that was connected to the 0.75-in. diameter stainless steel core (Figure 17). The range of the LVDTs was 1 in. and the maximum linearity of the sensors were -0.038%. Two LVDTs were mounted on either side of each test section (Figure 18a) in order to measure the joint opening/closing between the two PCC slabs during accelerated pavement testing.

Figure 17. Picture of a Macro Sensor GHS 750-100 LVDT

To mount the LVDTs, two steel bars were inserted into the sides of the concrete slabs on either side of the joint (between the two slabs) at a depth of 4-in. The steel bars were placed into the sides of the slabs during the construction of the slabs (i.e. before the cement mixture hardened). These bars along with mounting blocks (Figure 18b) were utilized to mount the LVDTs and record the horizontal joint movements. The assembly of the steel bars and mounting blocks was then covered by a sealed, prefabricated wooden box in order to protect the LVDTs from moisture damage (Figure 18c). This process was found to be sufficient as the measurements from the LVDTs yielded the expected joint opening and closing responses (per loading cycle).

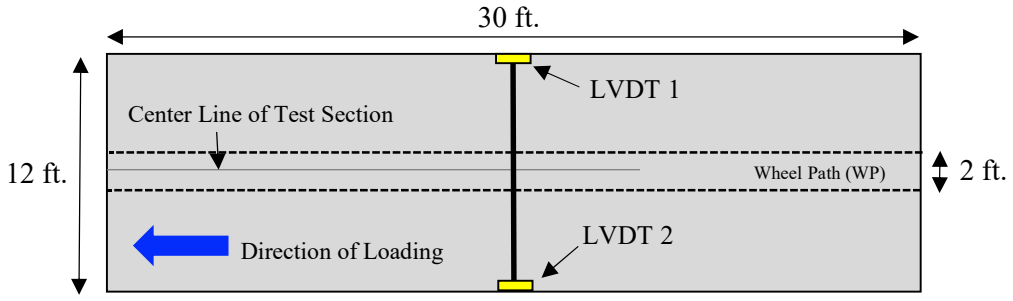

(a)

(b)

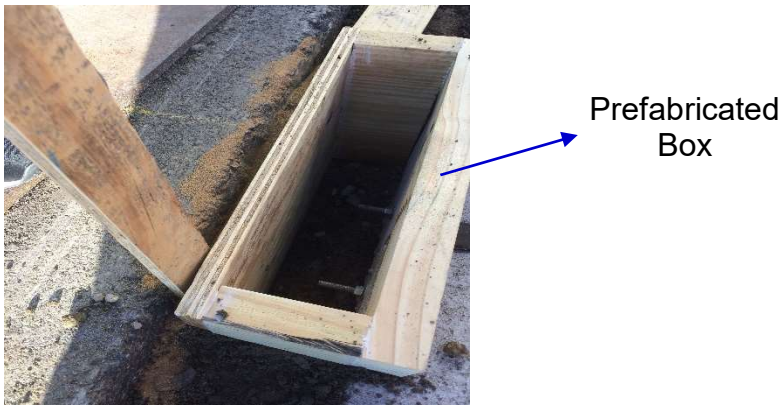

(c)

Figure 18. (a) Location of LVDTs and (b) Steel Bars for Attaching LVDTs to PCC Slabs (c) Prefabricated Wooden Box enclosure to protect LVDTs from moisture damage

Soil Compression Gauges (SCGs) Installation Procedure

Soil compression gauges SCGs are typically used to measure the compression of soil in response to loading at a particular depth within the granular layer(s) of a pavement structure. SCGs generally consist of two disc-shaped plates attached to either side of a cylindrical metal rod. (Figure 19). This cylindrical metal rod houses a sensor that measures the displacement of the plates and converts these measurements into an electrical voltage. The electrical voltage readings can then be translated back to displacement measurements using manufacturer provided calibration factors. It is important to note that SCGs do not contain springs that allow the disc-shaped plates to return to their original position after being compressed. Therefore, SCGs can only measure plastic, or permanent, compression in the soil. In regard to the SCGs utilized in this study, the distance between the disc-shaped plates when the sensor was fully extended was 6-in. and the distance between the plates when the sensor was fully compressed was 5-in. Thus, the SCGs was capable of measuring up to 1-in. of soil

movement (i.e. compression). In each test section, the SCGs were installed approximately 0.5-ft. on either side of the joint at a depth of 16-in. (Figure 20). The step by step procedure employed for installing the SCGs in all six sections at CREATEs is presented as follows:

Figure 19. Image of soil compression gauges utilized in test sections

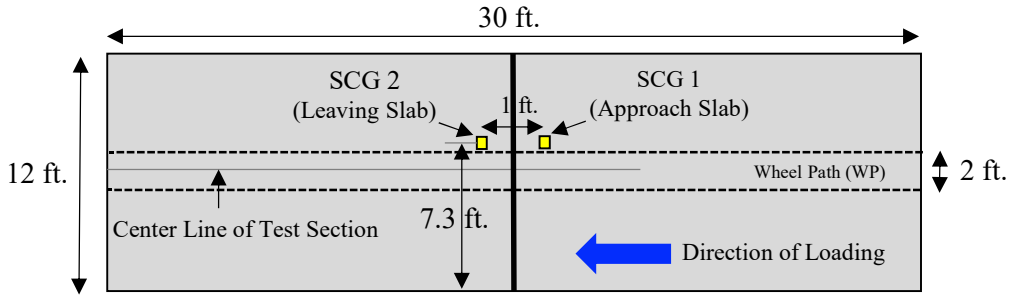

Figure 20. Location of soil compression gauges in test sections

- Step 1: Check if SCGs are working properly and calibrate if necessary: the SCGs were tested in laboratory prior to installation to verify if they were providing correct voltage readings (i.e., within expected ranges). The manufacturer provided calibration sheets which were also verified for the SCGs by applying a small measured displacement and recording the voltage from the sensor. Some SCGs' calibration sheets were found to be inaccurate; thus, new calibration sheets were developed for these sensors;
- Step 2: Dig a trench for placing the SCGs in position: At the desired locations of the SCGs (Figure 21), a 16-in. wide and 11-in. deep trench was prepared to place both SCGs (Figure 21a). The soil bed of trench was leveled using finely sieved soil to prepare the bedding for the compression gauge. A 3-in. wide trench, was also prepared to place the cords of the SCGs;
- Step 3: Compact representative soil around the SCGs: in order to place the SCGs fully extended in the soil, it was necessary compact soil around to be stuffed with finely graded damp soil (<1.2-mm or US 16). A 7.5-cm (3-in.) diameter PVC pipe (half of the pipe was cut) was utilized to facilitate the compaction of soil around the SCGs (Figure 21b). This technique was effective at keeping the SCGs fully extended while being compacted in the trench. Approximately 1500-grams of finely graded damp soil was

compacted around each SCGs when it was within the pipe assembly. Hands and small wooden piece were used for compaction;

- Step 4: Place the SCGs in their final location within the pavement structure: the SCGs placed in the PVC pipe assembly (i.e., with soil compacted around them) were placed in their final location inside the trench. Soil was then compacted around the PVC assembly manually inside the trench. At every 1-in. intervals of compacted soil within the trench, the PVC pipe was pulled out allowing the soil around the SGCs and the SCGs to rest in position. This compaction process was continued until the trench was fully compacted and PVC pipes were extracted (Figure 21c);
- Step 5: Place a layer of loose soil (I-3) to cover the placed SCGs: a layer of loose soil was then placed on top of the placed SCGs (Figure 21d). This layer was compacted using a manual tamper. This layer was necessary to ensure the SCGs survive construction operations (i.e., placement of PCC slabs and HMA overlays); and,
- Step 6: Obtain GPS coordinates of SCGs' locations: the SCGs' were located using a Global Positioning System (GPS) device.

(a)Step 2

(b)Step 3

(c)Step 4

(d)Step 5

Figure 21. Process for Installing the Soil Compression Gauges (SCGs).

Pressure Cells (PCs) Installation Procedure

Pressure Cells (PCs) are used to measure the total pressure in earth fills (i.e. granular layers of pavement structures. They generally consist of two 23-in. diameter stainless steel circular plates welded together around their periphery. The circular plates are

separated by a narrow cavity which is filled with de-aired oil. When the surfaces of the circular plates experience a change in pressure, the plates squeeze together and causes the fluid pressure inside the pressure cell to increase. A vibrating wire pressure transducer then converts this pressure into an electrical signal (voltage). The voltage readings obtained from the pressure cell can then be translated to pressure values using manufacturer supplied conversion factors. The type of pressure cell utilized in the test sections were Geokun 3500 pressure cells (Figure 22a). These pressure cell were capable of measuring changes in earth pressure up to 58-psi. The pressure cells were placed at a depth of 19.5-in. directly below the joint in each test section (Figure 22b). The step by step procedure employed for installing the PCs in all six sections at CREATEs is presented as follows:

(a)

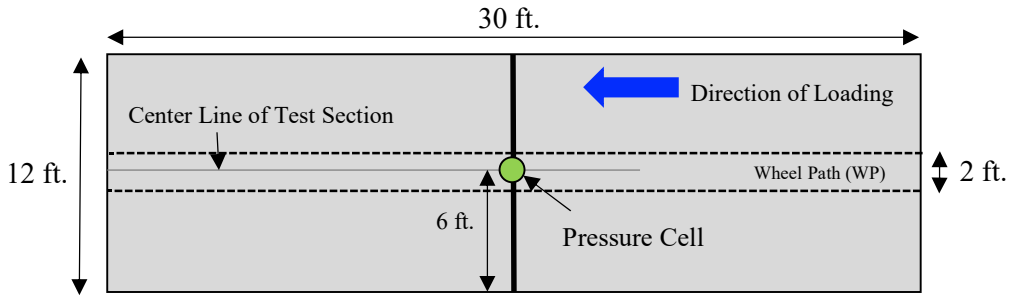

(b)

Figure 22. (a) Image of Geokun 3500 pressure cell (b) Location of pressure cells in test sections

- Step 1: Check if PCs are working properly and calibrate if necessary: the PCs were tested in laboratory prior to installation to verify if they were provided voltage readings when the plates of the PC were loaded;
- Step 2: Dig a trench for placing the PCs in position: At the desired locations of the PCs, a 30-in. wide and 2-in. deep trench was prepared to place the PCs. (Figure 23a). A 3-in wide and 2-in. deep trench was also prepared to place the cords of the PC. The

soil at the base of the two trenches were leveled using finely sieved soil and compacted by hand to prepare a soil bedding for the PCs;

- Step 3: Place the PCs in their final location within the pavement structure: The plates of the PCs were placed on the soil bed in the 30 in. wide trench the wires of the PC were placed in the 3 in. wide trench. In this step, it was verified that the plates of the PCs were levelled (Figure 23b). This was done in order to ensure that the plates experienced an even stress distribution when loading was applied to the test section during APT;
- Step 4: Place a layer of loose soil (I-3) material to cover the installed PCs: A layer of loose soil was placed on top of the placed PCs. This layer was compacted using a manual tamper (Figure 23c). This layer was necessary to ensure the PCs survive construction operations (i.e., placement of second layer of I-3, PCC slabs and HMA overlays); and,
- Step 5: Identifying the locations of the PC in each test section: the PCs were located using a Global Positioning System (GPS) device (Figure 23d).

(a) Step 2

(b) Step 3

(c) Step 4

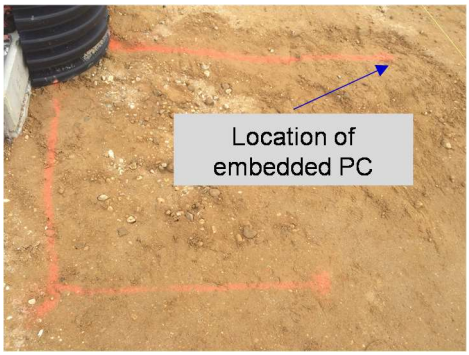

(d) Step 5

Figure 23. Process for installing the pressure cell (PCs)

Temperature Sensor Installation Procedure in I-3 Subbase

A total of 30 T-type thermocouples were utilized to measure the temperature of the I-3 subbase in all the test sections at various depths. The procedure employed to installation the thermocouples in the I-3 subbase layer was provided as follows:

- Step 1: Cut thermocouple wires to required length and pair corresponding thermocouple wires: The copper and constantan thermocouple wires were measured and cut at intervals of 8-ft. The respective copper and constantan wires were then labeled numerically in ascending order, and the paired according to their labels (i.e. 1-1, 2-2, etc). This step was critical because in correct pairing (i.e. pairing similar wires) would lead to erratic temperature measurements. ASGs were tested prior to installation in the test sections. The initial voltage readings were recorded to ensure that the sensors are working properly (i.e., responding to applied pulling action or tensile force);
- Step 2: Check if thermocouple wire pairs are working properly: The copper and constantan thermocouple wire pairs were inserted into a digital thermometer and it was verified whether the temperature readings fell within the 75^{o}F to 80^{o}F range (Figure 24a). This is because the verification process was conducted at room temperature;
- Step 3: Connect the thermocouple wire pairs at one end: Quick tip connectors were used to connect the copper and constantan wire pairs. Shrink tubing was then placed over the Quick tips connectors and heat was applied to the shrink tubing in order to seal and hold the quick tip connections in place and to protect the thermocouple from damage;
- Step 4: Mount thermocouples on wooden dowel at predetermined intervals: Five thermocouple wire pairs were mounted on a 10-in. wooden dowel at 2-in. intervals. To achieve this, the sealed end of the thermocouple wire pairs were tied to the dowel using nylon cable ties (Figure 24b) and the free end of the thermocouple wire pairs was fed through a rubber tubing which had opening on both ends. The mounted thermocouples were labelled numerically on both the mounted and free ends of the thermocouple wire pairs in order to ensure that accurate temperature readings were recorded the desired depths in the subbase;
- Step 5: Dig a trench for placing the thermocouples in position: At the desired locations of the mounted thermocouples in each test section, an 11-in. deep hole was dug in subbase in preparation for embedding the mounted thermocouples. A 3-in wide and 3-in. deep trench was also prepared to place the cords of the thermocouple (i.e. rubber tubing). The soil at the base of the two trenches were leveled using finely sieved soil (< 1.2-mm or US 16) and subsequently compacted using a dowel to prepare a soil bedding for the thermocouples (Figure 24c);
- Step 6: Place the mounted thermocouples in their final location within the pavement structure: The thermocouples were inserted vertically in the trench and the rubber tubing was placed on the compacted soil bed (Figure 24c);
- Step 7: Place a layer of loose soil (I-3) material to cover the installed thermocouples: Loose I-3 soil was used to fill the voids in the dug trenches and cover the

thermocouples. The loose material was then compacted by hand using a manual tamper (Figure 24d);

- Step 5: Identifying the locations of the PC in each test section: the embedded thermocouples were located using a Global Positioning System (GPS) device.

(a) Step 2

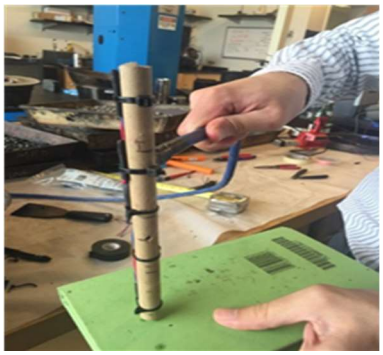

(b) Step 3

(c) Step 4

(d) Step 5

Figure 24. Process for installing the thermocouples in the I-3 subbase layer.

Sensor Installation Summary

Field evaluation of pavement structure through accelerated pavement testing is generally centered on two main objectives: performance comparison pavement treatments, and collection of performance data under controlled environmental and loading conditions for model calibration Harvey (2009). [24] In order to achieve these objectives, appropriate instrumentation and collection of reliable continuous data is necessary. The sensors installation process is one of the most critical stages in field testing because the measurements recorded from installed sensors during testing are used to draw conclusions about the pavement response to loading. Additionally, care should be taken during the sensor installation process because it is not practical to excavate and fix the sensors once they are embedded in test sections. This is due to the fact that artificial fractures will be introduced in the pavement test sections and the results will not be conclusive. It is noted that the protection of sensor cables from water and other construction activities are is also necessary to avoid signal disruption during field testing.

Damage due to any activity, (installation or construction) then the entire purpose of careful application of sensor is jeopardized.

All the sensors embedded in the six test sections at CREATEs were checked after the entire construction process to verify whether they were damage or survived the test section construction. The success of the installation process for each sensor was measured based on a quantity referred to as the sensor survival rate. The sensor survival rate was defined as the ratio of the total number of sensors (of a specific type) that recorded reasonable measurements after test section construction to the total number of sensors (of a specific type) installed in the test section. This ratio was computed for each type of sensor installed in the test sections at CREATEs. The survival rate of each type of sensor is provided in Table 3. From this table it can be seen that all of the thermocouples in the HMA overlay and I-3 subbase were functional after construction. It can also be seen that the LVDTs and Pressure Cells in all test sections worked after construction concluded. In regard to the ASGs and SCGs, both of the ASGs in test section 1 were damaged during the placement of the HMA overlay and one SCG was damaged in test section 4 during installation. Therefore the survival rate of the ASGs and SCGs was 83% and 92% respectively.

Table 3 – Survival rates of Sensors Installed in Test Sections

Sensor Type	Total No. of Sensors	No. of Sensors Failed during Construction	Sensor Survival Rate (%)
Asphalt Strain Gauge (ASG)	12	2	83
Thermocouples (HMA Overlay)	18	0	100
Linear Variable Displacement Transformer (LVDT)	12	0	100
Soil Compression Gauge (SCG)	12	1	92
Pressure Cell	6	0	100
Thermocouples (Subbase)	30	0	100

FIELD EVALUATION PLAN

This chapter presents a detailed description of the field evaluation testing that was performed on the six test sections considered in this study. The field evaluation consisted of three components: (1) heavy weight deflectometer testing, (2) accelerated pavement testing using an HVS, and (3) visual pavement distress evaluation. The details of each component of the field evaluation is provided in the following subsections.

Heavy Weight Deflectometer Testing

Heavy Weight Deflectometer (HWD) testing is a nondestructive test that is used to simulate the deflection of a pavement surface under the action of fast moving traffic. It involves the application of variable loads on the surface of a pavement via a spring loaded plate. Generally, the variable loads are released from set heights and allowed to fall under gravity. The deformation of the pavement due to the applied loads causes a deflection basin to form within the pavement structure. The pavement response to the applied impulse load (i.e., pavement deflections) is measured by velocity transducers or geophones which are placed at specific radial distances from the center of the applied load. The measured deflections are then used to compute the estimated layer stiffness through an ill-posed, iterative process referred to as back-calculation. As such, HWD testing is generally used to determine the structural conditions of pavement layers with time (i.e. the instantaneous and recurring in-situ pavement layer modulus).

In this study, raw pavement deflections obtained from HWD testing were utilized to determine the impact of accelerated pavement testing on the overall structural capacity of the various layers of the full-scale test sections. Raw pavement deflections were used to assess the structural conditions of the test sections as opposed to back-calculated layer moduli because the nature of the pavement structure of the test sections (i.e., 3-in. asphalt layer overlaid on 8-in. rigid pavement layer) made it difficult to perform back-calculation. This is because currently available back-calculation software are limited in terms of their capability to adequately compute reasonable asphalt layer moduli for composite pavement sections when the deflection basin is dominated by a significantly thicker and stiffer rigid layer.

HWD testing was performed immediately before and after HVS testing on each test section. The HWD test locations for each full-scale section evaluated in this study is shown in testing Figure 25. As can be seen from this figure, there were a total of six HWD test locations on each test section. Two of these test locations were evaluated in the direction of accelerated pavement testing (HVS loading) (i.e., TS-1 and TS-2) while the remaining four test locations were evaluated in the opposing direction. HWD tests were conducted in the following sequence: TS-1, followed by TS-2, TS-3, TS-4, TS-5, and TS-6 respectively. This testing sequence was selected in order to easily align the device on testing locations. The selected testing pattern facilitated the maneuvering (or towing) and placement of the HWD at the desired testing position within a short period of time. The arrows shown in Figure 25 indicate the position of the geophones used to measure pavement deflections. Figure 25 also presents a schematic of the HWD trailer configuration along with its dimensions.

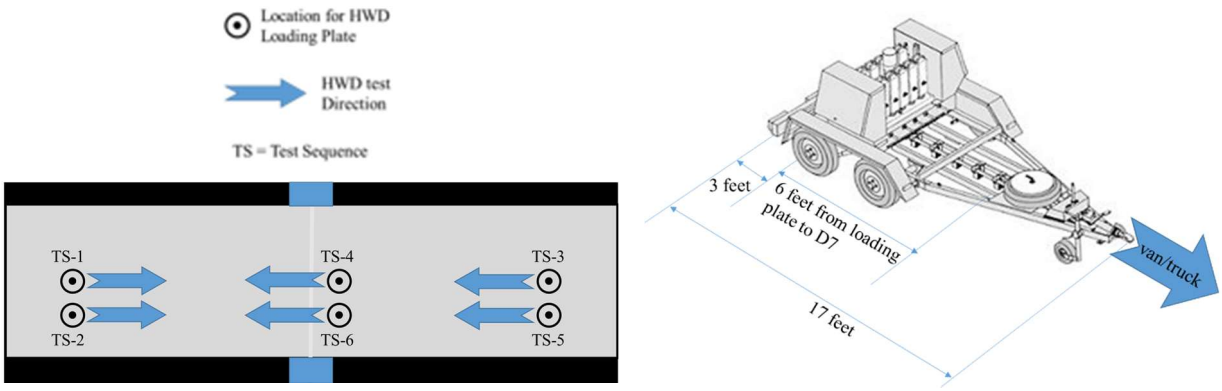

Figure 25. HWD test locations on the full-scale pavement sections

The HWD test points were located in two zones on each section as shown in Figure 26. As can be observed in Figure 26, HWD Test Zone 1 consisted of the region loaded by the HVS while Test Zone 2 consisted of the area outside the HVS loading area. By comparing the HWD results obtained from both test zones, the effect of applied HVS loading on pavement section deterioration was evaluated. A set of seven geophones were utilized to measure the pavement deflections at the various HWD test locations on each full-scale section evaluated in this study. These geophones were spaced at the following intervals from the applied HWD load: 0-in, 8-in, 24-in, 36-in, 48-in., and 72-in respectively. It is noted that the HWD test locations and geophone spacing selected for this study provided a basis for obtaining the structural integrity information at the PCC layer joint and at various locations away from the PCC layer joint in each test section. For instance, when HWD testing was performed at the TS-4 and TS-6 locations sensors, geophones D1 (i.e. geophone located directly under applied load) through D3 (i.e., geophone located 24-in from applied load) captured deflections on one side of the PCC layer joint and the remaining geophones (i.e., D4 through D7) measured deformations on the other side of the joint. The data collected from these locations therefore, provided valuable information regarding the integrity of the joint between the two PCC slabs in the rigid layer on each test section. Similarly, HWD testing conducted on locations TS-1, TS-2, TS-3, and TS-5 provided valuable information with regard to the integrity of the overall pavement structure. The overall HWD test configurations used in this study is presented in Table 4.

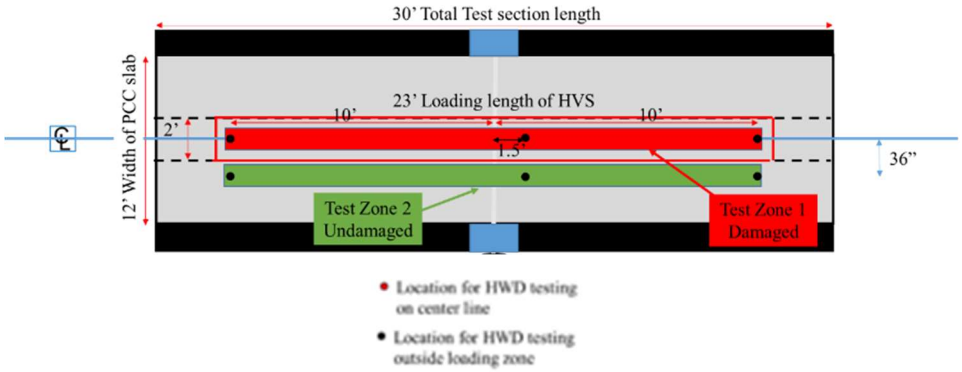

Figure 26. Two zones of HWD testing on each test section.

Table 4 – Test Parameters used during HWD Testing on Test Sections

Parameter		No. of Drops	Stress (psi)	Load (lb)
Load	Seating	4	60	7000
			85	9500
			110	12500
			140	16000
	Drop Height 1	4	60	7000
	Drop Height 2	4	85	9500
	Drop Height 3	4	110	12500
	Drop Height 4	4	140	16000
Loading Plate	Diameter	12 in.		

Heavy Vehicle Simulator Testing

A heavy vehicle simulator is a fully automated electrically powered mobile loading machine that accelerates the deterioration of pavements by simulating several years of traffic in a condensed period of time. All the pavement sections evaluated in this study were subjected to accelerate testing using a heavy vehicle simulator. On each test section, a 60-kN, dual-wheel single axle load (truck tire) was applied in a unidirectional manner at a speed of 5-mph.The tire pressure utilized during HVS testing was 110-psi and the tests were conducted at a temperature of 25ºC. Additionally, each test section was subjected to approximately 200,000 HVS wheel repetitions during accelerated pavement testing.

Pavement response data obtained from embedded sensors in each test section (i.e., asphalt strain gauges, LVDTs, pressure cell, soil compression gauges, and thermocouples) were recorded using a National Instruments cDAQ, data acquisition system. The HVS and embedded sensors were connected to the system in order to simultaneously collect data from the installed sensors and synchronize data collection in relation to the number of HVS wheel repetitions. The measurements collected from the embedded sensors during each HVS wheel pass were captured by the cDAQ at a frequency of 2000 data points per second while the data sampling frequency (i.e. data recorded by the cDAQ) was higher during the initial stages of APT and reduced as HVS loading progressed on each test section. This type of data sampling frequency was selected based on the typical response of pavements to repeated loading; i.e., rapid changes (reduction) in material properties during the initial stages of repeated loading and less variation in stiffness as repeated loading continues. In this study, data was recorded using the following sampling frequency: every of 100 passes between HVS passes 1 and 1000, every 500 passes between HVS passes 1000 and 10,000, every 1000 passes between HVS passes 10,000 and 20,000, every 22,500 passes between HVS passes 20,000 and 50,000, every 10,000 passes between HVS passes 50,000 and 100,000, and every 20,000 between HVS passes 100,000 and 200,000.

Transverse Pavement Profile Evaluation

Transverse pavement profile evaluation is usually conducted to assess the extent of permanent deformation on the surface of pavement sections. In this study, pavement profile evaluation was conducted using a manual laser profilometer as shown in Figure 27. The laser profilometer measured the distance from a reference point on the device to the pavement surface at various points across the pavement width. This measured data was then used to compute an estimate of the permanent deformation on the pavement surface.

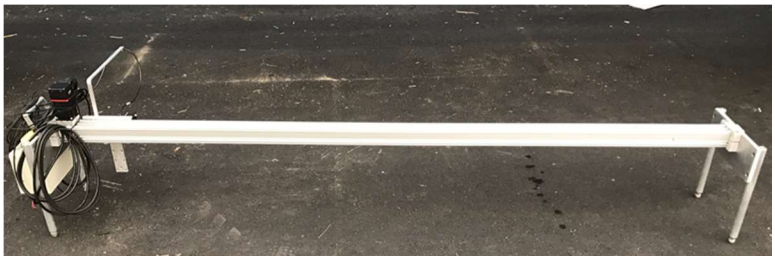

Figure 27. Photograph of manual laser profilometer

Figure 28 illustrates the locations at which pavement profiles were obtained on each test section. As can be seen from this figure, the laser profilometer was utilized to determine the transverse pavement profile at seven different locations on each test section evaluated in this study. Measured data at these seven locations provided comprehensive information related to the field rutting potential of the asphalt overlays evaluated in this study. It is noted that an initial transverse profile evaluation was conducted on each test section before HVS testing and subsequent transverse profile evaluations were performed on a weekly basis (i.e. at intervals of approximately 40,000 HVS loading passes) during accelerated pavement testing. This transverse profile evaluation testing scheme was adopted in order to facilitate establish the extent of rutting on each section and facilitate comparisons between test sections with respect to rutting potential.

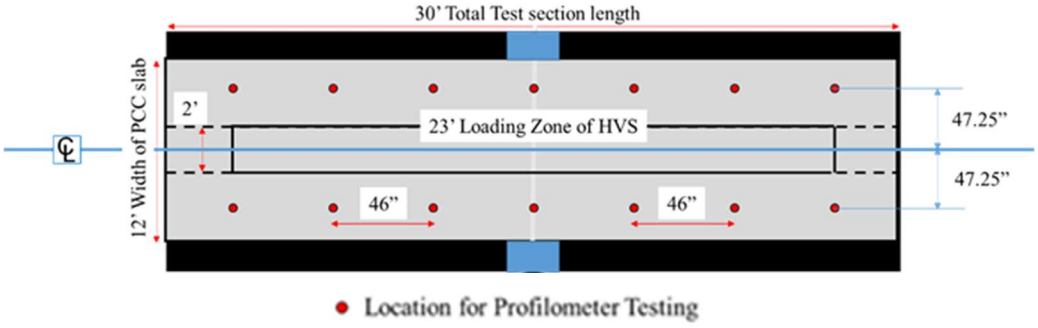

Figure 28. Transverse Profilometer Test Locations on each Test Section

FIELD TESTING RESULTS

Heavy Weight Deflectometer Testing

As was previously mentioned, HWD tests were conducted on all the test sections before and after accelerated pavement testing. This testing scheme for HWD testing was developed as a means of comparing the change in layer stiffness in the respective test sections before and after HVS loading. Figure 30 presents the raw pavement deflection data obtained before and after HWD testing on the six test sections evaluated in this study. As can be observed in this figure the pavement deflections obtained at each test location on all the test sections generally decreased with distance from the applied load. This trend was expected because the deflections recorded by the geophones nearest to the applied HWD load are typically associated with the pavement layers closer to the pavement surface and deflections recorded further from the applied HWD load generally correspond to the lower layers of a pavement system. It can also be observed from Figure 30 that on each test section there was an increase in measured deflections between geophones D2 and D3 (located 8-in. and 16-in. from the applied HWD load respectively) at HWD test locations TS-4 and TS-6. It is noted that this spike in deflections was due to the presence on the discontinuity (i.e. lack of load transfer) at the joint in each test section.

As can be seen in Figure 30, the measured deflections obtained after HVS testing on each test section were noticeably different from those obtained before HVS testing. This difference in measured deflections was more prominent at the HWD test points located near the joint (i.e., TS-4 and TS-6). Since the impact of the joint on the overall performance of the asphalt overlays was a primary concern in this study, the change in deflections recorded at TS-4 and TS-6 before and after HVS testing were used to compare the relative change in structural capacity of the test sections due to accelerated pavement testing. The outer-AREA method was adopted in this study to analyze the measured deflections and draw conclusions about the structural capacity of the test sections. This method hinges on the computation of a deflection basin curvature index (i.e., the *Outer AREA* parameter) that is used together with a composite modulus (E_o) to forward calculate an approximate modulus for the upper, bound layer of a pavement system. [25] The composite modulus represents an overall modulus for the entire pavement system beneath the loading plate while the *Outer AREA* parameter represents a normalized area with respect to one of the measured deflections. Therefore the *Outer AREA* parameter compensates for effect of the magnitude of the applied HWD load. Additionally, the *Outer AREA* ignores the deflections obtained directly under the load because in order to minimize the compression effect in the HMA layer.

The *Outer AREA* parameter is a deflection basin shape factor that is related to the ratio between pavement stiffness and the underlying subgrade stiffness. It is strongly influenced by the thickness of a pavement structure and the stiffness of the materials that make up the structure. Generally, higher *Outer AREA* values indicate higher pavement stiffness or thickness. However it should be noted that temperature also influences the magnitude of the *Outer AREA*. For instance the *Outer* AREA is inversely related to the mid-depth temperature of the asphalt layer within a pavement system. This implies that

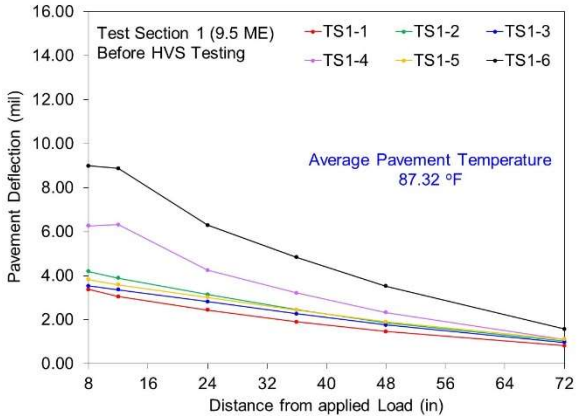
Test Section 1 (9.5 ME)
Before HVS Testing
TS1-1
TS1-2
TS1-3
TS1-4
TS1-5
TS1-6
Average Pavement Temperature
87.32 °F
Pavement Deflection (mil)
Distance from applied Load (in)

(a)

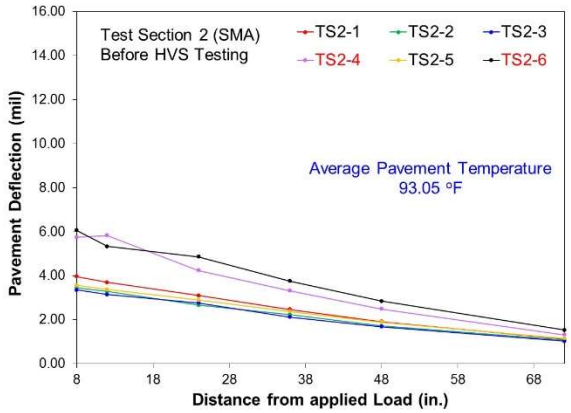
Test Section 2 (SMA)
Before HVS Testing
TS2-1
TS2-2
TS2-3
TS2-4
TS2-5
TS2-6
Average Pavement Temperature
93.05 °F
Pavement Deflection (mil)
Distance from applied Load (in.)

(b)

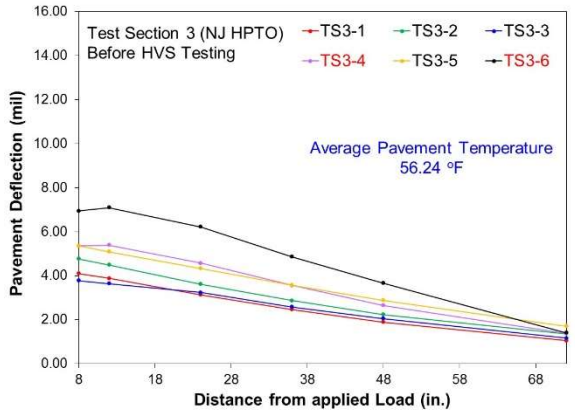
Test Section 3 (NJ HPTO)
Before HVS Testing
TS3-1
TS3-2
TS3-3
TS3-4
TS3-5
TS3-6
Average Pavement Temperature
56.24 °F
Pavement Deflection (mil)
Distance from applied Load (in.)

(c)

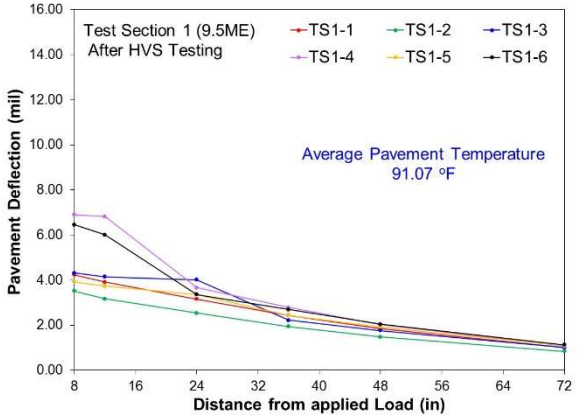
Test Section 1 (9.5ME)
After HVS Testing
TS1-1
TS1-2
TS1-3
TS1-4
TS1-5
TS1-6
Average Pavement Temperature
91.07 °F
Pavement Deflection (mil)
Distance from applied Load (in)

(d)

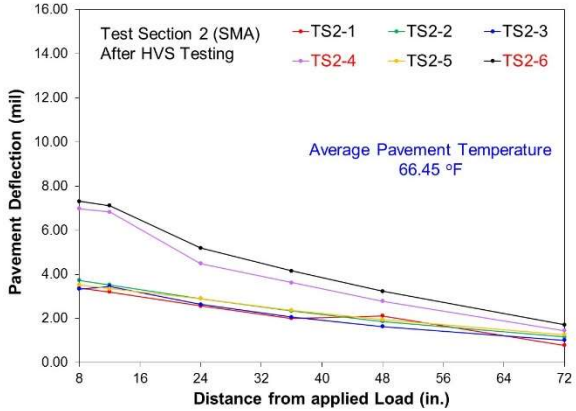
Test Section 2 (SMA)
After HVS Testing
TS2-1
TS2-2
TS2-3
TS2-4
TS2-5
TS2-6
Average Pavement Temperature
66.45 °F
Pavement Deflection (mil)
Distance from applied Load (in.)

(e)

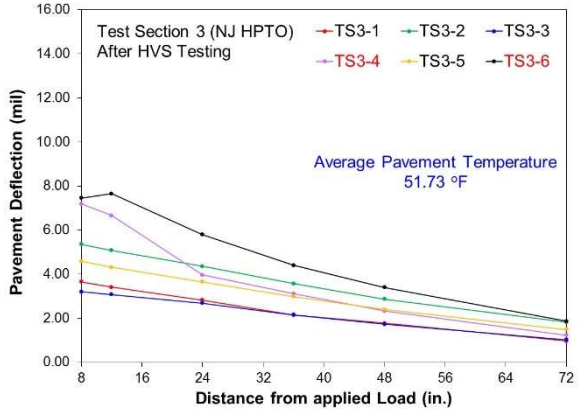
Test Section 3 (NJ HPTO)
After HVS Testing
TS3-1
TS3-2
TS3-3
TS3-4
TS3-5
TS3-6
Average Pavement Temperature
51.73 °F
Pavement Deflection (mil)
Distance from applied Load (in.)

(f)

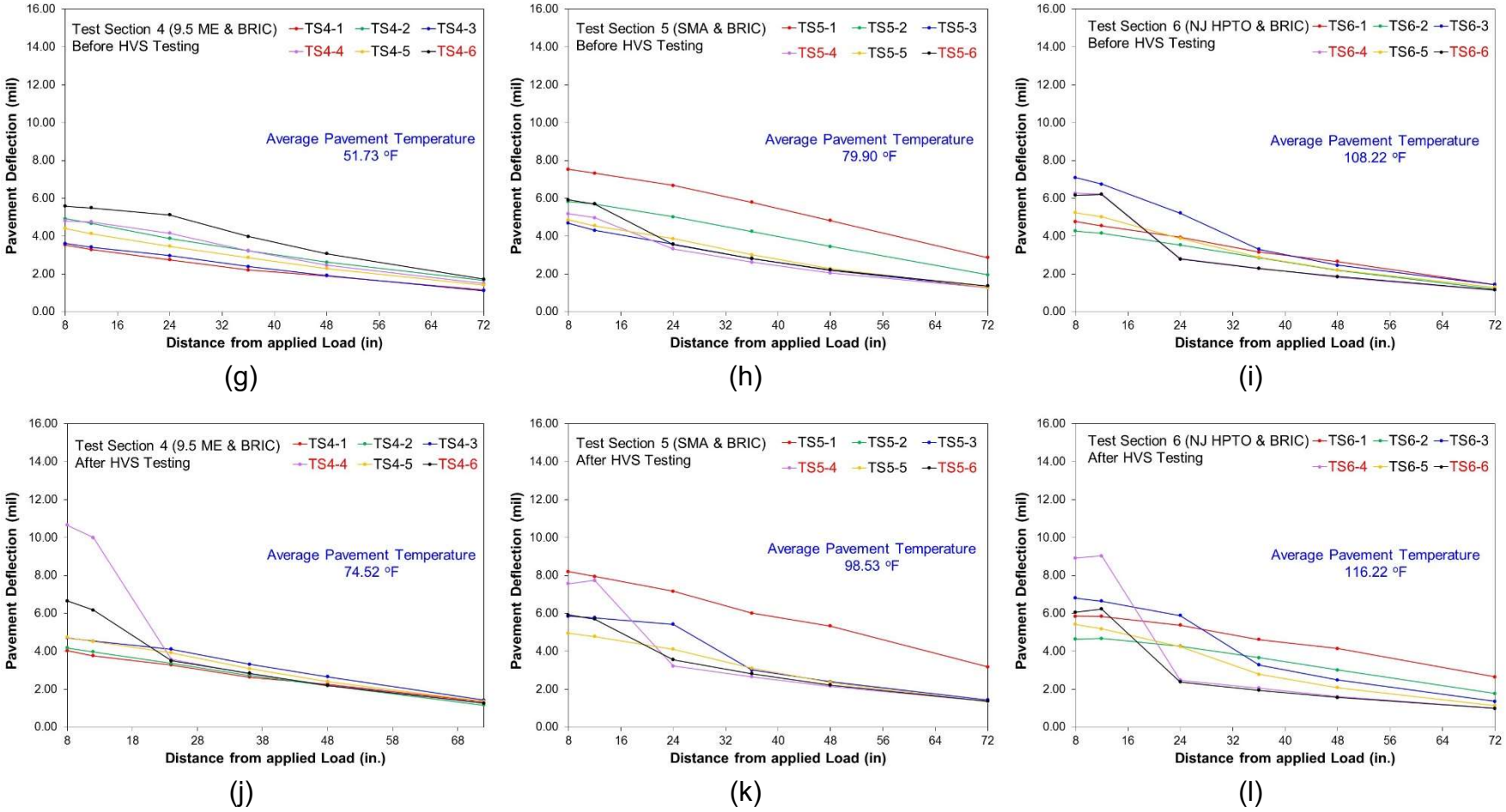

Figure 29. Pavement deflections obtained during HWD testing before and after accelerated pavement testing

$$\mathrm{E}o = \frac{(1.5 * \mathrm{a} * \sigma_o)}{\mathrm{Do}} \quad (1)$$

$$Outer\ AREA = 6(1 + 2\left(\frac{D3}{D2}\right) + 2\left(\frac{D4}{D2}\right) + 2\left(\frac{D5}{D2}\right) + 2\left(\frac{D6}{D2}\right) + \left(\frac{D7}{D2}\right)) \quad (2)$$

$$\mathrm{AF} = \left(\frac{k_2 - 1}{k_2 - (\frac{AREA}{k_1})}\right)^2 \quad (3)$$

$$\mathrm{E}S = \mathrm{E}o * AF * k_3{}^{(\frac{1}{AF} - 1)} \quad (4)$$

Where: - $(\mathrm{E}o)$ composite modulus of pavement
- (a) radius of HWD plate
- (σ_o) Peak pressure of HWD impact load under plate
- (Do) Peak center HWD deflection
- $(Outer\ AREA)$ Area parameter
- (D3, D4, D5, D6, D7) Measured pavement deflections
- (AF) Area factor
- (k_1) = 11.037(*AREA* when stiffness of upper layer is same as that of lower layers)
- (k_2) = 3.262 (maximum possible improvement in *AREA* (36/11.037))
- (k_3) Thickness of upper layer / load plate diameter

Table 5 – Inputs Used to Compute Equivalent Area for Dual-Tire Single Axle Configurations

Test Section	HWD Test Location	Effective Stiffness (psi)		Percent Difference (%)
		Before HVS Testing	After HVS Testing	
Test Section 1 (9.5 ME)	TS-4	98,922	56,389	42.9
	TS-6	47,466	39,065	17.7
Test Section 2 (SMA)	TS-4	125,850	19,690	84
	TS-6	23350	16362	30
Test Section 3 (NJHPTO)	TS-4	73,095	15,991	78.1
	TS-6	60,981	19,169	68.5
Test Section 4 (9.5ME and BRIC)	TS-4	64,436	1,226	98.0
	TS-6	21,679	6,933	68.0
Test Section 5 (SMA and BRIC)	TS-4	10,636	2,933	72.5
	TS-6	8,652	4,219	51.2
Test Section 6 (NJHPTO and BRIC)	TS-4	7,477	4,364	41.6
	TS-6	7,721	2,834	63.3

as temperature increases, the *Outer AREA* decreases and vice versa. Therefore when adopting the *Outer* AREA method for HWD analysis, temperature corrections should be utilized in order to minimize the effect of temperature on the pavement stiffness calculations.

The analysis of the measured pavement deflections began with the computation of the E_o and the *Outer AREA* parameter for each test section before and after HVS testing using Equations 1 And 2 respectively. The computed *Outer AREA* was then used to calculate and AREA factor (AF) (Equation 3). The composite modulus and AREA factor were subsequently utilized to calculate the effective stiffness (ES) of the surface layers of the test sections (Equation 4).

The computed effective stiffness obtained for all the test sections before and after HVS testing is presented in Table 5. From this table, it can be seen that the effective stiffness of the test sections at HWD locationsTS-4 and TS-6 generally decreased after the test sections were subjected to HVS loading. It can also be observed from this table that the reduction in effective stiffness at TS-4 was generally larger than the effective stiffness reduction seen at TS-6. This observed trend was expected because TS-4 was located 1.5-in. from the joint in the Test Zone 1 (i.e., region loaded by the HVS) while TS-6 was located near the joint (1.5-in.) in Test Zone 2 (i.e., region not loaded by the HVS). Therefore the decrease in structural capacity captured at TS-4 was expected to be more significant than that captured at TS-6. With respect to the relative change in structural capacity of the test sections, it can be observed from Table 5 that the Section 4 (9.5 ME & BRIC) experience the largest reduction in effective stiffness followed by Section 2 (SMA), Section 3 (NJHPTO), Section 5 (SMA and BRIC), Section 6 (NJHPTO and BRIC) and Section 1 (9.5 ME) respectively. These observations suggests that Section 4 (9.5 ME and BRIC) experienced the most deterioration (i.e. damage accumulation) during HVS testing while Section 1 (9.5 ME) experienced the least deterioration (i.e. reduction in stiffness during APT.

Reflective Cracking Susceptibility of Overlays

Typically, the presence of fully propagated cracks in a rigid layer of composite pavement leads to reflective cracking in the layer(s) above (i.e. asphalt overlay).[26] This is because local points of stress concentration form at the bottom of the asphalt overlay (at the locations directly above the cracks in the rigid layer) as trafficking progresses on the composite pavements. These points of local stress concentrations lead to increased tensile strains at the bottom of the asphalt overlay and eventually cause cracks to initiate and propagate through the overlay. To determine the susceptibility of the asphalt overlays to reflective cracking, the strain at the bottom of the overlays directly above the joint, were measured using H-gauges installed adjacent to and directly in the wheel path as mentioned previously. Embedded H-gauges are generally used in APT to measure the dynamic material response (i.e., strain) of asphalt layers in full scale test sections to moving traffic loads. [27] The strain at the bottom of an asphalt layer is typically monitored during APT to capture the load-associated, cracking failure mechanism of such layers. This is because load-related, strain accumulation beyond the allowable strength of

asphalt mixtures typically leads to cracking.[28] Since cracking is considered the least understood distress in flexible pavements and generally leads to a rapid decrease in pavement service life, the measurement of strain at the bottom of the asphalt layer during APT is vital. Such measurements assist APT users in quantifying or comparing the fatigue behavior (i.e., fatigue life) of full-scale pavement sections.

The following subsections presents an overall procedure established for analyzing the strain data obtained from the H-gauges installed in each test section considered in this study. An approach to compute pavement damage response parameters is also presented in this section. The developed approach is based on the concept of reduction in modulus and damage accumulation as HVS loading is being applied. The computational procedure consists of five steps the details of which are presented below.

Step 1: Processing Data and Defining Strain Signal Time History Phases

In this step, the strain measurements were obtained by converting the voltage signal recorded by H-gauges embedded in the pavement section. Calibration factors provided by the manufacturers, were used for this purpose. The strain signal time history response was then filtered using a signal processing technique to remove any noise that may be present in the data. This is because typical strain time history signals are usually obtained from a large amount of recorded data points (i.e., data points ranging from 1000–2000 data points per section) from each strain gauge installed in full-scale test sections. [29] For this purpose, a 25-data-point moving average was performed on the 10,000 data points are recorded during APT to reduce the number of data points required to capture the strain response at a particular loading pass. This process for reducing the amount of data point per loading pass was found to accurately capture the trend in strain response as will be highlighted in the upcoming sections.

Step 1 of the analysis procedure also involved defining various phases representing the change in strain response recorded for a particular pass. To establish these phases, it was necessary to first identify the critical (or turning) points on the strain time history for each loading pass (Figure 30). The critical points were defined as a local maximum or minimum point on the strain time history pulse where the slope changed from positive to negative or vice versa. Using these turning points, four phases in the strain signal time history pulse were defined (Figure 30b). As illustrated in Figure 30, Phase I represented the start of the strain time history pulse up until Turning Point 2 (TP2) (Figure 30. This phase captured the initial compressive strain occurring in the pavement followed by the tensile strain response as the load is approaching the sensor. Phase II captured the compressive strain when the load was directly on top of the strain gauge (TP2 to TP3 in Figure 30). Phase III (Figure 30) captured the tensile strain (TP3 to TP4) measured for the pavement when the load started to depart from the location of the strain gauge and Phase IV (TP4 to End Point (EP) in Figure 30) captured the gradual reduction in strain when the load did not impact the pavement anymore (at the location of the embedded strain gauge). The establishment of these critical phases was essential for calculations in the following steps of the developed strain data analysis method.

Step 2: Calculating Maximum Strain and Tensile Strain Phase Ratio (TP_R)

For each loading pass, the phases defined in Step 1 were utilized to compute two parameters representing the strain response of the pavement structure. The first parameter, referred to as the "maximum tensile strain ($\varepsilon_{t\text{-}max}$)," was computed as the absolute difference between the maximum tensile strain (TP4) and the maximum compressive strain (TP3) for each loading pass. The $\varepsilon_{t\text{-}max}$ represented the most critical tensile strain the asphalt overlays experienced in a loading pass. Generally, higher $\varepsilon_{t\text{-}max}$ values for a particular asphalt mixture, indicated that more damage was being applied to the section. Thus, this parameter provided insights related to the amount of damage being applied in a particular loading pass. It is noted that the $\varepsilon_{t\text{-}max}$ has been successfully used in other studies to compare the response of different asphalt overlays to various APT conditions such as: distance from the wheel path, load magnitudes, and loading rates among others.[30 and 31]

The second parameter, referred to as "tensile strain phase ratio (TP_R)," was also computed for each strain time history pulse obtained for each loading pass during APT. This parameter was defined as the ratio of tensile strain representing the smaller of Phases I (i.e., |TP2 – TP1|, Figure 30) or III (i.e., |TP4 – TP3|) to the other tensile strain Phase (I or III) representing the strain phase which had the larger magnitude of the two (Equation 5). This mathematical definition was employed to ensure that the TP_R values followed a logarithmic growth trend as the loading passes applied on the sections increased regardless of the strain response obtained from the H-gauges. This was important because strain time history pulses in APT depend on the wheel loading configurations and asphalt mixtures types. [30 and 32] Similar to $\varepsilon_{t\text{-}max}$, higher TP_R (approaching 1 and higher) indicated that the asphalt layer was experiencing more tensile strains (or more damage) at a particular loading pass. This parameter also captured the critical tensile strain the asphalt layers underwent while at the same time captured the potential "elasticity" of the asphalt mix (or its ability to stretch and flex under applied loading).

$$TP_R = \begin{cases} \frac{Phase\ I}{Phase\ III} & if\ \ |TP2 - TP1| < |TP4 - TP3| \\ \frac{Phase\ III}{Phase\ I} & if\ \ |TP2 - TP1| \geq |TP4 - TP3| \end{cases} \quad (5)$$

Where: - (TP_R) Tension Phase Strain Ratio
- (TP1) Turning Point 1
- (TP2) Turing Point 2
- (TP3) Turning Point 3
- (TP4) Turning Point 4

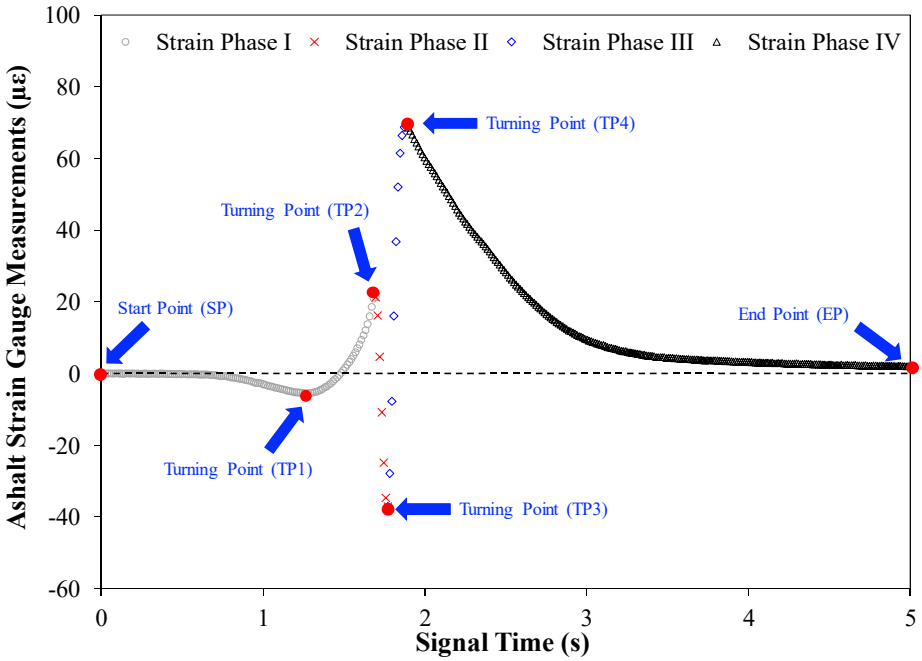

Figure 30. Illustration of critical points and critical strain phases

Step 3: Calculating Asphalt Layer Modulus and Rate of Change of TP_R

Step 3 involved the computation of an APT asphalt layer modulus based on the measured strain data (i.e., either $\varepsilon_{t\text{-}max}$ or $\varepsilon_{t\text{-}max}$ and TP_R) and loading applied. Equation 6 below presents the mathematical representation of the suggested APT asphalt layer modulus, computed for all loading passes applied using $\varepsilon_{t\text{-}max}$. The applied stress was computed using a tire imprint (circular) representing the wheel area through which full-scale HVS loading was applied. An equivalent circular tire imprint representative of the dual-tire configuration [30], was used to compute the applied stress when the wheel was on top of the strain gauge.

$$E_{APT} = \frac{Applied\ Stress}{t-max} \quad (6)$$

Where: - (E_{APT}) Asphalt Layer Modulus
- ($\varepsilon_{t\text{-}max}$) Measured Maximum Tensile Strain

To account for the "elasticity" of the various asphalt mixtures utilized in the overlays, the rate of change in the TP_R parameter was used a means of computing a "Damage Index (DI)." To compute the damage index, it was first necessary to obtain the relationship between TP_R and the applied equivalent single axle loads (ESALS). This relationship was described using a logarithmic growth function (i.e.,$TP_R = a\ln(ESALS) + b$; where a and b were model parameters). Using this relationship for a particular test section, the rate of change in TP_R (ΔTP_R) was calculated as shown in Equation 7:

$$\Delta TP_R = \frac{d\,TP_R}{d\ loading\ cycle} = \frac{a}{ESALS} \quad (7)$$

Where: - (ΔTP_R) Rate of Change in Tension Strain Phase Ratio
- (a) Model Parameter

Once ΔTP_R was obtained for all passes, the damage applied at a particular loading pass (PD) was then defined as shown in Equation 8. Using this definition, the effect of both the tensile and compressive strains during loading (or stretching and flexing due to loading) as well as the change in layer modulus were considered when accounting for damage in an asphalt pavement layer.

$$PD_i = (E_{APT} \times \Delta TP_R)_{pass\ i} \quad (8)$$

Where: - (PD_i) Damage Applied at Particular Loading Pass
- (E_{APT}) Asphalt Layer Modulus
- (ΔTP_R) Rate of Change in Tension Strain Phase Ratio

The DI was then computed as summation of damage applied for all loading passes as shown in Equation 9. Higher values of DI for an asphalt pavement layer indicate that this layer has experienced more damage when compared to an asphalt layer showing lower DI values.

$$Damage\ Index\ (DI) = \sum PD_i \quad (9)$$

Where: - ($\sum PD_i$) Cumulative Damage Applied for all Loading Pass

Step 4: Correlating E_{APT} and DI to Applied Loading Passes

In this step, correlations between the computed asphalt layer moduli values (E_{APT}) and the number of loading passes applied were established through regression analyses. This was important for comparing the fatigue performance of the various asphalt overlays and their ability to withstand damage from applied loading. For the purpose of this analysis, loading passes were converted to ESALS using the empirical relationship shown in Equation 10. [33] A logarithmic decay model was utilized to model the relationship between E_{APT} and number of loading cycles. This model was selected because it accurately captured the reduction in asphalt layer modulus with the increase in loading passes. The relationship form is presented in Equation 11.

$$\text{ESALS} = (\frac{HVS\ Applied\ Loadi}{40})^4 \text{ x HVS Loading Pass} \quad (10)$$

$$E_{APT} = a \times \ln(No.of\ Cycles\ Applied) + b \quad (11)$$

Where: - (a and b) Model parameters

In the case of the DI parameter, the cumulative increase in DI and the number of applied ESALS were related using a logarithmic growth function. This is because this function

represented the realistic behavior of the asphalt overlays in that damage accumulates at a faster rate during in early stages of an asphalt overlay's life followed by a slower damage accumulation rate in the later stages of the pavement life. It is noted that this trend is similar to that typically observed when permanent strain accumulates of in asphalt mixtures.

Step 5: Comparing the Fatigue Performance of Asphalt Layers

The computed regression models with respect to E_{APT} and cumulative DI for different asphalt pavement layers (Step 4) were then utilized to compare the relative performance of these layers. For instance, a pavement section which showed a high rate of reduction in E_{APT} values (i.e., derivative of E_{APT}) indicated a higher susceptibility to fatigue cracking than those which showed a lower rate of reduction in E_{APT} values. In addition, the E_{APT} values for the various overlays were compared at the same number of loading cycles applied, in order to determine the susceptibility of these mixtures to fatigue cracking. It is noted that higher E_{APT} values, at the same applied loading passes, indicated the asphalt layer or mix was more resistant to fatigue cracking than those with lower E_{APT} values.

The DI (Equation 9) was also compared for various asphalt pavement layers at the same number of applied loading passes. With the same load applied on all sections evaluated in this study (e.g., (60-kN)), sections which demonstrated lower DI values were less susceptible to fatigue damage. The rate of change of cumulative DI also provided an indication of the susceptibly of asphalt pavement layers to fatigue cracking. Higher cumulative DI values indicated that the overlay was deteriorating faster and therefore it was more susceptible to fatigue cracking.

Comparison of Asphalt Overlay Fatigue Cracking Susceptibility

The stain data analysis procedure outlined in the previous section was utilized to compare the relative fatigue cracking susceptibility of the asphalt overlays evaluated in this study. Strain data obtained from Sections 2 through 6 were used to demonstrate how the developed strain data analysis procedure can be employed to compare the relative fatigue performance sections. Strain data from Section 1 was omitted from the analysis because the asphalt strain gauges in this test section were damaged during test section construction as previously mentioned. The different steps of the strain data analysis procedure previously outlined were followed closely to analyze the strain data. The following subsections provide the details of this strain data analysis and subsequent fatigue performance comparison of the asphalt overlays.

Filtering and Processing of Strain Data

Figure 31 presents an example strain-time history pulse obtained from a strain gauge (H-gauge) embedded in one of the sections evaluated in this study. As can be seen from Figure 31, the strain-time history response for this particular HVS loading pass was smooth with low noise in the recorded data (a total of 10,000 data points recorded over five seconds). Based on this observation, it was concluded that no signal processing was necessary to remove noise from the data. This was the case for all strain-time history responses collected from all five pavement sections considered in this study. Figure 31

also illustrates the reduced strain time history response as obtained using a moving average (25 data points period). It is evident from Figure 31 that the reduced strain-time history response (25-period moving average) was able to accurately capture the trend of the full strain-time history response. Therefore, for ease of data handling, the reduced strain-time history, which only amounted to 400 points as opposed to 10,000 data points, was calculated for all strain-time history responses obtained from all HVS loading passes, all five pavement sections. To automate the process of reducing all recorded strain-time history responses, an Excel Macro (visual basic for applications program) was developed. Similarly, the process for establishing the various turning points along with the four strain phases (Step 1 of the developed strain data analysis procedure) was completed as described previously and automated using an Excel Macro.

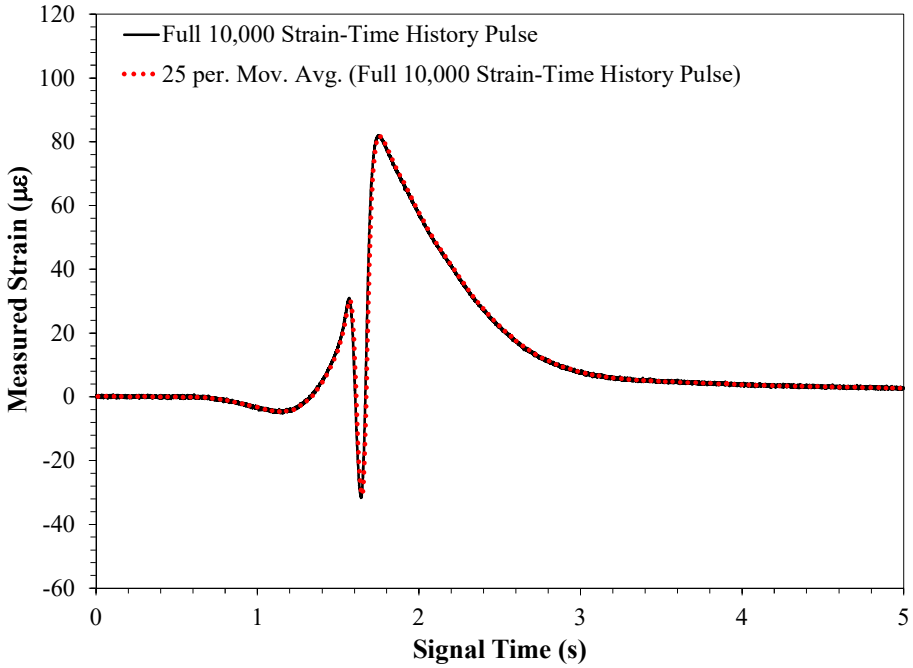

Figure 31. Example of measured and reduced strain-time history response obtained from a strain gauge embedded in one of the five sections

Maximum Tensile Strain and Tensile Strain Phase Ratio

The $\varepsilon_{t\text{-}max}$ and TP_R parameters were computed for all strain-time history responses recorded from all five pavement sections at all loading passes where strain-time history data was sampled. It is noted that the damage associated with the loading passes Figure 32 presents the computed $\varepsilon_{t\text{-}max}$ and TP_R values obtained for all five sections; plotted versus the number of applied ESALS. As evident from Figure 32a, the $\varepsilon_{t\text{-}max}$ computed for all five sections increased, i.e., followed a logarithmic growth trend, with the increase in number of applied ESALS. This trend was expected because the increase in applied loading passes typically amounts to an increase in permanent strain (or damage) within the pavement sections; thus, explaining the increase in $\varepsilon_{t\text{-}max}$ with the increase in applied loading passes. In addition, given the constant loading applied on top of all five pavement

sections (i.e., (60-kN)), it can be seen from Figure 32a that $\varepsilon_{t\text{-}max}$ parameter was able to differentiate between all the mixes. This is the case because $\varepsilon_{t\text{-}max}$ values for Section 2 (SMA) were higher than those for Sections 6 (NJHPTO), 4 (9.5 ME and BRIC), 3 (NJHPTO), and 5 (SMA and BRIC) respectively. Similarly, Figure 32b presents the TP_R values obtained for all five sections and plotted versus the number of applied ESALS. As illustrated in this figure, the TP_R values followed a logarithmic growth trend; that is, with the increase applied ESALS, there was an increase in TP_R values. This parameter was also capable of differentiating between the five asphalt overlays.

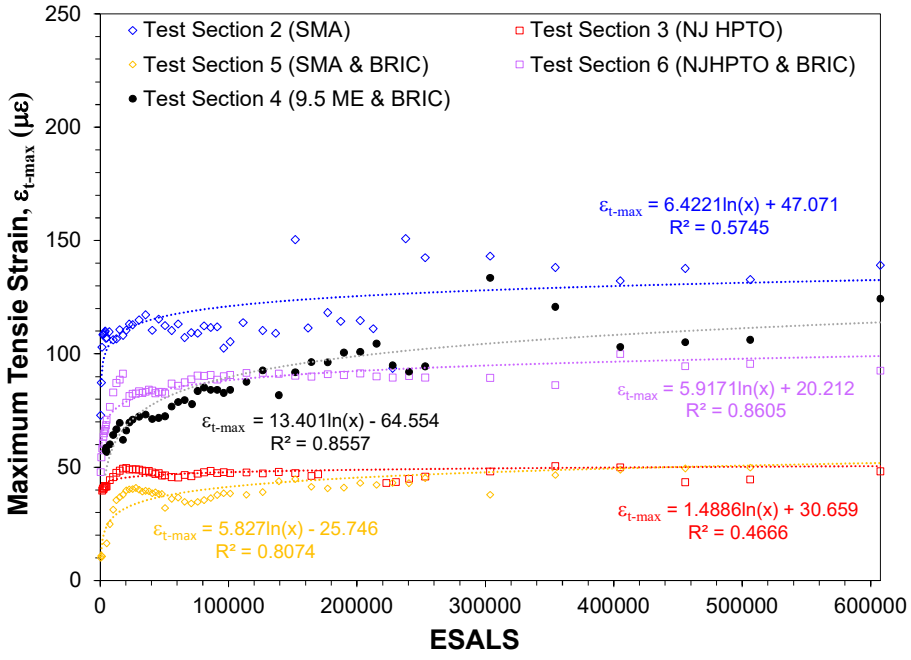

(a)

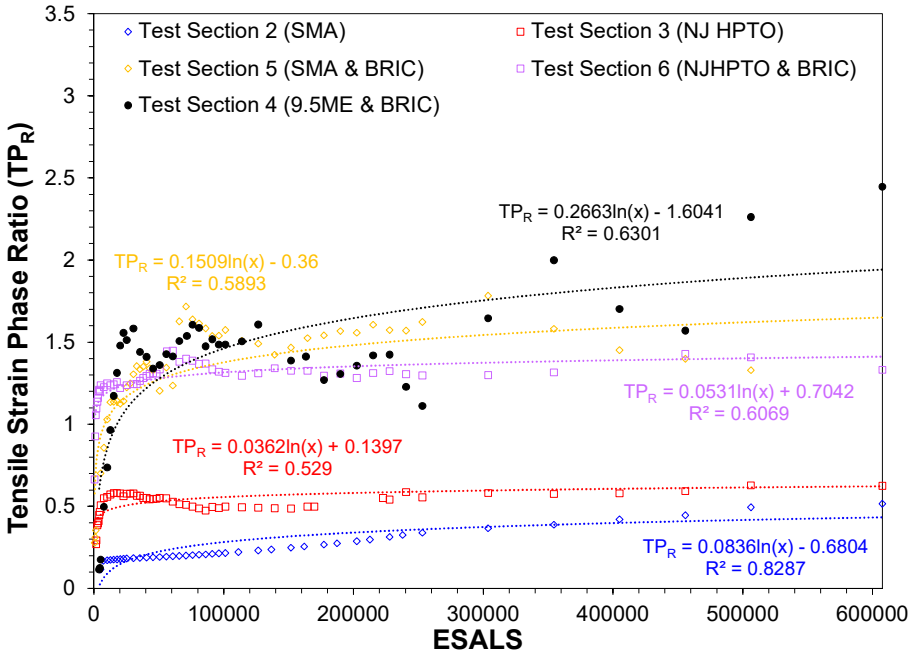

(b)

Figure 32. (a) Maximum tensile strain ($\varepsilon_{t\text{-}max}$) and (b) Tensile Strain Phase Ratio (TP_R) versus number of applied HVS loading passes for all five sections.

Asphalt Layer Moduli

To compute the asphalt pavement layer moduli values for all loading passes (Equation 6), the stress applied from the dual-tire configurations utilized in this study, was first determined. Table 6 presents the inputs used for computing this equivalent area over which loading was applied. The radius of an equivalent circular tire imprint was then determined using Equation 12. [32] Subsequently, the applied stress was computed as the applied HVS load (Table 6) over the equivalent circular tire imprint area using (Equation 12). Using the computed applied stress (i.e., 44.29-psi) and the maximum tensile strain measured at each loading pass, E_{APT} of the five test sections were calculated using Equation 2.

$$a = \sqrt{\frac{0.8521\,P_D}{q\pi} + \frac{S_d}{\pi}\left(\frac{P_D}{0.5227q}\right)^{\frac{1}{2}}} \qquad (12)$$

Area = πa^2
(89)

Where: - (a) Equivalent circular radius of applied loading
- (q) Stress applied to pavement sections
- (P_D) Load applied to pavement sections
- (S_d) Center to center tire spacing

Figure 33 presents the E_{APT} values computed for all five pavement sections. As can be seen from Figure 33, the computed moduli values followed a logarithmic decay trend. This trend was expected because E_{APT} values were directly computed using the $\varepsilon_{t\text{-}max}$ parameter which followed a logarithmic growth trend (i.e., $\varepsilon_{t\text{-}max}$ increase as applied ESALS increase). It is noted that the trend observed in Figure 33 with respect to E_{APT} is also similar to what is typically observed during the laboratory assessment of asphalt mixtures' fatigue properties. This is significant because existing literature attributes the reduction in moduli values for an asphalt mixture to damage accumulation as loading cycles are applied; which is closely associated with the overall fatigue life of the asphalt layer. For instance, Shen and Carpenter (2007) [33] reported that a 50% reduction in modulus for an asphalt mixture constitutes the stage at which fatigue cracking initiates. Therefore the observations from Figure 5, along with supporting literature indicate that the use of E_{APT} in characterizing the fatigue performance of full-scale instrumented asphalt pavement layer is practical (i.e., easy to compute) and may correlate well to fatigue life of asphalt mixtures.

Moreover, Figure 33 shows that the logarithmic decay relationships between E_{APT} and ESALS obtained for all five test sections are different from one another. For instance, as illustrated in this figure, layer moduli values obtained for Section 2 (SMA overlay) are lower than those obtained for Section 3 (NJHPTO). This observation suggested that these relationships were dependent on the asphalt overlay mixture type as well as the thickness of the asphalt overlay. This is the case because loading applied on all five sections was similar (i.e., 60-kN using dual-tire single axle configuration). In addition, the results presented in Figure 32 show that the rate of reduction in E_{APT} values for Section 5 (SMA and BRIC) were the highest followed by that for Sections 6 (NJHPTO) Section 4 (9.5ME and BRIC), Section 3 (NJ HPTO) and Section 2 (SMA), respectively. Therefore, it can be concluded that the rate of reduction in E_{APT} was capable of distinguishing between various asphalt mixtures with respect to their fatigue characteristics.

Table 6 – Inputs Used to Compute Equivalent Area for Dual-Tire Single Axle Configurations

Axle Configuration	Value
Loading Magnitude	13488.54 lb.
Axle Type	Single Axle
Tire Center to Center Spacing (Sd)	13.0635 in.
Tire inflation pressure (q)	110 psi
No. of Tires	2 (Dual)
Equivalent Circular Imprint and Applied Stress	
Equivalent radius (a)	7.852-in.
Equivalent area	193.71 square-in
Applied Stress (σ) (Load/Area)	44.29 psi

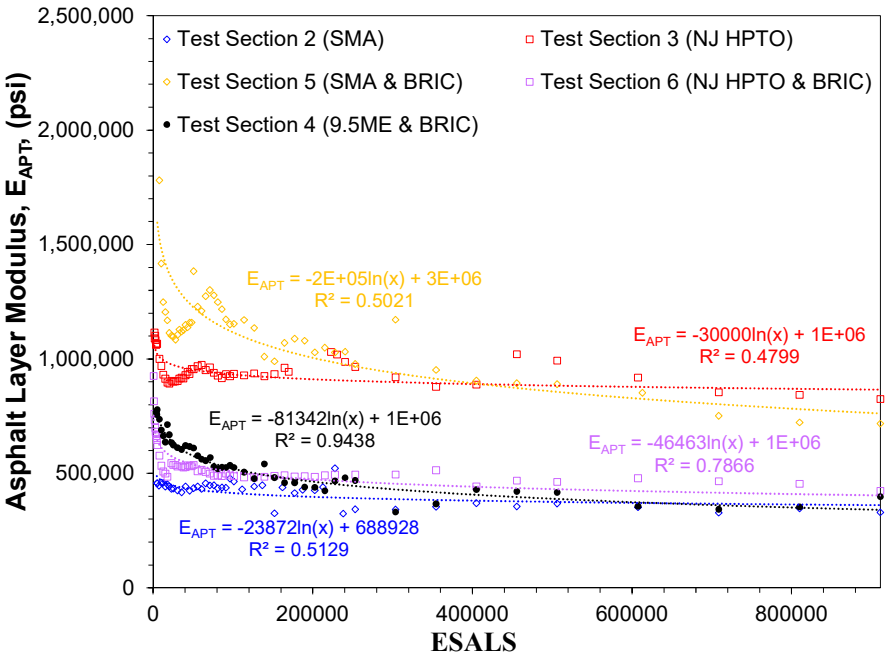

Figure 33. Computed asphalt pavement layer moduli values (E_{APT}, Equation 2) for all loading passes

Damage Index

To determine the damage index (DI) values for all loading passes, the rate of change in TP_R was first determined at each loading pass. Using the empirical relationships illustrated in Figure 32b, the ΔTPR was computed for all five pavement sections using Equation 7. Additionally, using the empirical relationships in Equation 10, the loading passes applied were converted to ESALS. Table 7 presents the equations for determining the ΔTPR relationships of all five pavement sections considered in this analysis. Using the ΔTPR relationships presented in Table 7 and the computed E_{APT} for each loading pass, the DI index was determined using Equation 8 as discussed previously. The cumulative DI values for each of the five asphalt overlays were then be determined using Equation 9.

Figure 34 presents the cumulative DI values computed using Equation 9 for each pass. As can be seen from this figure, the DI values shown in Figure 34 increased at different rates for the different asphalt overlays (or sections). Additionally, by comparing the accumulated damage after applying 160,000 loading passes for example, it can be seen from Figure 34 that Section 2 (SMA) had the lowest accumulated damage, followed by Section 3 (NJHPTO), Section 5 (SMA and BRIC), Section 6 (NJHPTO and BRIC) and Section 4 (9.5ME and BRIC), respectively. These results indicated that Section 2 had the best fatigue cracking resistance followed by Sections 3, 5, 6 and 4, respectively. This is the case because for Section 2 to reach the same level of damage seen for Section 4 after applying 160,000 ESALS, the application of more ESALS is required on this section (Section 2). Based on these observation, it was deduced that the rate of increase in DI

and the cumulative DI values for all six sections was adequately able to differentiate the fatigue resistance of the asphalt overlays considered in this study.

Table 7 – Rate of Change in Tensile Strain Phase Ratio (ΔTP_R) as Determined from Logarithmic Growth Relationships Presented in Figure 32(b)

Section Designation	Value
Test Section 2 (SMA)	$\frac{0.0836}{ESALS}$
Test Section 3 (NJHPTO)	$\frac{0.0362}{ESALS}$
Test Section 4 (9.5ME and BRIC)	$\frac{0.2663}{ESALS}$
Test Section 5 (SMA and BRIC)	$\frac{0.1509}{ESALS}$
Test Section 6 (NJHPTO and BRIC)	$\frac{0.0531}{ESALS}$

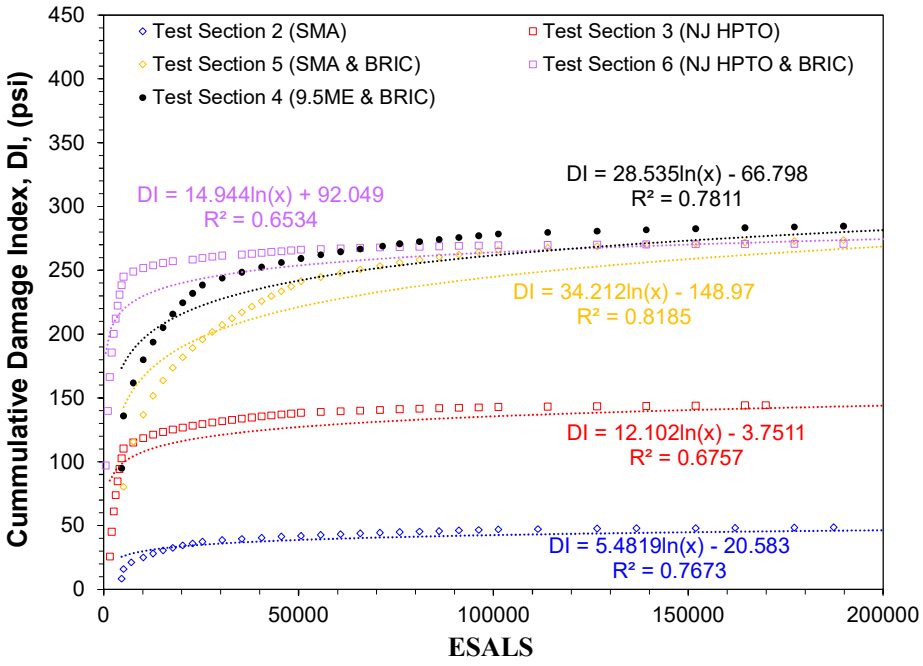

Figure 34. Computed cumulative damage index (DI, Equation 5) for all loading passes

Comparison of E_{APT} and Cumulative DI Analysis Parameters

In summary, it appeared that both parameters (E_{APT} and cumulative DI) were able to distinguish between the fatigue characteristics of asphalt pavement layers. However, it is noted that the fatigue performance ranking obtained from both parameters were slightly

different. To elaborate more, the E_{APT} showed that Section 5 (SMA and BRIC) was the most susceptible to fatigue cracking, followed by Sections 6 (NJHPTO) Section 4 (9.5ME and BRIC), Section 3 (NJ HPTO) and Section 2 (SMA) However, using the cumulative DI, Section 2 (SMA) was the best at resisting fatigue cracking followed by Section 3 (NJHPTO), Section 5 (SMA and BRIC), Section 6 (NJHPTO and BRIC) and Section 4 (9.5ME and BRIC), respectively. To determine which parameter gave a more accurate fatigue performance ranking for the asphalt overlays, the overall trends obtained for E_{APT} and cumulative DI were evaluated. Based on the results illustrated in Figure 33, it can be seen that E_{APT} values and overall reduction in E_{APT} were relatively similar for the Sections 2 (SMA) and 6 (NJHPTO and BRIC) and Sections 3 (NJHPTO) and 5 (SMA and BRIC) respectively. Based on Figure 34 it can be observed that the cumulative DI values and rate of increase in cumulative DI for Section 2 (SMA) was lower than Section 3 (NJHPTO) while those for Section 5 (SMA and BRIC) were lower than Sections 4 (9.5 ME and BRIC) and 6 (NJPTO and BRIC) respectively. It can also be observed from Figure 34 that the cumulative DI values and rate of increase in cumulative DI were higher for the overlays that contained the 1-in. layer of BRIC (i.e. Sections 4, 5, and 6). Based on these observed trends, it was concluded that the cumulative DI parameter demonstrated a more consistent fatigue performance ranking. This is because the cumulative DI and rate of increase in cumulative DI was lowest for the section containing the SMA overlay followed by those containing the 9.5 ME and NJHPTO overlays respectively even when the overlay contained an additional 1-in. layer of BRIC. Additionally, the cumulative DI and rate of increase in cumulative DI was also able to clearly distinguish between overlays that contained a layer of BRIC and those which did not. Therefore the cumulative DI was utilized to compare the fatigue performance of the asphalt overlays.

Asphalt Overlay Resistance to Horizontal Joint Movement

Horizontal joint movement in the rigid layer of the composite pavement test sections was of particular concern in this study because it simulated the behavior of cracks in rehabilitated rigid pavements under the action of repeated loading. This is important because the presence of cracks in the deteriorated rigid pavement layer typically leads to reflective cracking in asphalt overlays as previously mentioned. It has been well established that as the severity of cracking in the rigid layer of composite pavements increases (i.e. crack width and crack length of fully propagated cracks) the intensity of the stress concentrations and tensile strains at the bottom of asphalt overlays also increase. Therefore composite pavements are exposed to a greater risk of reflective cracking as the extent of cracking (i.e. crack width and length) in the rigid layer increases. [34] As such, the degree of horizontal joint movement that occurred in the test sections due to applied HVS loading were monitored using two LVDTs installed on either side of the joint as mentioned previously. These measurements gave some insight about the ability of the overlays to effectively transfer the applied loads across the joint as well as the overall susceptibility of the overlays to reflective cracking (i.e. larger the joint displacements, higher the risk of reflective cracking). However, these standalone LVDT measurements do not necessarily reflect a change in material properties of the asphalt overlays. Therefore caution must be taken when drawing conclusions about the reflective cracking susceptibility of the overlays strictly based on LVDT measurements. Nevertheless, since

the overlay stiffness influenced the overall load transfer efficiency across the joint, the joint displacement gave an indication of how the load transfer efficiency provided by the asphalt overlay was affected by HVS loading. That is, higher joint displacement, indicated less load transfer efficiency across the joint and lower joint displacement indicated greater load transfer efficiency across the joint.

This section presents the overall approach established to analyze the horizontal joint movement data obtained from the LVDTs installed in each test section evaluated in this study. The procedure developed to compute horizontal joint displacement is also outlined in this section. The computational procedure consists of two steps which are detailed in the following subsections.

Step 1: Processing Data and Identifying Peak Joint Opening

In this step, displacement measurements were obtained by converting the voltage signal recorded by LVDTs installed in the pavement sections. Calibration factors, which were provided by the manufacturers of the pressure cells were used for this purpose. The voltage was filtered using signal processing techniques (i.e. moving average) to remove any noise that was present in the data. A 25-data-point moving average of 10,000 data points was utilized in order to reduce the number of data points required to capture the horizontal joint movement during a particular loading pass. This was due to the fact that 10,000 data points were recorded during each HVS wheel pass. As with the strain data analysis procedure, this process for reducing the amount of horizontal displacement measurements per loading pass was found to be optimal since it accurately captured the trend in horizontal displacements measured as illustrated in Figure 35.

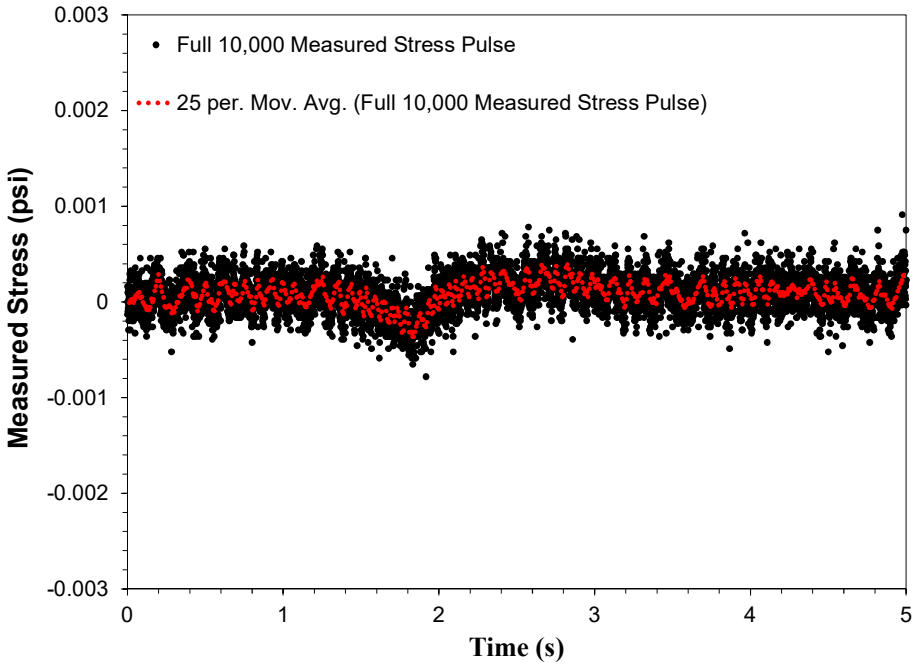

Figure 35. Example of measured and reduced horizontal displacement obtained from a LVDT in one of the six sections

Figure 36 illustrates a joint displacement pulse representative of the typical LVDT measurements obtained during each HVS loading pass on the six test sections. From this figure, it can be observed that the LVDT measurements consisted of several stages which corresponded with the movement of the test wheel of the HVS across the test section. These stages included an initial approach stage; where the LVDT measurements remained relatively constant, a second stage; where joint displacement measurements decreased (i.e., the joint closed), a third stage where the LVDT measurements increased considerably more than it decreased in the second stage (i.e. joint opened), and a fourth stage where the joint displacement measurements subsequently reduced toward its original position. The initial stage of the joint displacement pulse coincided with the movement of the wheel towards the joint, while the second and third stages coincided with the movement of the wheel over the edge of the approach and leaving PCC slabs respectively. The fourth stage of the joint displacement pulse corresponded with the movement of the HVS wheel away from the joint.

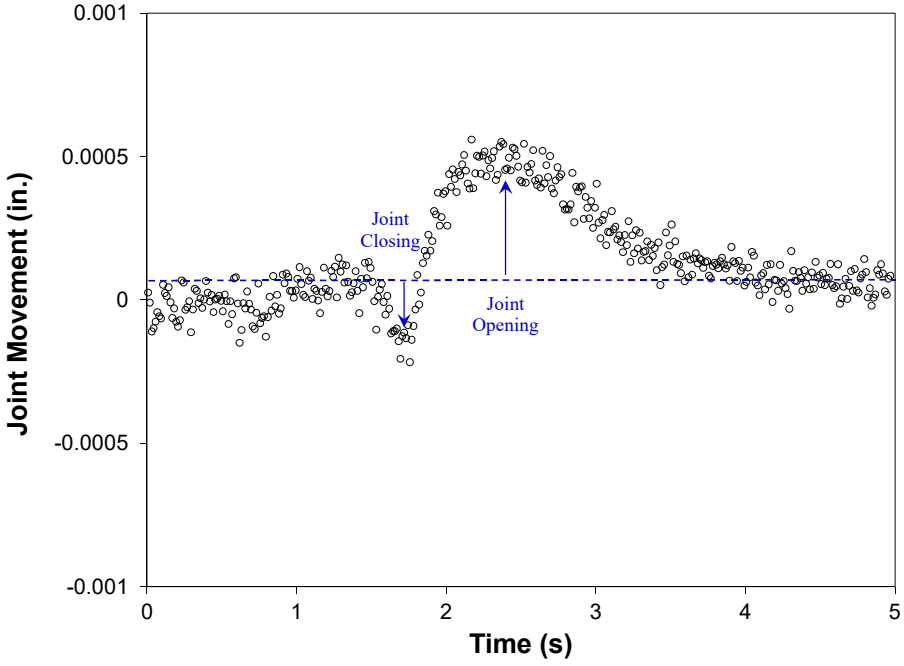

Figure 36. Typical joint displacement pulse recorded by installed LVDTs

Step 2: Calculating Joint Displacement for Each Pass

This step involved the computation of a parameter referred to as maximum joint displacement (ΔMax(JD)). The maximum joint displacement was computed for each loading pass by adding the overall change in joint displacement (i.e. the difference between the average LVDT measurements recorded for a particular pass and the average LVDT measurements recorded for the initial or reference pass) to the increase in joint displacement (ΔO_{Pn}) for a particular pass (i.e. the difference between maximum and average LVDT measurement recorded for that pass). This computational procedure for maximum joint opening is illustrated in Figure 37. From this computational procedure,

it can be seen that the maximum joint opening accounted for the most critical joint displacement experienced during each HVS loading pass on the test sections.

Asphalt Overlay Reflective Cracking Potential Based on Maximum Joint Displacement

The maximum joint displacement computed from the recorded LVDT measurements obtained from each test section is shown in Figure 38. The maximum joint displacement obtained from LVDT1 in each test section (i.e. the LVDT on the right side of the test section in relation to the direction of loading) is shown in Figure 38a and the ΔMax(JD) obtained from LVDT 2 in each test section (i.e. the LVDT on the left side of the test section in relation to the direction of loading) is illustrated in Figure 38b. From Figure 38, it can be seen that the maximum joint displacement computed for each asphalt overlay generally ranged between 0-in. and 0.01-in.

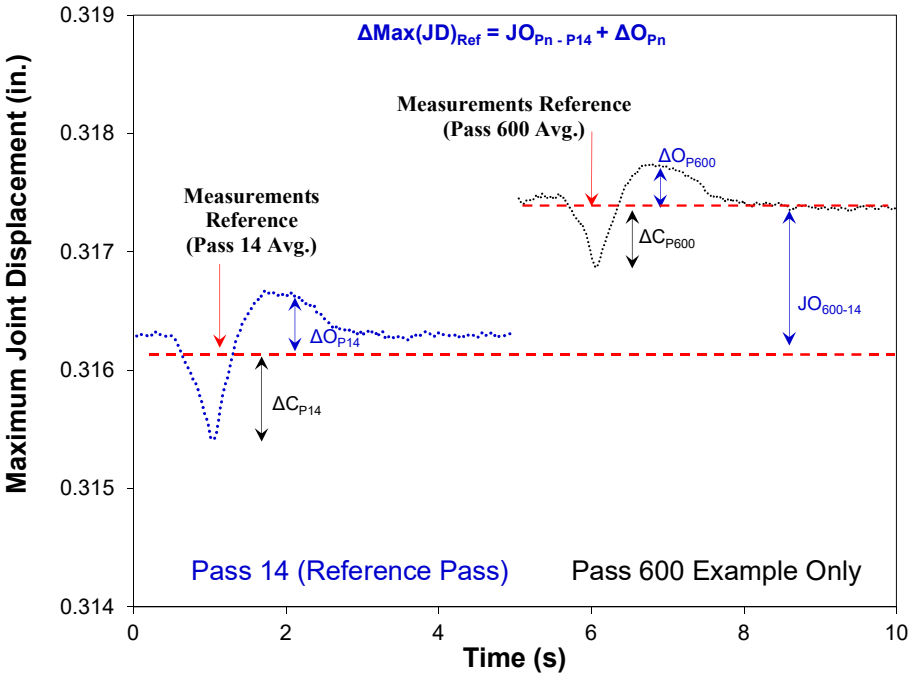

Figure 37. Computational method used to obtain maximum joint opening

This is significant because a study by Bennert (2010) [17] determined that dense asphalt mixtures were not capable of resisting cracks with movements greater than 0.01-in. Therefore since similar HVS loading was applied to the test sections, the computed maximum displacement values obtained for the test sections during HVS loading provided a means to directly compare the relative reflective cracking susceptibility of the asphalt overlays. It can also be seen from Figure 38 that the LVDT measurements recorded by LVDT 2 yielded higher computed maximum joint displacements values than those obtained from LVDT 1 for test sections except Sections 3. Therefore the maximum joint displacements obtained from LVDT 2 measurements were utilized to compare the reflective cracking susceptibility of the asphalt overlays on all test sections except Section 3. Based on the overall maximum joint displacement values presented in Figure 38, it

can be observed that the largest maximum displacement value recorded on Section 3 (NJHPTO) was 0.009-in. while that on Sections 1 (9.5ME), 4 (9.5 ME and BRIC), 2 (SMA), 6 (NJHPTO and BRIC), and 5 (SMA and BRIC) were 0.008-in., 0.007-in., 0.006-in., 0.005-in., and 0.004-in. respectively. Therefore it can be deduced that asphalt overlay on Section 5 had the highest load transfer efficiency across the joint followed by Sections 6, 2, 4, 1, and 3 respectively. This may also infer that the asphalt overlay on Section 3 might have the highest susceptibility to reflective cracking followed by Sections 1, 4, 2, 6, and 5 respectively.

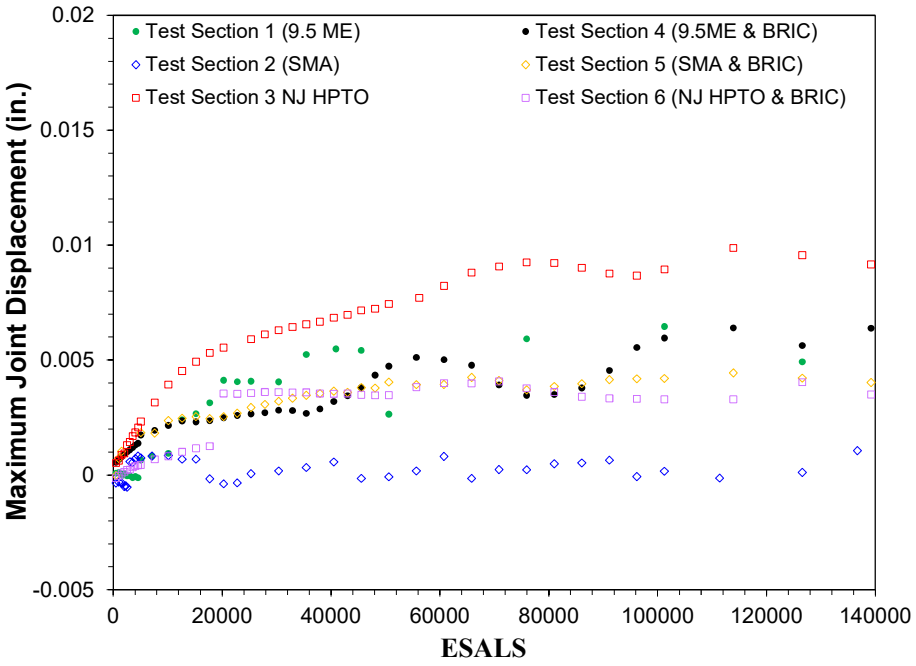

(a)

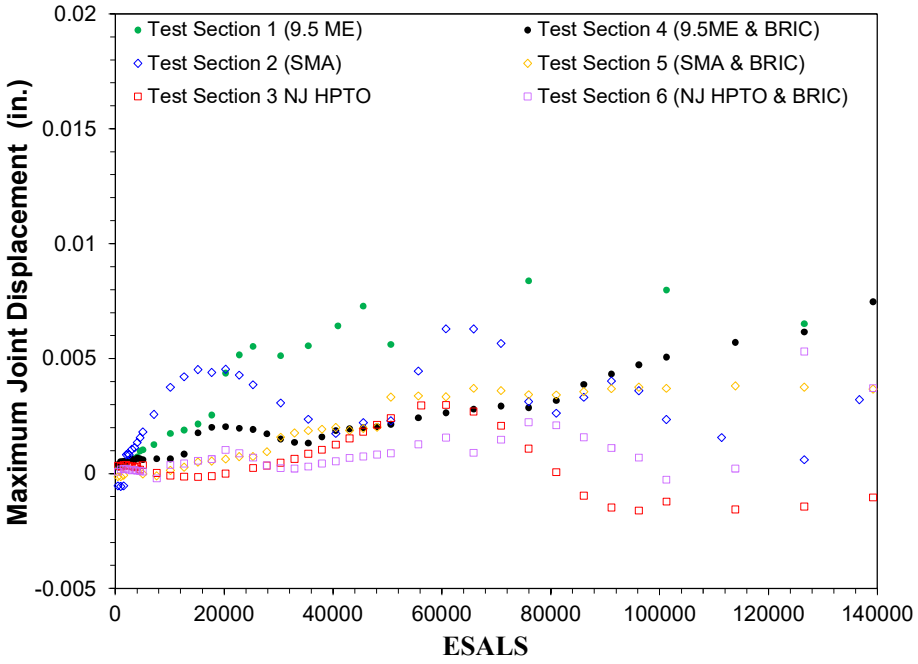

(b)

Figure 38. (a) Maximum Joint Displacement ΔMax(JD) obtained from (a) LVDT1 measurements (b) LVDT2 measurements in each test section

Asphalt Overlay Resistance to Vertical Joint Movement

In addition to the horizontal joint movement, the vertical joint movement was also of concern in n this study. This is because vertical joint movement replicates the behavior of fully propagated cracks in the rigid layer of composite pavement sections under the influence of applied loads. For instance, when a rehabilitated concrete pavement is subjected to repeated loading, the PCC slabs in the rigid layer of the composite section tends to deflect at the discontinuities (i.e., cracks). This bending action within the rigid layer leads to the formation of points of local stress concentration at the bottom of asphalt layer. At these points of local stress concentration, the asphalt experiences an increase in tensile strains; which eventually leads to reflective cracking. In this study, the vertical joint displacement in each test section was monitored by two embedded soil compression gauges on either side of the joint as mentioned previously. The embedded soil compression gauges measured the permanent vertical displacement of the PCC slabs at the joint in each test section. This is because the soil compression gauges were not equipped with a spring. The vertical PCC slab measurements obtained during HVS testing was used to compare the reflective cracking susceptibility of the overlays. However, like the LVDT measurements, it is noted that the standalone soil compression gauge measurements do not necessarily reflect a change in asphalt overlay material properties. Therefore caution must be taken when drawing conclusions about the resistance of the overlays to vertical joint movement strictly based on soil compression gauge measurements. Nevertheless, since the overlay stiffness influenced the overall load transfer efficiency across the joint, the relative vertical PCC slab movement (i.e.

vertical joint movement) gave an indication of how the load transfer efficiency provided by the asphalt overlay was affected during accelerated pavement testing. That is, higher relative vertical PCC slab movement, indicated less load transfer efficiency across the joint and lower relative vertical PCC slab movement indicated greater load transfer efficiency across the joint.

This section presents the overall approach established to analyze the vertical joint movement data obtained from the SCGs installed in each test section evaluated in this study. The procedure developed to compute vertical joint displacement is also outlined in this section. The computational procedure consists of two steps which are detailed in the following subsections.

Step 1: Processing Data and Determining

In this step, vertical displacement measurements were obtained by converting the voltage signal recorded by LVDTs installed in the pavement sections. As with the previous sensors discussed, calibration factors, provided by the manufacturers of the pressure cells were used for this purpose. The voltage was filtered using signal processing techniques (i.e. moving average) to remove any noise that was present in the data. A 25-data-point moving average of 10,000 data points was utilized in order to reduce the number of data points required to capture the vertical joint movement during a particular loading pass.

The reduced soil compression gauge data was utilized to determine the loading passes at which the soil compression gauges were functional (i.e., provided reasonable readings). This was done because the soil compression gauges had a tendency to become defective very rapidly during accelerated pavement testing as was illustrated in Figure 39. From this figure it can be seen that at least one soil compression gauge in each test section measured fluctuations in measured vertical displacement. Since the SCGs installed in the test sections were not spring loaded (i.e. only capable of measuring permanent displacements), these observation indicated that at least one failed during APT on each section except Section 4. In the case of Section 4, it can be seen from Figure 39d that SCG 2 measured fluctuations in vertical movement from the beginning of and throughout accelerated pavement testing. This was because the SCG utilized under the leaving slab in Section 4 was actually, an LVDT because the original SCG was damaged during installation. Hence this SCG was capable of measuring both vertical displacement in two directions.

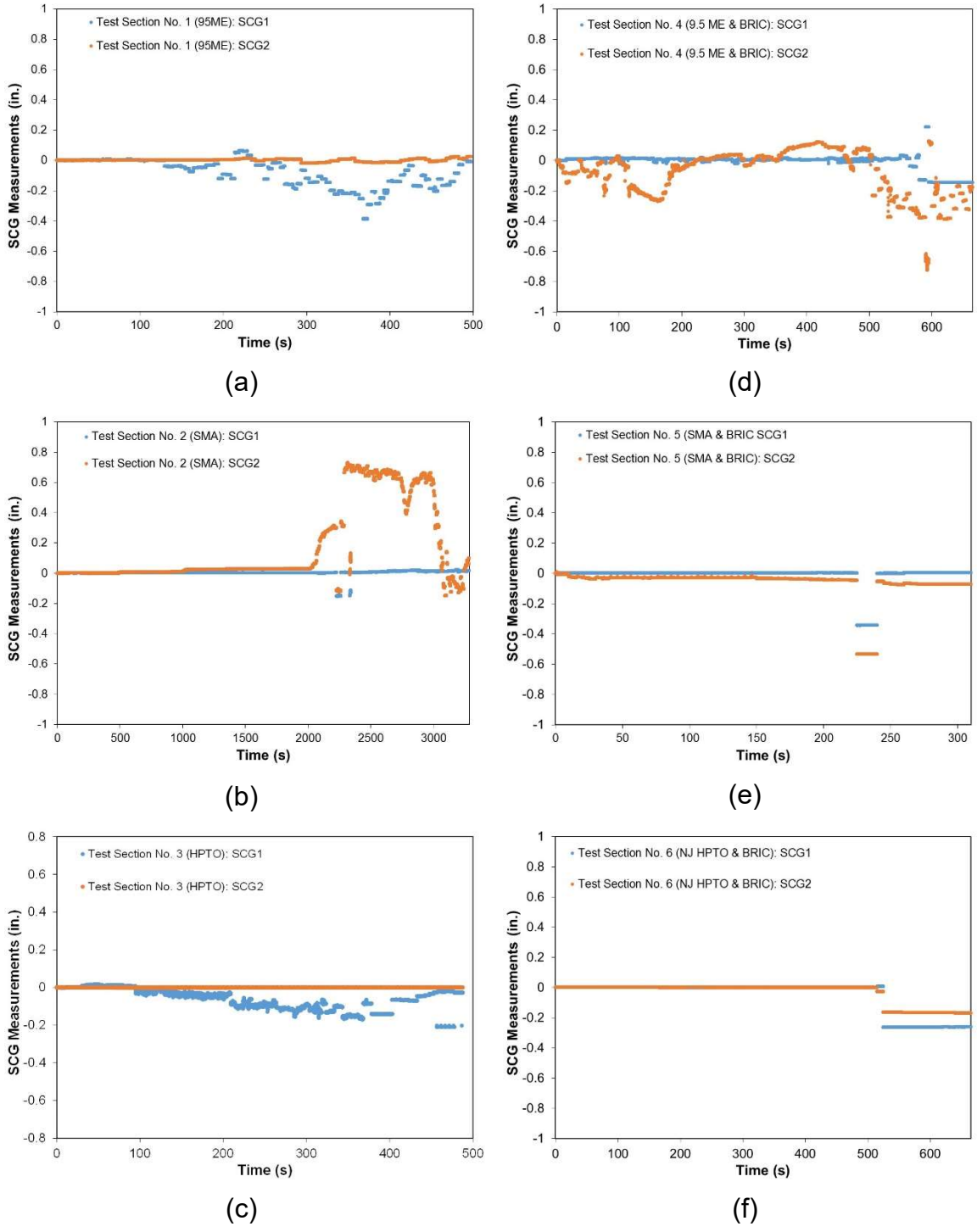

Figure 39. Vertical Displacement Measurements Obtained from Installed SCGs.

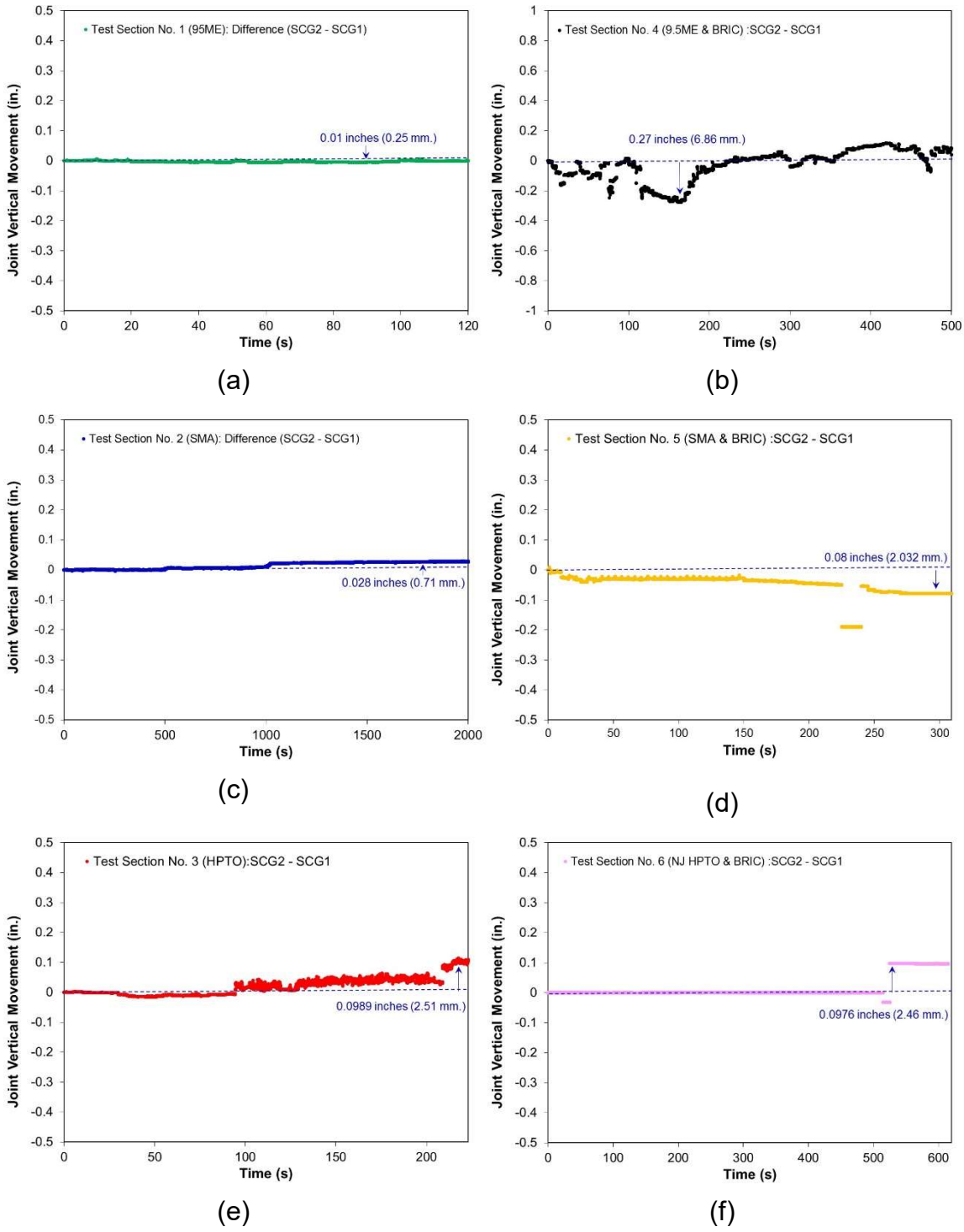

Figure 40. Vertical Displacement Measurements Obtained from Installed SCGs.

Step 2: Determining Relative Vertical Positions of the Approach and Leaving Slabs

In this step, the relative vertical position of the top of the PCC slabs in each test section was determined. To achieve this task; the vertical position of the top of the approach slab

was subtracted from the vertical position of the top of the leaving slab. Therefore the relative vertical position of the PCC slabs was determined by finding the difference between the vertical measurements recorded from the SCG under the approach slab and the vertical measurements recorded from the SCG under the leaving slab as shown in Figure 40. In general an increase in relative vertical position indicated that the top of the leaving slab was at a higher elevation than that of the leaving slab while a decrease in relative vertical position indicated that the top of the approach slab was at a higher elevation than that of the leaving slab.

From Figure 40 it can be observed that the maximum relative vertical joint displacement obtained on all test sections did not exceed 0.01-in. except in the case of Section 4 (9.5ME and BRIC); which had a maximum relative vertical joint displacement of 0.27-in. Section 1 (9.5 ME) had the next highest maximum vertical joint displacement; 0.01 in., followed by sections which was followed by Sections 3 (NJHPTO), 4 (NJHPTO and BRIC), 5 (SMA and BRIC), and 2 (SMA) which had maximum vertical joint displacements of 0.099-in., 0.098-in., 0.08 in., and 0.076-in. respectively.

Vertical Load Distribution of Asphalt Overlays

Typically, the stress distribution within the layers of a pavement structure gives an overall indication of the load transfer across the layers of the pavement. Pavement systems generally perform better when the upper layers (i.e. surface and base) of the pavement are able to reduce the stresses that the lower layers (i.e. subbase/subgrade) experience due to applied loads. This is because as depth increases within a pavement system, the quality and durability (i.e. performance) of layer material decreases. Therefore if the lower layers are subjected to higher stresses, the pavement system is likely to experience severe structural failure.

This section presents the overall approach established to analyze the stress data obtained from the pressure cells installed in each test section evaluated in this study. The procedure developed to compute a stress response parameter that accounts for the influence of overlay stiffness on the stress distribution within a pavement structure is also outlined in this section. The developed procedure is based on the theory that overlay or surface layer deterioration of a pavement structure due to applied APT loading leads to an increase in stress in the lower layers (i.e. subbase and subgrade) of the structure. The computational procedure consists of two steps which are detailed in the following subsections.

Step 1: Processing Data and Identifying Peak Measured Stress

In this step, the stress measurements were obtained by converting the voltage signal recorded by pressure cells installed in a pavement section. Calibration factors, which were provided by the manufacturers of the pressure cells were used for this purpose. The stress response pulse was then filtered using signal processing techniques (i.e. moving average) to remove any noise that was present in the data. A 25-data-point moving average of 10,000 data points were utilized in order to reduce the number of data points required to capture the stress response at a particular loading pass. This process for

reducing the amount of stress measurements per loading pass was found to be optimal since it accurately captured the trend in stress response as illustrated in the Figure 41a. A stress response pulse representative of the typical subbase stress responses obtained during each HVS loading pass on the six test sections is illustrated in Figure 41b.

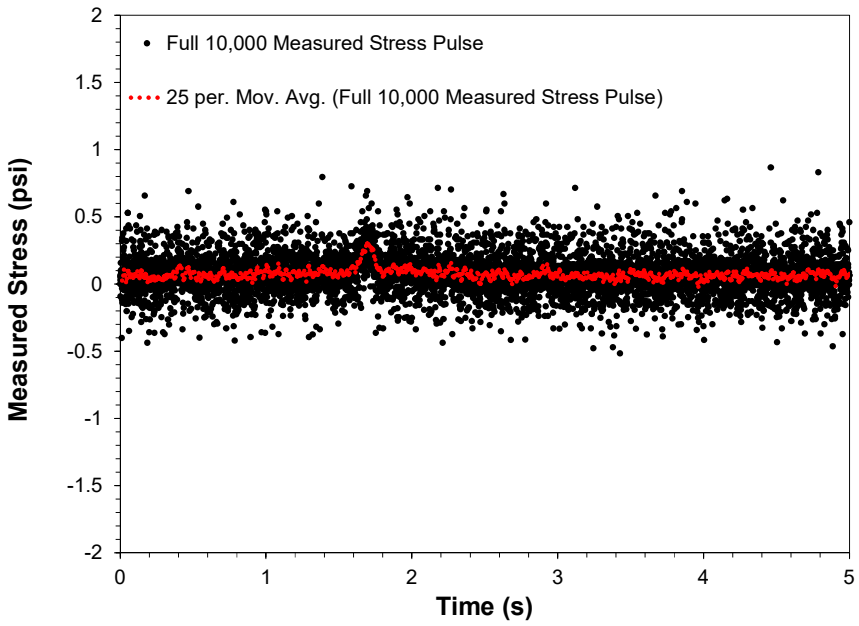

(a)

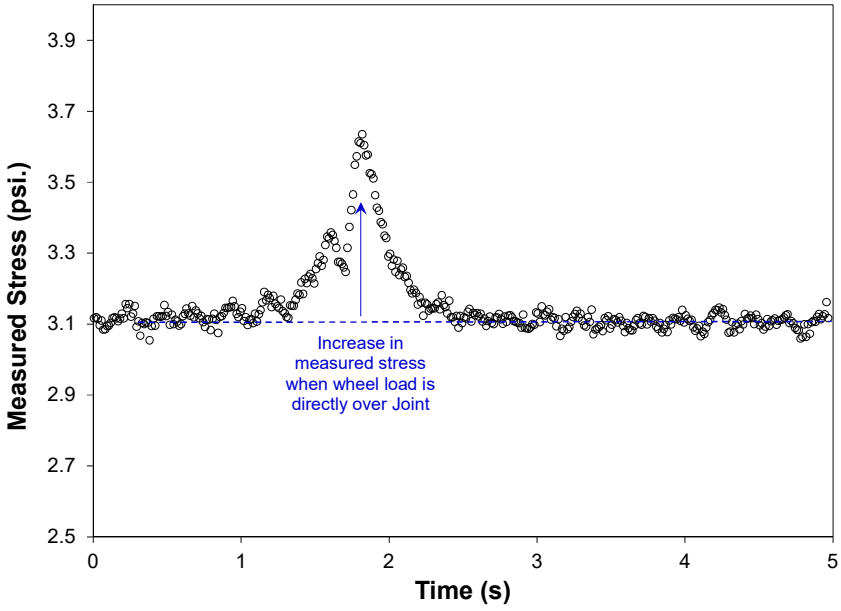

(b)

Figure 41. (a) Example of measured and reduced stress obtained from embedded Pressure Cell in one of the six sections and (b) Typical Stress Response Pulse Recorded by Embedded Pressure Cells.

From this figure it can be seen that the measured stress was constant as the HVS wheel approached the joint. However as the wheel moved over the joint in each test section, a noticeable spike measured stress was observed. The measured stress subsequently decreased toward a particular stress value as the wheel moved away from the joint. In addition to processing the stress data obtained from the pressure cells, Step 1 of the stress data analysis procedure also entailed identifying the maximum stress recorded for a particular pass. This task was performed in order to facilitate the computation of the developed stress response parameter discussed in the following step of the overall procedure.

Step 2: Calculating Total Measured Stress for Each Pass

This step involved the computation of a stress response parameter referred to as the total measured stress (σ_{total}). The total measured stress was computed for each loading pass by adding the overall change in stress (i.e. the difference between the average stress recorded for a particular pass and the average stress recorded for the initial or reference pass) to the change in stress ($\delta\sigma$) for a particular pass (i.e. the difference between the peak stress for that pass and the average stress recorded for that pass). This computational procedure for total measured stress is illustrated in Figure 42(a). From this computational procedure, it can be seen that the total measured stress accounted for the most critical stresses the lower layers (subbase layer) experienced during each passage of the HVS test wheel over the test section. It can also be seen from this figure that the total measured stress parameter (σ_{total}) also accounted for the overall increase in stress recorded within the subbase (due to overlay deterioration or damage accumulation) as loading passes increased on the test sections.

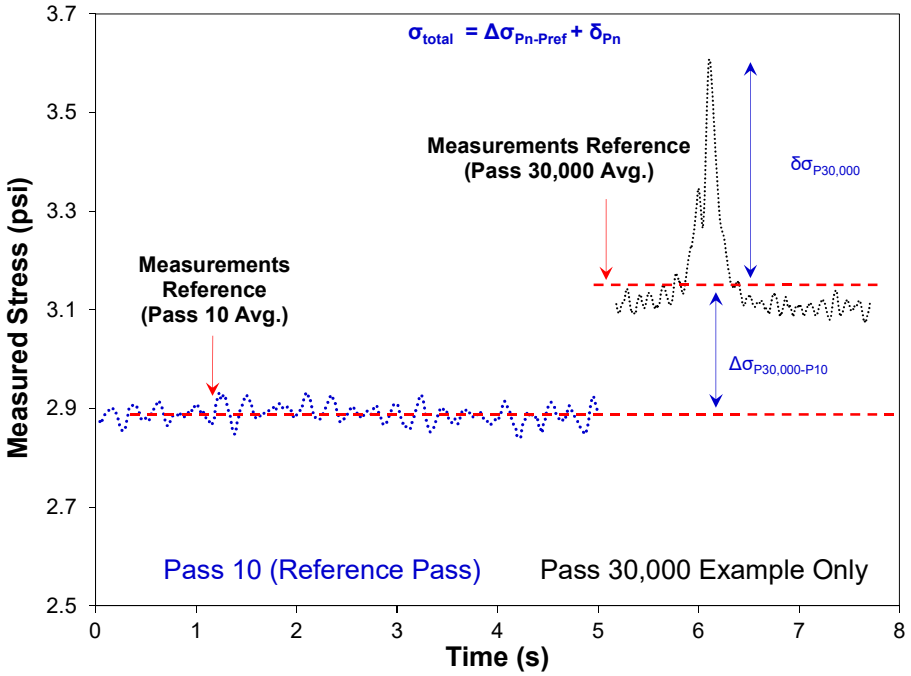

(a)

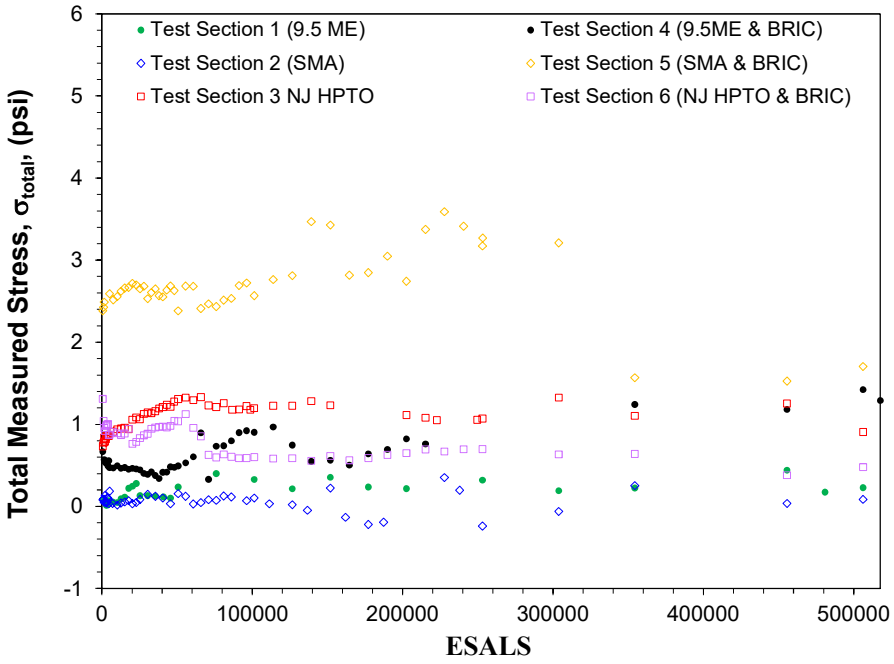

(b)

Figure 42. (a) Illustration of Peak Measured Stress Computational Procedure and (b) Total Measured Stress (σ_{total}) computed for all six sections with ESALS.

Figure 42(b) presents the total stress computed for on all six test sections evaluated in this study. From this figure it can be seen that the computed σ_{total} obtained from the embedded pressures measurements were relatively similar for all Sections except Section 5 (SMA and BRIC). By determining the magnitude of the maximum change in total stress $\Delta\sigma_{total}$, during APT, the overall vertical load distribution of the asphalt overlays can be compared. Additionally, by comparing the computed σ_{total} values of the various mixes at a particular amount of ESALS, the vertical load distribution capacity of the asphalt overlays can also compared since similar loading conditions were maintained for all test sections. It is noted that the computed σ_{total} values for all test sections were only compared up to 300,000 ESALS in this analysis because the drastic decrease in σ_{total} Section 5 (SMA and BRIC) after 300,000 ESALS may have been due to the sensor being damaged (i.e., recording unreasonable stress measurements). Based on the maximum change in computed σ_{total} it can be observed that Section 1 (9.5ME) had a maximum change in σ_{total} of 0.31-psi while Sections 2, 3, 4, 5 and 6 had a change in σ_{total} of 0.59-psi, 0.5-psi, 0.51-psi, 0.82-psi, and 0.67-psi respectively. These results implied that the both the σ_{total} and maximum change in σ_{total} were not capable of differentiating between the test sections since the values obtained for all test sections were similar. This was expected because the pressure cells were embedded at a 19.5 in below the surface of the pavement structure in all test sections. Due to the presence of an 8-in thick rigid (PCC) base layer, the impact of accelerated loading at such a depth (i.e. 19.5 in below the pavement surface) was expected to be minimal.

Transverse Pavement Profile Evaluation

As was previously mentioned, transverse pavement profile evaluation was conducted in this study in order to assess the extent of permanent deformation on the surface of pavement sections due to applied HVS loading. Pavement profiles were taken at seven locations along each test section however, particular focus was placed on the pavement profiles obtained at the joint in each test section. The transverse pavement profiles obtained on each test section at the joint after 200,000 HVS passes were used for the comparisons presented in this section. Figure 43 (a) illustrates the methodology utilized to compute the surface permanent deformation on each of the six test section. From this figure, it can be seen that the permanent surface deformation on each test section was computed by finding the difference in depth between a transverse reference line and the surface depression recorded in each test section. Figure 43(b) presents the surface permanent deformation obtained for each test section at the joint after 200,000 HVS passes. Based on the results presented in Figure 43(b), it can be seen that Section 2 (SMA) had the lowest surface permanent deformation followed by Section 1 (9.5 ME), Section 4 (9.5 ME and BRIC), Section 3 (NJHPTO and BRIC), Section 5 (SMA and BRIC), and Section 6 (NJHPTO & BRIC) respectively. This trend in the permanent surface deformation results was expected because SMA mixes are typically designed to resist rutting while binder rich asphalt mixtures such as NJHPTO and BRIC are generally highly susceptible to rutting

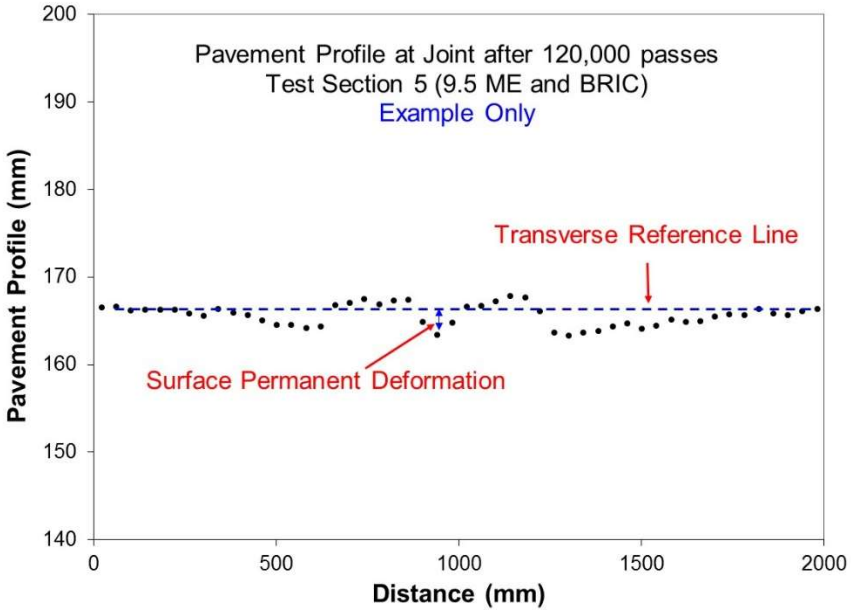

(a)

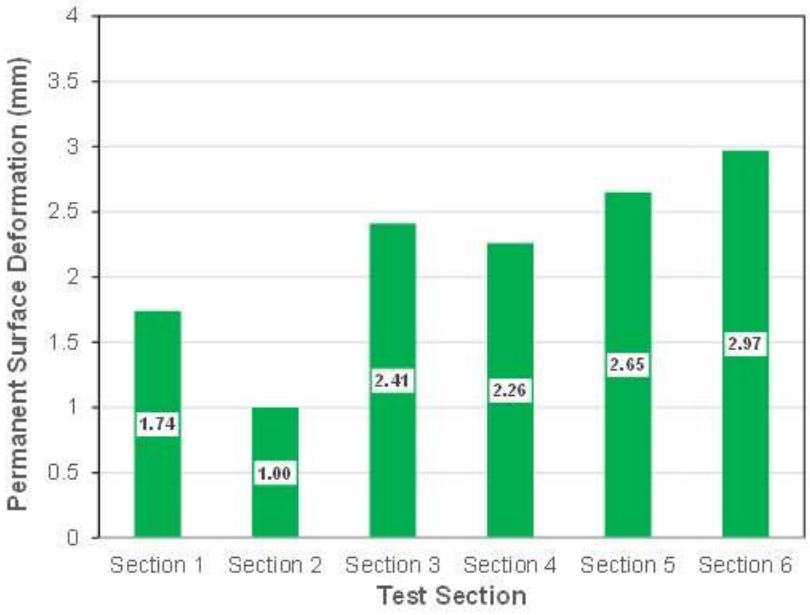

(b)

Figure 43. (a) Method used to compute surface permanent deformation (b) suface permanent deformation obtained for all test sections at joint after 200,000 HVS passes.

Performance Ranking of Test Sections

Table 8 presents the ranking system used to determine which asphalt overlay had the best overall field performance. The ranking system was based on two performance criteria.

These performance criteria included the following:

- Reflective cracking susceptibility; characterized by the cumulative DI and rate of change in cumulative DI,
- Asphalt layer permanent deformation during HVS evaluation.

The highest performance criterion ranking score was designated to the test section which had the lowest cumulative DI and rate of change in cumulative DI and the least permanent deformation after being subjected to HVS testing. The overall performance ranking score for the test sections was then computed by using a weighted average of the individual performance criterion ranking scores for each test section. The weighted average placed greater significance on performance criteria that were directly related to the material properties of the asphalt overlay (i.e. fatigue and rutting performance). In regard to permanent surface deformation, the ranking scores were computed by finding ratio between permanent surface deformation observed and the NJDOT rutting requirement for each specific mix. Asphalt overlays that had a permanent surface deformation percentage between 0-20% received a score of 5, while those which had percentages ranging between 20-40%, 40-60%, 60-80%, and 80-100% hade ranking scores of 4, 3, 2,

and 1 respectively. The section with the highest average ranking score (i.e. raking score 5) was considered as the best performing field section while the section with the lowest average ranking score was considered as the worst performing test section (i.e. ranking score 0).

Based on the results presented in Table 8 it can be seen that Section 2 (SMA) had the best overall performance with an average ranking score of 4.5 followed by Sections 1 (9.5 ME) and 3 (NJHPTO) with an average ranking scores of 3. The test sections with the next best overall performance were Section 4 (9.5ME and BRIC), Section 5 (SMA and BRIC), and Section 6 (NJHPTO and BRIC) with average ranking scores of 2.5, and 2 respectively. The section with the worst overall performance were Section 5 (SMA and BRIC) and Section 6 (NJHPTO and BRIC) with an average performance ranking score of 2. Based on the overall performance ranking of the test sections and data analysis presented in the previous sections it can be deduced that the addition of a 1-in. layer of BRIC did not improve the field performance of the overlay. This was because the performance criterion ranking scores generally indicated that the addition of the 1-in. BRIC layer slightly worsened the performance of the test sections in regard to reflective cracking susceptibility and surface permanent deformation.

Table 8 – Overall Performance Ranking of Test Sections

Section Designation	Ranking (5 Best, 1: Worst)		Average Ranking Score
	Reflective Cracking Susceptibility (Weight; 1)	Permanent Deformation (Weight; 1)	
Test Section 1 (9.5 ME)	N/A	3	3
Test Section 2 (SMA)	4	5	4.5
Test Section 3 (NJHPTO)	3	3	3
Test Section 4 (9.5ME and BRIC)	2	3	2.5
Test Section 5 (SMA and BRIC)	2	2	2
Test Section 6 (NJHPTO and BRIC)	2	2	2

SUMMARY OF FINDINGS, CONCLUSIONS AND RECOMMENDATIONS

Summary of Findings

This study focused on evaluating the field performance and life expectancy of various asphalt overlay treatments commonly used in New Jersey through full-scale accelerated pavement testing. Six 30-ft. long and 12-ft. wide full-scale, composite field sections were evaluated in this study. All six field sections contained a similar substructure (i.e. 8-in. thick Portland cement concrete (PCC) base, 16-in thick New Jersey I-3 (A-1-a) granular subbase, and 12-in. thick compacted natural soil subgrade). The differences between the sections came from the hot mix asphalt (HMA) overlay placed over the PCC layer. The overlay on the test sections consisted of the following mixes a 3-in. thick 9.5 mm Superpave mix for Section 1, a 3-in thick Stone Matrix Asphalt (SMA) mix for Section 2, and a 2-in. thick New Jersey High Performance Thin Overlay (NJHPTO) for Section 3. The overlays on sections 3 through 6, consisted of a combination of 1-in. thick layer of BRIC and a 2-in. layer of 9.5 ME Superpave, SMA, and NJHPTO respectively. All sections were instrumented with two asphalt strain gauges, linear variable differential transorfmers, soil compression gauges, and one pressure cell. The test sections were subjected to accelerated pavement testing at the Rowan University Accelerated Pavement Testing Facility (RU-APTF) using a Heavy Vehicle Simulator (HVS). The accelerated pavement testing involved the application of 60-kN, dual-tire, single axle load configuration for 200,000 repetitions. The test sections were also evaluated through heavy weight deflectometer testing and transverse pavement profile assessment. Additionally, a ranking system was developed to determine which asphalt overlay had the best overall field performance. The ranking system was based on six performance criteria. These performance criteria included the following: (1) reduction in effective stiffness obtained from HWD testing, (2) reflective cracking susceptibility, (3) resistance to horizontal joint movement, (4) resistance to vertical joint movement, (5) vertical load distribution capacity and (6) asphalt layer permanent deformation during HVS evaluation.

Based on the testing results, data collected from the embedded sensors and the subsequent data analyses, the following conclusions were drawn:

- The Outer AREA method was successfully used to analyze the measured HWD deflections and draw conclusions about the structural capacity of the test sections. This is because it facilitated the ranking of the pavement sections by comparing the relative reduction in effective stiffness the test sections experienced after being subjected to HVS testing. Based on the computed effective stiffness values, it was concluded that Section 4 (9.5 ME & BRIC) experienced the largest reduction in effective stiffness followed by Section 2 (SMA), Section 3 (NJHPTO), Section 5 (SMA and BRIC), Section 6 (NJHPTO and BRIC) and Section 1 (9.5 ME) respectively.
- The strain data processing and analysis approach presented in study was successfully used to rank all six sections based on their relative fatigue performance. This is the case because the computed analysis parameters (E_{APT} and cumulative DI) were able to distinguish between the sections.

- Two measures ($\varepsilon_{t\text{-}max}$ and TP_R) were directly computed from the strain time history pulses measured during APT. These parameters quantify the response of pavement layers to applied loading. The $\varepsilon_{t\text{-}max}$ represented the critical tensile strain that an asphalt layer experiences in a loading pass while The TP_R captured the critical tensile strain an asphalt layer undergoes while at the same time accounted for the potential "elasticity" of the asphalt mix (i.e. its ability to stretch and flex under applied loading). These measures were necessary for computing the reduction in layer modulus (E_{APT}) and cumulative damage index (DI).
- The E_{APT} is defined as the ratio of the applied full-scale stress to the $\varepsilon_{t\text{-}max}$ in a particular loading pass. The rate of reduction in E_{APT} values was successfully able to distinguish the fatigue characteristics of the six asphalt overlays evaluated in this study. Based on the rate of reduction in E_{APT}, Section 5 (SMA and BRIC) was ranked as the most susceptible to fatigue cracking, followed by Sections 6 (NJHPTO) Section 4 (9.5ME and BRIC), Section 3 (NJ HPTO) and Section 2 (SMA).
- The cumulative DI is computed as summation of DI for all loading passes. The DI is defined as the rate of change in TPR (ΔTP_R) multiplied by E_{APT} for a particular loading pass. Therefore, this parameter accounts for the "elasticity" of the asphalt overlay as well as the loading being applied (asphalt modulus reduction). The cumulative DI was also found to be capable of distinguishing the fatigue performance of the six asphalt overlays as different cumulative DI values were calculated for the six overlays. Using the cumulative DI parameter, Section 2 (SMA) was the best at resisting fatigue cracking followed by Section 3 (NJHPTO), Section 5 (SMA and BRIC), Section 6 (NJHPTO and BRIC) and Section 4 (9.5ME and BRIC), respectively.
- The cumulative DI parameter demonstrated a more consistent fatigue performance ranking. This is because the cumulative DI and rate of increase in cumulative DI was also able to clearly distinguish between overlays that contained a layer of BRIC and those which did not. Additionally, the cumulative DI and rate of increase in cumulative DI maintained a similar fatigue performance ranking for the overlay mixtures even when there was a layer of BRIC added to the overlay.

- The LVDT data processing and analysis approach presented in study was successfully used to rank all six sections based on their relative susceptibility to horizontal joint movement. This is the case because the computed analysis parameter (maximum joint displacement (ΔMax(JD)) was able to distinguish between the six test sections. The maximum joint displacement computed for each asphalt overlay generally ranged between 0 and 0.01-in. This coincides with the findings of a previous study which found that dense graded asphalt mixtures were not able to resist crack movements more that 0.01-in. Based on the overall maximum joint displacement values obtained for the test sections, Section 3 (NJHPTO) was found to have the largest maximum displacement (or susceptibility to reflective cracking) followed by Sections 1 (9.5ME), 4 (9.5 ME and BRIC), 2 (SMA), 6 (NJHPTO and BRIC), and 5 (SMA and BRIC) respectively. It is noted however that caution must be taken when drawing conclusions about the reflective cracking susceptibility of the overlays strictly based on LVDT measurements. This is because standalone LVDT

measurements do not necessarily reflect a change in material properties of the asphalt overlays.

- The soil compression gauge data processing and analysis approach presented in study was successfully used to rank all six sections based on their susceptibility to vertical joint movement. Based on the maximum vertical joint displacement obtained, it was found that Section 4 (9.5ME and BRIC had the highest a maximum relative vertical joint displacement of 0.27-in. followed by Section 1 (9.5 ME), Sections 3 (NJHPTO), Section 4 (NJHPTO and BRIC), 5 (SMA and BRIC), and 2 (SMA) respectively. As in the case of horizontal displacement measurements, it is noted that caution must be taken when drawing conclusions about the reflective cracking susceptibility of the overlays strictly based on soil compression gauge measurements. This is because standalone SCG measurements do not necessarily reflect a change in material properties of the asphalt overlays.
- The stress data processing and analysis approach presented in study was could not be utilized to rank the six sections based on their relative vertical load distribution capacity. This is the case because the computed analysis parameter (total measured stress (σ_{total})) was not able to distinguish between the sections. That is, the computed σ_{total} values obtained for all test sections were similar. This was expected because the pressure cells were embedded at a 19.5 in below the surface of the pavement structure in all test sections. Due to the presence of an 8-in thick rigid (PCC) based layer, the impact of accelerated loading at such a depth (i.e. 19.5 in below the pavement surface) was expected to be minimal.
- The transverse pavement profile evaluation was able to successfully assess the extent of permanent deformation on the surface of pavement sections due to applied HVS loading. Based on the results of the transverse profile evaluation, it was found that Section 2 (SMA) had the lowest surface permanent deformation after 200,000 HVS passes followed by Section 1 (9.5 ME), Section 4 (9.5 ME and BRIC), Section 3 (NJHPTO and BRIC), Section 5 (SMA and BRIC), and Section 6 (NJHPTO & BRIC) respectively.

Conclusions

Based on the results of the ranking system, the following conclusions were drawn:

- Section 2 (SMA) had the best overall performance with an average ranking score of 4.5 followed by Section 1 (9.5 ME) and Section 3 (NJHPTO) with average ranking scores of 3.
- The sections with the worst overall performance rankings were Section 5 (SMA and BRIC) and Section 6 (NJHPTO and BRIC) with an average ranking score of 2 followed by Section 4 (9.5 ME and BRIC) with an average ranking score of 2.5.
- Additionally, the overall performance ranking of the test sections presented in this study indicated that the addition of a 1-in. layer of BRIC did not improve the field performance of the overlay. This was because the performance criterion ranking scores generally indicated that the addition of the 1-in. BRIC worsened the

performance of the test sections in regard to some criteria such as the reflective cracking susceptibility and surface permanent deformation.

Recommendations for Future Research

It is recommended that further field evaluation is required to estimate the life expectancy of the overlays considered in the study. Though the research present in this study provides tools to successfully measure and rank the field performance of the six asphalt overlays considered in this study, further field evaluation is necessary in order to predict the expected life of these overlays. Estimation of the expected life of the six overlays evaluated in this study would provide verification for the parameters developed in this study to characterize the asphalt overlays' reflective cracking susceptibility, resistance to horizontal and vertical joint movement, and vertical load capacity.

REFERENCES

[1] Watson, D. E., and M., Heitzman, "**Thin Asphalt Concrete Overlays."** In *NCHRP Synthesis 464*, TRB, National Research Council, Washington, D.C. 2014, pp. 6-7.

[2] Cooley, L. A., and R., Brown, **"Potential of Using Stone Matrix Asphalt for thin Overlays"** *In Transportation Research Record 1749*, TRB, National Research Council, Washington, D.C. 2003, Paper No. 01-0367.

[3] Xie, H., L.A., Cooley, and M. H. Huner, *4.75 mm NMAS Stone Matrix Asphalt (SMA) Mixtures*. NCAT Report 03-05. National Center for Asphalt Technology, Auburn University, 2003.

[4] Cooley, L. A., R. B., Mallick, M. R. Teto, R. L. Bradbury, and D. Peabody, *An Evaluation of Factors Affecting Permeability of Superpave Designed Pavements*. Report 03-02. National Center for Asphalt Technology, 2003.

[5] Cantrell, L., *Design and Evaluation of 4.75 mm Mixture for Thin Asphalt Overlay in Washington State*. Doctoral dissertation, Washington State University, 2013.

[6] Al-Qadi, I. L., S. Son, and T. Zehr, "4.75 mm SMA Performance and Cost-Effectiveness for Asphalt Thin Overlays." *International Journal of Pavement Engineering*, Vol. 17 No. 9, (March 2015), pp 799-809.

[7] Mogawer, M., A. Austerman, R. Kluttz, "**High Performance Thin-Lift Overlays with High Reclamed Asphalt Pavement Content and Warm-Mix Asphalt Technology"** In *Transportation Research Record 2293*, TRB, National Research Council, Washington, D.C. 2012 pp. 18-28.

[8] Kandhal, P. and L. A. Cooley, *Coarse Versus Fine-Graded Superpave mixtures: Comparative Evaluation of Resistance to Rutting*. NCAT Report 02-02. National Center for Asphalt Technology, Auburn University, 2002.

[9] Rahman, F., M. Hossain, S. A. Romanoschi, and C. Hobson, **"Experience with Thin Superpave Mixture Overlay of Small Aggregate Top Size in Kansas."** In *Transportation Research Record 2205*, TRB, National Research Council, Washington, D.C. 2014, pp. 3-10.

[10] Suleiman, N. **"Evaluation of North Dakota's 4.75mm Superpave Mixes for Thin Overlay Applications."** *In Transportation Research Record 2204*, TRB, National Research Council, Washington, D.C. 2011, pp.58-64.

[11] Gilbert, T. M., P. A. Olivier, and N. E. Galé, "Ultra-thin Friction Course: Five Years on in South Africa." In *Proceedings of the 8th Conference on Asphalt Pavements for Southern Africa (CAPSA'04)*, Vol. 12, (2004), p. 16.

[12] Ahmed, S., E. V. Dave, B. Behnia, W. G. Buttlar, and K.M. Exline, "Fracture Characterization of Gap-Graded Asphalt Mixtures and Thin Bonded Wearing Courses." *Journal of the Pavement Research and Technology,* Vol. 3, No. 3 (May 2010), pp. 128-134.

[13] Huffman, M. *Comparison of Reflective Crack Retardation by Fabric Material (Petromat), Open-Graded Friction Courses and Conventional Hot Mix.* Report FHWATX78-606-3, FHWA, U.S. Department of Transportation, 1978.

[14] Belshe, M., K. E. Kaloush, J. S. Golden, M. Mamlouk, and P. E. Phelan. **"Asphalt Rubber Asphalt Concrete Friction Course Overlays as Pavement Preservation**

Strategy for Portland Cement Concrete Pavement." *In Transportation Research Record*, TRB, National Research Council, Washington, D.C. 2007, Paper No. 07-1916

[15] Qing, L. and J. T. Harvey **"Laboratory Evaluation of Open-Graded Asphalt Mixes with Small Aggregates and Various Binders and Additives"** *In Transportation Research Record 2209*, TRB, National Research Council, Washington, D.C. 2011, pp 61-69.

[16] Gibney A., G. Lohan, and V. Moore, **"Laboratory Study of Bituminous Overlays to Reflective Cracking."** *In Transportation Research Record 1809*, TRB, National Research Council, Washington, D.C. 2002, Paper No. 02-2201.

[17] Bennert, T. A. *Flexible Overlays for Rigid Pavements*. Report FHWA-NJ-2009-014, FHWA, U.S. Department of Transportation, 2010.

[18] Druta, C., L. Wang, and K. K. McGhee, *Performance Evaluation of Thin Wearing Courses Through Scaled Accelerated Trafficking*. Report FHWA/VCTIR 14-R7. FHWA, U.S. Department of Transportation, 2014.

[19] Powell, R. B., and S. Buchanan, **"Long Term Performance of a Thin Asphalt Overlay on the NCAT Pavement Test Track."** *In Transportation Research Record*, TRB, National Research Council, Washington, D.C., 2012.

[20] Li, X., N. Gibson, X. Qi, T. Clark, and K. McGhee. **"Laboratory and Full-Scale Evaluation of 11 4.75 mm NMAS Superpave Overlay."** *In Transportation Research Record 2293*, TRB, National Research Council, Washington, D.C. 2012, pp. 29-38.

[21] Nur A., M., Khattak, M. J., and Bhuyan, M. R. U. K. "Rutting Model for HMA Overlay Treatment of Composite Pavements." *International Scholarly Research Notices Civil Engineering*, Vol. 2013 (January 2013).

[22] Al-Qadi, I. L., W. Buttlar, J. Baek, and K. Minkyum, *Cost-effectiveness and Performance of Overlay Systems in Illinois Volume 1: Effectiveness Assessment of HMA Overlay Interlayer Systems used to Retard Reflective Cracking*. Report FHWA-ICT-09-044, FHWA, U.S. Department of Transportation, 2009.

[23] Gokhale, S., T. Byron, S. Iyer, and B. Choubane. **"Evaluation of Pavement Strain Gauge Repeatability: Results from Accelerated Pavement Testing."** *In Transportation Research Record 2094*, TRB, National Research Council, Washington, D.C. 2009. pp. 30-40.

[24] Harvey, J. T. **"Use of Accelerated Pavement Testing to Evaluate Maintenance and Pavement Preservation Treatments: Introduction."** *In Transportation Research Circular E-C139,* TRB, National Research Council, Washington, D.C. 2009. pp. 1-10.

[25] Smith, K.D., J. E. Bruinsma, M. J. Wade, K. CHatti, J. M. Vandenbossche, and H. T. Yu. *Using Falling Weight Deflectometer Data with Mechanistic-Empirical Design and Analysis, Volume 1: Final Report.* Report FHWA-HRT-16-009, FHWA, U.S. Department of Transportation, 2017.

[26] Dhakal, N., M. A. Elseifi, and Z. Zhang. "Mitigation Strategies for Reflection Cracking in Rehabilitated Pavements-A Synthesis" *International Journal of Pavement Research and Technology,* Vol. 9 No. 3 (May 2016) pp 228-239

[27] Hammons, M. I., D. Timm, and J. Greene. *Instrumentation Data Interpretation*. State Materials Office, Florida Department of Transportation, 2007.

[28] Rodrigues de Mello, L. G., M. Muniz de Farias, and K.E. Kaloush. “Using Damage Theory to Analyze Fatigue of Asphalt Mixtures on Flexural Tests”. *International Journal of Pavement research and Technology*, Vol. 11 No. 4, (February 2018).

[29] Timm, D. H., and A. L. Priest. *Dynamic Pavement Response Data Collection and Processing at the NCAT Test Track*. NCAT Report 04-03. National Center for Asphalt Technology, Auburn University, 2004.

[30] Qi, X., T. Mitchell, K. Stuart, J. Youtcheff, K. Petros, T. Harman, and G. Al-Khateeb. “Strain Responses in ALF Modified-Binder Pavement Study.” *In 2nd International Conference on Accelerated Pavement Testing.* TRB, National Research Council, Washington, D.C (2004)

[31] Garg, N. and G.F. Hayhoe, "Asphalt Concrete Strain Responses at High Loads and Low Speeds at the National Airport Pavement Test Facility (NAPTF)." *Presented at the Airfield Pavement Specialty Conference*, American Society of Civil Engineers. Chicago, I.L., (2001)

[32] Huang, Y. H. *Pavement Analysis and Design*. Pearson Education, Inc., Upper Saddle River, N.J., 2004.

[33] Li, H., Jones, D., R., Wu, and J. T. Harvey, *Development and HVS Validation of Design Tables for Permeable Interlocking Concrete Pavement: Final Report*. Report UCPRC-RR-2014-04, Institute of Transportation Studies, University of California, Davis, 2014.

[34] Joeseph P. E., and R. Haas, **“Evaluating Alternative Solutions to Reflection Cracking Through Asphalt Overlays.”** *In Transportation Research Record 1215*, TRB, National Research Council, Washington, D.C. 2000. pp. 282-291.